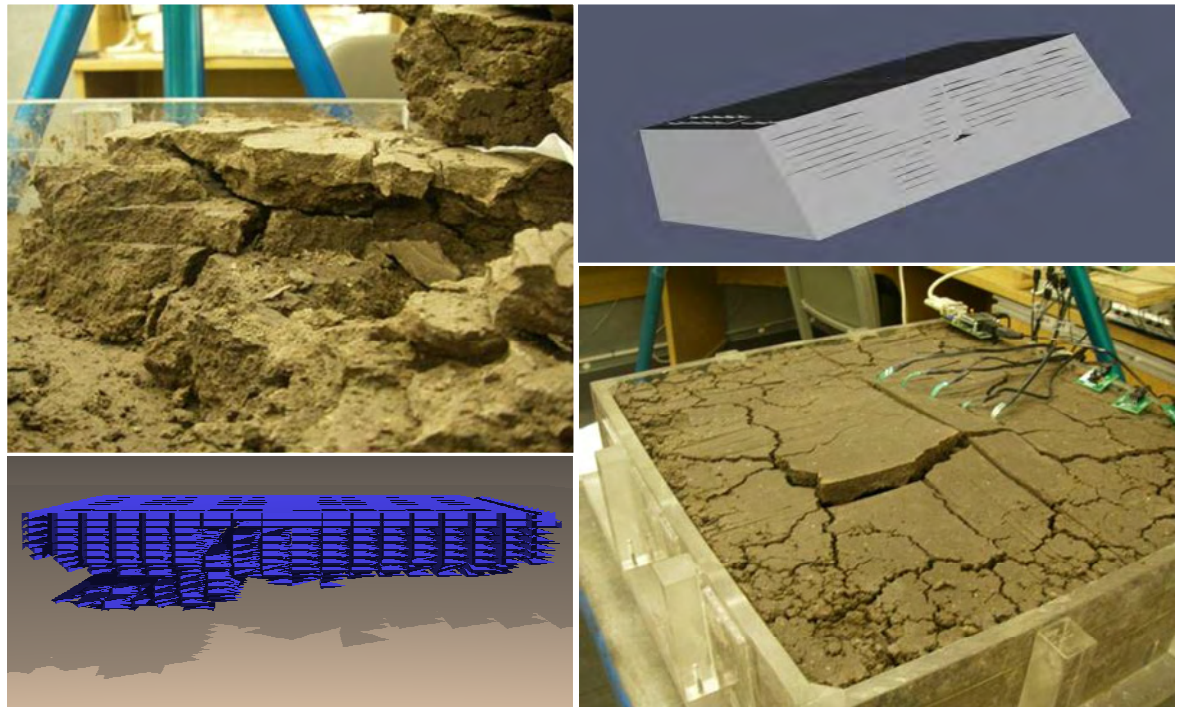Engineer Research and Development Center

US Army Corps of Engineers®
Engineer Research and Development Center

Assessment of the Effectiveness of Clay Soil Covers as Engineered Barriers in Waste Disposal Facilities with Emphasis on Modeling Cracking Behavior

Ernest S. Berney IV, Wayne D. Hodo, John F. Peters, Tommy E. Myers, Richard S. Olsen, and Michael K. Sharp

June 2008

Assessment of the Effectiveness of Clay Soil Covers as Engineered Barriers in Waste Disposal Facilities with Emphasis on Modeling Cracking Behavior

Ernest S. Berney IV, Wayne D. Hodo, John F. Peters, Richard S. Olsen, and Michael K. Sharp

Geotechnical and Structures Laboratory
U.S. Army Engineer Research and Development Center
3909 Halls Ferry Road
Vicksburg, MS 39180-6199

Tommy E. Myers

Environmental Laboratory
U.S. Army Engineer Research and Development Center
3909 Halls Ferry Road
Vicksburg, MS 39180-6199

Final report

Approved for public release; distribution is unlimited.

Abstract: This research investigated the nature of cracking behavior in compacted clay liners used for nuclear waste disposal facilities. A literature review found that, in all documented in-place clay liner studies, cracking occurred in the clay liner within 10 years, leading to failure of the liner system. Further, all moisture-flow models studied failed to capture clay cracking and the resultant high permeability associated with these failed liner systems. A laboratory investigation was undertaken to define the mechanics of the clay cracking process for a numerical model. Visual and numerical observations of cracking during drying of a highly expansive clay showed that crack formations are very diverse along the surface layer and as they migrate downward. Shapes of cracks are neither uniform nor symmetric, evolving from thin webs of microcracks to a select number of wide primary cracks that, in turn, can seal off existing microcracks. A finite element model of the soil shrinkage process was then developed, which included crack formation. Stresses within intact soil are caused by self weight (gravity stresses) and changes in water content, which induce shrinkage as a result of suction-induced tensile stresses. Two numerical simulations were run on a digital test bed similar to the laboratory study. The simulations agreed well with laboratory experimental observations, capturing all the relevant crack phenomena. The report concludes that a change in the current design criteria for clay liner systems is necessary to enable the clay to remain in a fixed, as-compacted state.

Contents

Figures and Tables

Figures

Tables

Preface

This is the final report from a 4-year study conducted during the period 2003–2007, prepared for and sponsored by the U.S. Nuclear Regulatory Commission's Office of Nuclear Regulatory Research, entitled "Assessment of the Effectiveness of Clay Soil Covers as Engineered Barriers in Waste Disposal Facilities with Emphasis on Modeling Cracking Behavior," project agreement number RES-02-2003.

This publication was prepared by personnel of the U.S. Army Engineer Research and Development Center (ERDC), Geotechnical and Structures Laboratory (GSL), Vicksburg, MS. The findings and recommendations presented in this report are based upon tests and analyses conducted at the Waterways Experiment Station. The research team consisted of Dr. Ernest S. Berney IV, Wayne D. Hodo, and Roosevelt Felix, Jr., Airfield and Pavements Branch (APB), GSL Engineering Systems and Materials Division (ESMD), and Dr. John F. Peters, Research Group, ESMD; Drs. Michael K. Sharp and Richard S. Olsen, Wipawi Vanadit-Ellis, and Eric Smith, Geotechnical Engineering and Geosciences Branch (GEGB), GSL Geosciences and Structures Division (GSD); Tommy Carr and David Daily, ERDC Information Technology Laboratory; and Tommy E. Myers of the ERDC Environmental Laboratory (EL). Dr. Berney and associates prepared this publication under the supervision of Dr. Gary L. Anderton, Chief, APB; Dr. Larry N. Lynch, Chief, ESMD; Dr. William P. Grogan, Deputy Director, GSL; and Dr. David W. Pittman, Director, GSL.

COL Richard B. Jenkins was Commander and Executive Director of ERDC. Dr. James R. Houston was Director.

Recommended changes for improving this publication in content and/or format should be submitted on DA Form 2028 (Recommended Changes to Publications and Blank Forms) and forwarded to Headquarters, U.S. Army Corps of Engineers, ATTN: CECW-EW, Kingman Bldg., Rm. 321, 7701 Telegraph Rd., Alexandria, VA 22315.

Unit Conversion Factors

Multiply	By	To Obtain
feet	0.3048	meters
inches	0.0254	meters
pounds (force)	4.448222	newtons
pounds (force) per square foot	47.88026	pascals
pounds (force) per square inch	6.894757	kilopascals

Executive Summary

This report investigates the nature of cracking behavior in compacted clay liners. A thorough literature review on the current state of practice for construction of compacted clay liners revealed that significant infiltration of water into clay barriers occurs despite predictions of hydrologic models that such infiltration should be minimized by the low permeability of the clay. Numerous field studies have revealed that the cause of the high water intrusion is a direct result of cracks occurring as a result of vertical water vapor transport at the surface of the clay layer. These cracks will form, and quickly, in compacted clay liners independently of current techniques to mitigate cracking. Even composite caps that include clay liners overlain with geomembranes fail to provide effective resistance to water vapor transport because of defects that occur during the construction process. The studied hydrologic models do not account for the crack formation caused by drying, which induces a secondary porosity that greatly increases the bulk permeability of the clay mass.

As a preliminary step to a numerical model to capture this secondary porosity observed in field studies, an experimental program was undertaken to monitor and describe the phenomenology of crack formation and propagation in a clay mass. A series of drying experiments were carried out on a highly plastic clay, typical of clay liners, in a large area drying box with L × W × H dimensions of 18 in. × 18 in. × 5 in. (45.7 mm × 45.7 mm × 12.7 mm) instrumented with pressure sensors and time-lapse photography to capture quantitative and qualitative cracking response. The test bed was designed to encourage cracking in one dimension to optimize the readings obtained on lateral pressure sensors during the experiment. Several important conclusions were drawn from the results:

- Crack formations are very diverse along the surface layer and as they migrate downward. Shapes of cracks are neither uniform nor symmetric—evolving from thin webs of microcracks to a select number of wide primary cracks that, in turn, can seal off existing microcracks.
- The crack behavior was validated by pressure sensor readings exhibiting initially high compressive lateral stress that decreased to zero after 4 hr during microcrack formation (full tension), followed by a

> rebound to a compressive stress state after 20 hr when the formation of large primary cracks began to cause the small microcracks to close.

- Unbalanced stress loads from top to bottom of a horizontal crack induce a curling effect on the clay surface. As the soil continues to dry with depth and the boundary moisture conditions on the surfaces of the horizontal crack become balanced, an uncurling effect is noted.
- Time-lapse photography showed that the coupling of soil curling with primary crack formation leads to formation of "clay islands" that are free to shift and move along interfaces between compacted lifts. The exposed soil also allows drying to continue to deeper levels within the clay mass.
- Any imperfections in compaction, including scoring between compacted lifts, causes propagation of deep cracks, suggesting field defects can expedite cracking.

Once the mechanics of the cracking process were better defined, numerical parameters for shrink-swell models necessary for a quantitative model of cracking were obtained. The model development is based on the hypothesis that cracking in clay barriers is progressive and can extend to considerable depths despite the low permeability of the clay mass. Once an initial crack is formed at the surface, increasing the width of the crack by additional shrinkage will drive the crack deeper into the soil mass, exposing new surfaces to air, which enables further drying and cracking both horizontally and vertically within the soil mass. The cracking model consists of a finite element model of the soil shrinkage process that includes crack formation. Stresses within the intact material are caused by self weight (gravity stresses) and changes in water content, which induce shrinkage as a result of suction induced tensile stresses. The cracks are assumed to occur at the element boundaries, forcing the crack system to conform to the geometry of the finite element system. This was assumed a satisfactory approximation to capture the simple geometry of the experimental program.

Two numerical simulations were run on a digital test bed designed as close to the experimental drying box as possible, complete with constrained sides—the first on a uniform soil mass and the second with a pre-crack along the center of the specimen. The simulations agreed well with experimental observations. The model was dominated by horizontal cracking, not as a result of the influence of compaction lifts but because the soil is confined in the horizontal direction, which favors vertical shrinkage

strains resulting in horizontal cracks. Also, the size of the horizontal crack openings is enhanced by the curling tendency that results from the variation in shrinkage strain across the layers. In the second pre-crack simulation, little change was observed in the overall cracking response from the first analysis. From an exaggerated view of the cracking pattern, vertical cracks are evident at each element seam but with irregularly sized horizontal cracking with depth. This is a phenomenon very similar to the observed experimental behavior where primary crack locations varied with layer position. The fact that the essential features of the cracking process can be captured without appealing to arguments based on immeasurable lift properties simplifies interpretation of the cracking experiments. Therefore, the numerical model is able to capture the irregular cracking pattern indicative of typical field response versus a symmetric, uniform crack distribution.

The weight of the evidence from the published field studies, experiments, and numerical simulation clearly documents the inevitability of cracking in clay liners. The atmospheric suction potential, computed from relative humidity, is sufficient to cause cracking, even in temperate climates. The overburden stress is insufficient to offset the tensile stresses. It is concluded that clay liners are generally not adequate as a long-term moisture barrier. Change to the current design criteria for engineered barriers is necessary to enable the clay surface environment to remain in a fixed, as-compacted state.

1 Introduction

Background

The Office of Nuclear Regulatory Research (RES) furthers the regulatory mission of the U.S. Nuclear Regulatory Commission (NRC) by providing technical advice, technical tools, and information for identifying and resolving safety issues, making regulatory decisions, and promulgating regulations and guidance. RES conducts independent experiments and analyses, develops technical bases for supporting realistic safety decisions by the agency, and prepares the agency for the future by evaluating safety issues involving current and new designs and technologies. A portion of the RES research program is devoted to radionuclide transport in the environment. The radionuclide transport research program addresses the effect on public health and safety and the environment from nuclear material that enters the environment from NRC-licensed activities. The technical issues of concern (Office of Nuclear Regulatory Research 2002) include the following:

- Source-term characterization,
- Effectiveness of engineered and natural containment systems surrounding radioactive material,
- Multi-phase flow of water, including episodic infiltration, into and through contaminated systems,
- Transport of radioactive material through the geosphere,
- Transport of radioactive material through the biosphere, and
- Exposures of members of the public to radiation from these materials.

The second technical issue—effectiveness of engineered and natural containment systems surrounding radioactive material—includes research on engineered barrier systems at waste disposal facilities, e.g., shallow land burial of low-level radioactive waste (LLW). These facilities are typically constructed with an engineered cap or cover designed to eliminate or significantly limit infiltration of water into the waste. Conventional landfill covers are barrier-type systems that include a barrier layer among other layers that maybe installed above the waste. Compacted clay is usually the material of choice for the barrier layer. The primary purpose of an engineered cover is to isolate the underlying waste. A key element to isolating

the wastes from the environment is to prevent water from infiltrating into the landfill and coming into contact with the waste.

Figures 1 and 2 show widely used cap designs. These are conventional barrier-type caps that isolate waste and eliminate or significantly reduce infiltration of water into waste. Figure 1 is a schematic of a Resource Conservation and Recovery Act (RCRA) Class C landfill cover design. This design is in extensive use and meets the minimum requirements set forth for RCRA Subtitle "C" regulated landfills (40 CFR 264). RCRA Subtitle C regulations are commonly known as the hazardous waste regulations promulgated by the U.S. Environmental Protection Agency.
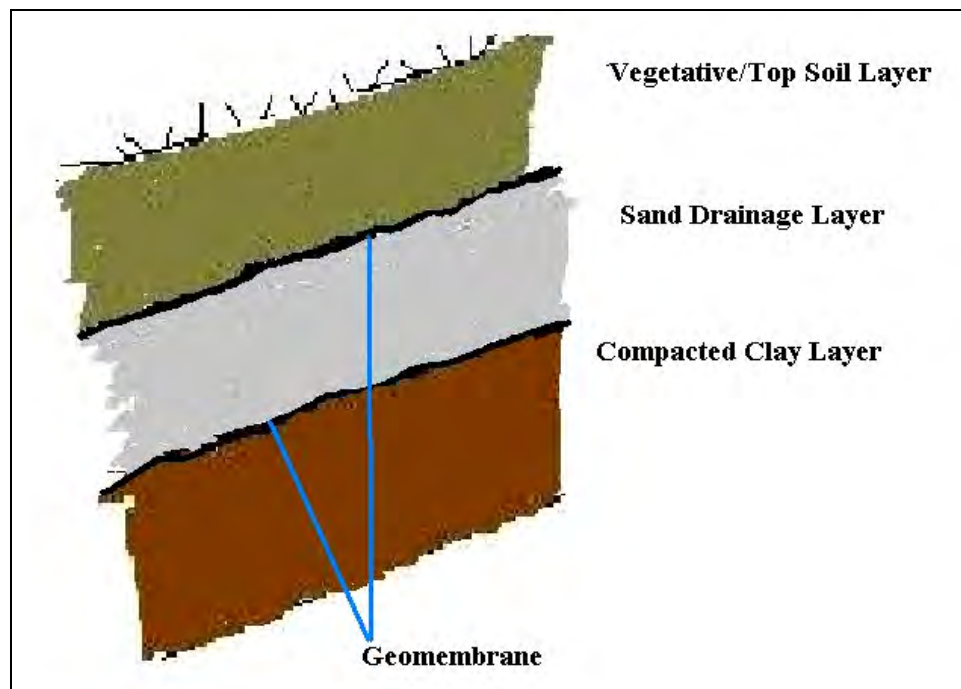
Figure 1. Prescriptive RCRA Subtitle C cap design.
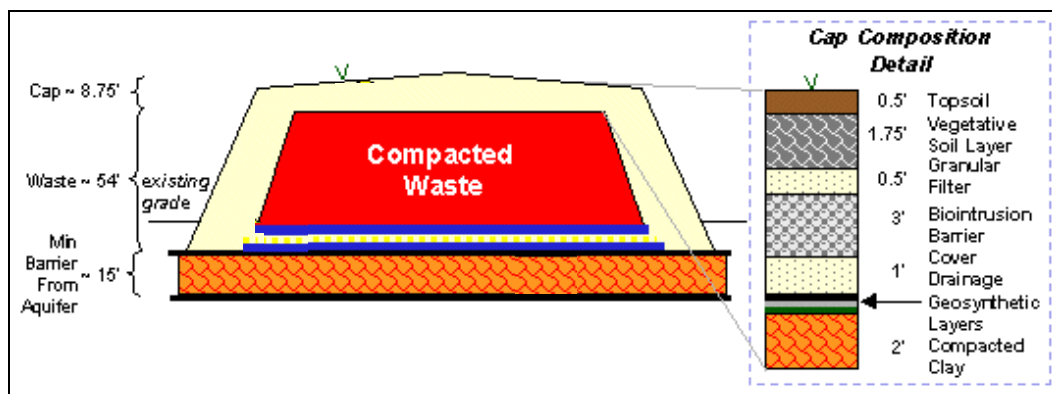
Figure 2. LLW disposal unit with cap detail.

Figure 2 shows a typical LLW facility design. This design and ones similar to it are often considered for shallow-land burial of LLW and is actually global in application, e.g., see Ziehm (2003).

The defining characteristic of the barrier-type covers illustrated in Figures 1 and 2 is the compacted clay barrier layer. It is this layer that blocks infiltration of water through the cover into the waste. The compacted clay layer is frequently specified to have a saturated hydraulic conductivity of 10^{-7} cm/sec or less. If the layers above the barrier layer cannot store or divert the infiltrating precipitation during an unusually large storm event, the barrier layer must stop or significantly inhibit downward flow. Guides to design and construction of barrier-type landfill caps are available in Landreth et al. (1991) and Koerner and Daniel (1997).

Alternative cover designs that do not use compacted clay barriers have recently been developed (Benson 1997; Hauser et al. 2001; Department of Energy 2002). Climate is a primary determinant of the applicability of these alternative cap designs. Arid and semi-arid climates are the most favorable (Hauser et al. 2001). Barrier-less cap designs are not given further consideration in this report.

The RES research program plan (Office of Nuclear Regulatory Research 2002) recognized long-term modeling of engineered barrier performance as a research need. Piet et al. (2003a, 2003b) discussed this same need in detail and pointed out that cap assessments treat the barrier layer structure as static throughout the lifetime of the cap. Current modeling approaches used to assess the long-term performance of caps treat probably the most important property of the clay barrier, hydraulic conductivity, as a fixed value over the life of the assessment. Piet et al. (2003a, 2003b) argued that this static approach to barrier layer material properties is unrealistic. Suter et al. (1993) reviewed and analyzed the likelihood of barrier failure at landfills and concluded that long-term avoidance of failure requires perpetual maintenance. Long-term failure mechanisms identified by Suter et al. (1993) included flaws in barrier construction, shrink-swell cycles, freeze-thaw cycles, erosion, subsidence, root intrusion, and animal intrusion.

At many Department of Energy facilities, caps and barriers will play a major role in cleanup strategies and need to be designed with maximum long-term integrity to minimize future risk. The longevity and

effectiveness of the barrier-type caps are influenced primarily by the ability of the clay layer to retain low-permeability characteristics. A key technical issue that needs to be addressed for the barrier-type cover system is the effective lifetime performance (hundreds of years) of the low-permeability clay layer in disposal facility caps. For example, in the disposal of LLW, the earthen cover over the wastes needs to be effective for 1000 years to the extent reasonably achievable and, in any case, for at least 200 years (40 CFR 40). In the case of near-surface disposal of LLW, the integrity and structural stability of covers for disposal must be demonstrated (10 CFR 61).

Objective

This research effort is designed to accomplish the following tasks:

- Conduct an extensive literature review documenting the state of knowledge concerning engineering waste barriers and their associated flaws.
- Develop and institute an experimental program designed to measure and document clay cracking phenomena in highly plastic clay soils.
- Develop a numerical model to predict the extent of clay cracking for varying soil properties calibrated from obtainable laboratory data.
- Recommend future studies to enable a transfer of the knowledge obtained in this research to clay barrier design solutions in the field.

Scope

The purpose of this report is to review and evaluate the literature on compacted clay barriers in landfill caps to identify the weaknesses inherent in their current application. The literature is reviewed with special attention to degradation mechanisms that affect the performance and effectiveness of compacted clay barriers with focus on their influence on the hydraulic conductivity of the clay. Results of this study guided the design of several laboratory experiments to further define the mechanisms of cracking phenomena and to clarify the certainty of cracking in clay barriers during long-term performance. Drainage layers, vegetative soil covers, and geomembranes are not within the scope of this review except for how they may affect the long-term performance of the compacted clay layer. Geosynthetic clay liners (GCLs) are of interest only as the response of the GCL to test conditions may be generally informative about clay barriers.

Alternative cap designs, i.e., designs that do not include a compacted clay layer, are also outside the scope of this review.

After completion of the experimental program, a thermodynamically based numerical model to simulate the cracking response observed in literature and experimentation will be developed and applied to the relevant problems. This report provides a summary of the degradation mechanisms present in clay barriers and the means to authoritatively state that, without careful protection, these clay barriers will fail well before the regulatory time frame allows.

2   Literature Review

Compacted clay barrier performance

The first engineered landfill caps were barrier-type caps, sometimes with only a vegetated surface soil layer and a compacted clay layer. The low saturated hydraulic conductivity of the clay layer was expected to encourage runoff and evapotranspiration and limit infiltration into the waste compartment. When compacted clay barriers began to be used in landfill covers and liners, it became standard practice to compact the clay layer on the wet side of optimum with a shearing type compaction, i.e., sheepsfoot roller. Mitchell et al. (1965) showed that the hydraulic conductivity of compacted clay depends on the molding water content and method of compaction. A shearing compaction effort coupled with compaction on the wet side of optimum develops a dispersed soil fabric with minimal hydraulic conductivity rather than the flocculated and more permeable soil fabric achieved with compaction on the dry side of optimum.

Is there really a problem with compacted clay layers in landfill caps? The early designers of engineered caps were concerned about construction quality control, slope stability, and settlement of the waste pile, but concern about the protectiveness of well-designed and properly constructed clay barriers was virtually unheard of in the regulatory and consulting engineer communities of the time. In the sections that follow, evidence of performance degradation of compacted clay layers in caps is reviewed. Laboratory studies have established, in principle, degradation by desiccation and frost action, and field studies have shown that the performance of compacted clay layers in landfill caps can be significantly degraded by these processes.

Desiccation

Albrecht and Benson (2001) investigated the effects of wetting and drying on eight natural clayey soils in laboratory studies. Each of the soils had been used for construction of landfill liners and covers, and came from natural deposits in the United States. Four of the eight soils formed cracks when compacted on the wet side of optimum, and two of the soils cracked regardless of the compaction water content. Volumetric shrinkage strains occurring after the first (initial) cycle of drying tended to be constant,

suggesting that the major changes in soil structure took place during the initial drying. Mineralogy affected the tendency to crack, with more severe cracking and volumetric change observed as clay activity increased. The resultant cracking caused increases in hydraulic conductivity by as much as 500 times. The largest increases in hydraulic conductivity occurred after the first drying cycle. Two of the soils that cracked were permeated for 350 days to evaluate the potential for healing. Although decreases in hydraulic conductivity were observed, neither soil returned to its initial as-compacted hydraulic conductivity, suggesting that permanent damage to the integrity of the soil mass had occurred.

Paruvakat (2002) discussed and commented on the Albrecht and Benson (2001) paper, indicating that he was hesitant to accept extension of the laboratory results to the field. The main points made by Paruvakat (2002) were as follows:

- In landfill covers, the clay barrier thickness is typically larger than the shrinkage crack depths, and flow is therefore controlled by the lower portion of the barrier with no cracks and lower hydraulic conductivity than the cracked portion.
- The laboratory tests did not simulate the overburden effects on cracks, in particular the potential for the cover soil to fill desiccation cracks.
- The lack of self-healing observed in the laboratory is in part an artifact. Piping (displacement of fines) in the small samples tested would not be expected in the field because the uncracked portion of the barrier would impede flow, prevent piping, and allow self-healing.

In their response to comments, Albrecht and Benson (2002) cited and discussed the field studies of Montgomery and Parsons (1989), Corser and Cranston (1991), Melchior (1997), Benson and Khire (1995), Albrecht (1996), Khire et al. (1997), and some unpublished case histories summarized below. The field studies and case histories show that desiccation cracking of compacted clay layers in caps can be a serious problem in all climates, humid and semi-arid. The cracks typically penetrate the entire compacted clay layer and do not self-heal.

Montgomery and Parsons (1989) found desiccation cracks in a cap 4 years after construction that penetrated a 1.2-m-thick compacted clay layer overlain by a vegetated soil cover. The study site was conducted in Milwaukee, WI. Lysimeters installed beneath test sections showed that

preferential flow through cracks allowed percolation completely through the cap shortly after precipitation events.

Corser and Cranston (1991) examined two test sections constructed in southern California several months after and 3 years after landfill construction. Both test sections had a 0.9-m compacted clay layer. In one test section, the clay layer was overlain by a geomembrane and a cover soil 0.6 m thick. The other test section was similar, but did not have the geomembrane. Several months after construction, the clay layer without the geomembrane cover was extensively cracked. The clay layer with the geomembrane was unaffected. Inspection 3 years later showed that the cracks in the clay layer without the geomembrane cover penetrated the entire thickness of the clay layer. No significant cracking of the clay layer overlain with the geomembrane was noted.

Benson and Khire (1995) reported extensive cracking of a clay barrier in southern Wisconsin 5 years after construction. The clay barrier was covered by 0.75 m of cover soil, but none of the cracks were filled with or contained cover soil.

Albrecht (1996) excavated test pits in a barrier-type cap in central Wisconsin. The clay layer was 0.6 m thick overlain by 0.15 m of vegetated soil. The clay layer was described as hard and dry and had a blocky structure created by numerous cracks. The hydraulic conductivity of the blocky material was 7.2×10^{-5} cm/sec (the as-constructed hydraulic conductivity was 10^{-8} cm/sec).

Melchior (1997) obtained water balance data for several cap designs in field tests at a landfill in Hamburg, Germany. The climatic conditions at the site were described as wetter than Seattle, WA. Composite caps with a geomembrane above the clay layer performed best. An extended capillary barrier also performed well. Within 5 years, the performance of compacted clay caps without geomembranes was severely degraded by desiccation cracking, with about 50% of the water reaching the compacted clay layer percolating through it.

Khire et al. (1997) reported hydrological data from a test section on a landfill in central Washington. The cap consisted of a 0.6-m-thick compacted clay layer overlain by a 0.15-m-thick vegetated surface cover. Within 2 years after construction, an increase in percolation through the

cap was observed, and pulses of percolation were observed after rainfall events. This was attributed to desiccation cracks in the clay layer, and the presence of desiccation cracks was confirmed by excavation and inspection. No filling of the cracks by cover material was noted.

Albrecht and Benson (2002) and Benson (2001) discussed data from a site in southwestern Georgia. The cap consisted of a compacted clay layer 0.46 m thick overlain by a vegetated protective cover 0.15 m thick. For the first 9 months after construction, percolation through the cap was very low due to unseasonable dry conditions. During this period, the clay layer apparently desiccated (Benson 2001). After the dry period, percolation through the cap increased by an order of magnitude. Later, it was observed that percolation followed precipitation events, indicating preferential flow, most likely through cracks, given the low percolation observed prior to the drying event (Benson 2001). An examination of the cap showed desiccation cracks.

Albrecht and Benson (2002) described excavation of a 9-year-old cap in the upper midwestern United States. The cap consisted of a 0.6-m-thick layer of lean, compacted clay overlain by a 0.15-m-thick sand drainage layer and a 0.46-m-thick vegetated layer. Numerous small cracks were observed in the clay layer. Laboratory testing determined that cracked samples taken from the clay barrier had a hydraulic conductivity of 2×10^{-5} cm/sec as opposed to 1×10^{-8} cm/sec in the uncracked samples, a value nearer the as-constructed conditions.

Desiccation of compacted clay barriers can apparently happen quicker than expected. Miller and Mishra (1989), Basnett and Bruner (1993), and Hewitt and Philip (1999) observed development of desiccation cracks in compacted clay liners during or shortly after construction. Hewitt and Philip (1999) described the mechanism of desiccation at a landfill in England as a temperature-driven process. The clay layer was overlain by a flexible membrane liner (FML). Heating of the FML during the day resulted in wrinkle formation and evaporation of water from the clay barrier. Upon cooling at night, water vapor condensed and collected in the wrinkles. On side slopes, this water drained away by gravity. Inspection 7 months after construction showed accumulation of water under the FML at the base of slopes and desiccation cracks on the slopes up to 11 mm wide and 220 mm deep. The clay layer was 1 m thick.

While, ideally, geomembranes should perform well at preventing desiccation of the confined clay layer, defects in construction can limit their usefulness over long-term applications. Giroud and Bonaparte (1989) found that, statistically, at least two defects per constructed acre were typical of geomembrane construction, and these defects ultimately would be the points of eventual long-term failure of the liner. This was validated by a study performed on the 14-year performance of a 1.5-mm-thick, high density polyethylene (HDPE) geomembrane composite layer system (Lake and Rowe 2005). Failure within the geomembrane occurred within 6 years (the extent of the Melchior study above) as increased percolation was evident in the liner system originating at the defect points in construction. Later studies by Benson et al. (2007) validated the eventual failure of geomembranes over long-term exposure to overlying soil. Plant roots were effective at penetrating completely through the plastic liner, even at locations where no construction defect was evident. Once root-bound, the moisture withdrawal from plants will induce desiccation that can ultimately fail the compacted clay liner.

In summary, desiccation cracking of clay layers in landfill caps has been reported by several investigators. These studies have shown that desiccation cracks can form quickly, as most of these studies involved cover systems from 3 to 8 years old. The cracks do not self-heal, can penetrate the entire thickness of the clay layer, and are not filled by soil from overlying layers. Composite caps composed of a compacted clay layer overlain by a geomembrane performed well in short-term studies, but did not perform well in long-term evaluations. Further, there are reports of temperature-driven desiccation cracking of clay liners covered by FMLs.

Benson (2000, 2001) reviewed the technologies, strategies, and performance of liners and covers for land disposal of wastes and discussed the performance of barrier-type landfill covers. Compacted clay landfill liners usually perform as designed (Benson et al. 1999; Benson 2000, 2001), but clay barriers in caps without a protective geomembrane perform poorly due to the effects of desiccation. Geomembranes such as HDPE are good short-term barriers to water vapor transport but are difficult to effectively place during construction, as minor imperfections in its placement typically result in vapor transport avenues through the membrane, reducing its effectiveness (Giroud and Bonaparte 1989). As will be discussed in later sections, desiccation of clay barriers in caps may be due to water vapor transport in the unsaturated soils above the clay barrier.

Frost action

Several studies have shown that frost can degrade the effectiveness of compacted clay as a hydraulic barrier (Wong and Haug 1991; Kim and Daniel 1992; Benson and Othman 1993; Benson et al. 1995; Khire et al. 1997; McBrayer et al. 1997). Desiccation is induced by the formation of ice lenses (Benson and Othman 1993). Hydraulic gradients drive water into the lenses, which results in desiccation of the clay. However, with adequate protection, this type of damage can be minimized (Benson 2000, 2001).

Smith and Rager (2002) describe a design procedure for determining the minimum thickness of a protective soil cover over a barrier layer in a landfill cap. The procedure uses site-specific daily maximum-minimum temperature data compiled for a minimum of 30 years to compute frost depths. The computations are based on the modified Berggren equation (Aldrich and Paynter 1953) and are implemented on a personal computer version of the solution provided by Aitken and Berg (1968). Smith and Rager (2002) provide a design example for their procedure using a uranium mill tailings landfill constructed in Monticello, UT. In this case, 40 CFR Part 192 requires a design life of 1000 years where reasonably achievable and in no case less than 200 years. The predicted extreme frost depth for a 200-year recurrence interval was 1.14 m. Smith and Rager (2002) cautioned that the proposed method should be used only as an estimate. Further comparisons of predicted versus measured frost depths are required to validate the method.

Geosynthetic clay liners

GCLs are commercially manufactured and consist of a thin layer of bentonite sandwiched between two geotextiles or a geomembrane with bentonite attached to it. GCLs are typically about 1 cm thick. GCLs are said to be more cost-effective and resilient to settlement than compacted clay liners.

Boardman and Daniel (1996) investigated the performance of GCLs under one cycle of wetting and drying in large tanks (2.4 m × 1.4 m × 0.9 m). Drying caused desiccation of the bentonite, but the bentonite rehydrated and resealed the GCL when again permeated with water. Hydraulic conductivities of the GCLs were about the same at the end of test as the undesiccated GCL. In his discussion of the paper by Boardman and Daniel

(1996), Day (1997) presented some of his work on a sand-montmorillonite mixture and a natural clay containing montmorillonite. The cracks in both materials caused by freeze-thaw cycling and wetting-drying cycles sealed during testing for hydraulic conductivity, indicating that montmorillonites are not susceptible to permanent changes in hydraulic conductivity.

Kraus et al. (1997) investigated the effects of freeze-thaw cycling on GCLs in laboratory and field tests. Three GCLs and one sand-bentonite mixture were exposed to one or two winters of freeze-thaw cycling. An increase in hydraulic conductivity was observed in one field test with a GCL. There was no increase in hydraulic conductivity of the GCLs in the laboratory tests. The hydraulic conductivity of the sand-bentonite mixture was unaffected by freeze-thaw cycling in both laboratory and field tests.

James et al. (1997) described field experiences and some limited laboratory tests on a GCL application with unexpectedly poor performance. A GCL was used to provide seals to the roofs of Victorian era water supply reservoirs. The GCL was overlain by a layer of noncalcareous gravel to provide drainage and a layer of calcareous cover soil. Leakage through the cap was observed, and an inspection showed finely cracked regions in the bentonite interspersed with hydrated and swollen regions of bentonite. Testing showed that the GCL had a much reduced exchangeable sodium and increased exchangeable calcium content compared with the dry unused GCL. It is widely recognized that exchange of calcium for sodium in sodium bentonite will result in flocculation and shrinkage. The source of the calcium was thought to be the calcite in the GCL bentonite. Laboratory simulations of the field conditions over a short period of time produced less extensive ion exchange and shrinkage.

Melchior (1997) described some field results on GCLs at the Hamburg, Germany, site previously discussed in the section on compacted clay desiccation. Two GCLs were installed in test plots, with a cover above them that consisted of a 0.15-m gravel drainage layer and 0.3 m of topsoil. The GCLs desiccated the first dry summer of testing and then leaked significantly the following winter. Wetting of the GCLs did not significantly reduce percolation.

Benson et al. (2007) have shown that GCLs will increase in permeability as both a function of desiccation cracking and cation exchange of clay minerals within the GCL. The permeability of the observed field GCLs in the

study all equilibrated to a value of 5×10^{-5} cm/sec, far greater than the 1×10^{-8} cm/sec permeability values possible in the intact GCL. It has been shown that GCLs do not self-heal in the field, suggesting that once this increase in permeability is noted, it remains permanent. Last, Benson et al. (2007) suggested that GCLs should be used in final covers with caution unless cation exchange and dehydration can be prevented or another barrier layer is present, such as a geomembrane. The study by Lake and Rowe (2005) showed that cation movement is prevalent in the defect regions of a composite liner system, making even a geomembrane solution inadequate for long-term barrier protection.

The literature on GCLs reviewed in this report suggests caution on the part of designers and regulators considering montmorillonites such as bentonite for use as a self-sealing hydraulic barrier. Some of the literature shows self-sealing does take place, but the laboratory and field data to this effect are of short duration and limited scope. Also, there are reports from the field concerning bentonite desiccation and shrinkage that has not reversed upon rewetting. Cracking due to ion exchange has also been indicated as a cause of problems in the field with bentonite-based GCLs.

Performance modeling

The rapid and extensive desiccation cracking of compacted clay layers in landfill caps that has been reported points to the need for improved understanding and improved models of clay barrier performance. The desiccation that occurs suggests inadequate treatment of vertical water transport and the potential for desiccation, cracking, and material property changes induced by cracking. In this section, modeling approaches to clay barriers are reviewed with the intent of discerning what is missing. Emphasis is placed on why desiccation is underpredicted, if predicted at all. In no instance do models predict cracking or the increase in percolation due to preferential flow in crack openings resulting from this mechanical behavior.

Clay barrier models

Khire et al. (1997) compared the predictive capabilities of the Hydrologic Evaluation of Landfill Performance (HELP) model (Schroeder et al. 1994) and the Unsaturated Water and Heat Flow (UNSAT-H) model (Fayer and Jones 1990) for the water balance in landfill caps. Details on the models are available in the user manuals cited, and Khire et al. (1997) provide an

overview of the two model formulation schemes and computational approaches. Field data from the Live Oak Landfill, Atlanta, GA, and the Greater Wenatchee Regional Landfill, East Wenatchee, WA, were used to make the comparison. Hydrologic data were collected for 2.5 years at each site.

At the Georgia site, HELP underestimated overland flow while UNSAT-H provided a more accurate prediction. HELP provided an accurate prediction of evaporation, and UNSAT-H underestimated evaporation. HELP significantly underpredicted soil water storage, primarily because it overpredicted percolation. UNSAT-H captured the large seasonal variation in soil water storage, but slightly underestimated soil water storage during the winter. HELP significantly overpredicted percolation, and UNSAT-H slightly underpredicted percolation, which is problematic from a regulatory perspective. HELP overpredicted percolation because it underpredicted overland flow, and it uses a unit hydraulic gradient to route water in unsaturated soil. A downward unit gradient is assumed by HELP until the wilting point is reached in water content. Field data showed that the hydraulic gradient was upward near the interface between the cover soil and the barrier layer for much of the time.

At the site in Washington, HELP significantly overpredicted overland flow, and UNSAT-H underpredicted overland flow. Both models had trouble simulating winter conditions (snow cover, snowmelt, and thermal ground conditions). Both models tended to overpredict evapotranspiration. HELP underpredicted soil water storage, and UNSAT-H predictions of soil water storage were in good agreement with the field data. Both models overpredicted percolation until the last winter of observation. Apparently, the clay barrier had cracked, and with the onset of winter precipitation, preferential flow occurred in the cracks. This gave a large percolation pulse in the field data set that was not predicted by either model. Neither model allows for preferential flow through cracks.

He et al. (1998) applied the HELP model to infiltration rates at three closed landfills. The results indicated that the recommended ranges of parameters suggested in the HELP documentation were adequate for simulating landfill performance.

Choo and Yanful (2000) investigated unsaturated flow through multi-layered soil covers using computer models and laboratory physical models.

A commercially available finite-element model, SEEP-W, was used to simulate unsaturated flow in laboratory packed-soil columns. The ability of the model to predict pressure head and water content was evaluated by comparing the model solution to those obtained from analytical solutions to simplified problems for steady flow in a multilayered soil and transient flow in a homogenous soil. There was good agreement between the model and the experimental results for the first 3 days. For times longer than 3 days, agreement was not as good, due to the formation of discontinuous water pockets in the experimental column and the lack of a vapor transport algorithm in the model. The data showed that vapor phase transport of water controlled total head profiles after 3 days in the column that was not sealed at the top.

Aubertin and Bussière (2001) discussed the paper by Choo and Yanful (2000) and pointed out that, in addition to the difficulties encountered by Choo and Yanful in applying commonly used calculation methods to analyze one-dimensional unsaturated flow in columns, more difficulties arise when considering sloped surfaces. Aubertin and Bussière (2001) argued with cited literature that, on slopes (and practically all caps have sloped surfaces), flow involves both vertical and lateral components within and between different layers. The difference in elevation between the bottom and top portions of an inclined layered system induces a suction gradient that creates variation in water content depending on the location along the slope. Aubertin and Bussière also comment that another important finding from their work is that some portion of capillary barriers may actually desaturate, even though one-dimensional calculations may predict otherwise.

Döll (1997) described a numerical model (SUMMIT; Döll 1996) that couples heat, water, and water vapor transport in unsaturated media. The problem that Döll focused on was one involving landfills with heat generation and the impacts of temperature variations on the integrity of soil barriers beneath landfills. Data from the literature on nonisothermal laboratory and field experiments were simulated. In the laboratory experiments, a clay liner desiccated and cracked due to nonisothermal vapor diffusion into an underlying sand drainage layer. Fitting of SUMMIT to this experiment required simulating vapor diffusion in the sand drainage layer as if vapor diffusion were occurring in air. For the field experiment, fitted model parameters again suggested that water vapor transport from the liner to the underlying drainage layer was much higher than expected.

Döll concluded that nonisothermal vapor diffusion of water can be up to five times higher than is explainable with reasonable model parameters and that vapor phase diffusion can be expected to cause desiccation and cracking of soil liners.

Crack models

Models for soil desiccation typically are based on the properties of the intact soil, and only indirectly consider cracking—such as the work previously described by Döll (1997).

Döll (1996) describes the use of the SUMMIT model for evaluating desiccation risk. Döll found that the model gave reasonable qualitative agreement with field data. Quantitative agreements were difficult because of uncertainties in soil properties and the unknown effects of consolidation and desiccation. The SUMMIT model does not explicitly consider crack propagation or the creation of secondary porosity.

In a study by Abu-Hejleh and Znidarčić (1995) of soft saturated clay under self-weight consolidation, a finite element model was used to capture the general process of desiccation. The conditions described by the model are better suited for dredged fill containment versus compacted landfill barriers, although the processes corresponding to the latter stages of drying are equally applicable to both. The finite element model was based on an extension to the one-dimensional finite strain consolidation theory of Gibson et al. (1967). The analysis was broken into two stages. The first stage was idealized as one-dimensional consolidation. During the consolidation phase the vertical water migration exceeds or balances losses due to evaporation, and no shrinkage occurs. As consolidation slows, drying creates a tensile stress and shrinkage. Cracking occurs when the shrinking soil reaches a critical void ratio, at which point the model becomes two-dimensional. The developing cracks are modeled as equally spaced, and extend to equal depth. Properties do not vary in the horizontal direction. Thus, upon cracking, the model effectively corresponds to a single "pillar" of soil bounded by cracks. The cracking void ratio is determined from a relationship for tensile strength (σ_t), which in turn is expressed as $\sigma_t = FS_u$, where F is an experimentally determined factor and S_u is the undrained shear strength. The advantage of this approach is that S_u can be found from conventional experiments and F falls within relatively well-known bounds. According to Abu-Hejleh and Znidarčić (1995), the factor F has a lower bound of zero and is assumed to have an upper

bound of 0.5, based on values reported by Lau (1990). The undrained shear strength, and therefore the tensile strength, can be correlated to the void ratio. *(See Peters and Leavell (1986) and Leavell and Peters (1988) and for a detailed discussion of the relationship between compressive and tensile strengths for compacted materials.)*

An important aspect of the research reported herein is that, as cracking evolved, the boundaries of the soil domain are modified to expose the soil at depth to the atmosphere. The depth of the cracking is determined by the void ratio of the soil, which is indirectly controlled by the stress. Crack propagation is not considered in the Abu-Hejleh and Znidarčić (1995) model.

The evolution of soil cracking has been described extensively by Chertkov and his coworkers (Chertkov and Ravina 1998, 1999; Chertkov 2000, 2002), who recognized that the hydraulic properties of clayey materials depend on the geometries of crack networks. One important observation of Chertkov (2002) is that cracks form even in saturated clay under "desiccation in constrained conditions." Chertkov applies the concepts of linear fracture mechanics to derive the formula for the characteristic length, l_*, of a crack caused by a change in gravimetric water content from its initial value θ to a value of θ_o,

$$l_* = \frac{1}{\pi}\left(\frac{K_{Ic}}{\sigma_*}\right)^2 \tag{1a}$$

where K_{Ic} is the critical stress-intensity factor (fracture toughness) of the soil and σ_* is the maximum stress at the surface computed from the elastic stiffness parameters E and ν, the shrinkage coefficient, α, and the change in water content

$$\sigma_* = \frac{E\alpha}{3(1-\nu)}(\theta_o - \theta) \tag{1b}$$

This formula is based on Griffith's formula for a crack subjected to a uniform stress of σ_* and can be interpreted as follows: A crack with initial length $l < l_*$ will not propagate, but for $l > l_*$ the crack grows into a moving equilibrium state in which length increases with a constant velocity. The average crack length was determined by Chertkov to be $l_{av} = 1.22 l_*$.

The key conclusion derived from this model is that, in a saturated soil, cracks fall within two categories: shallow cracks that are incapable of further propagation and deep cracks that have the potential for propagation. Chertkov posits that two scales of crack length actually exist, consisting of larger seasonal cracks and smaller "interaggregate" microcracks. A detail that is not considered is the change in boundary condition by the creation of the crack itself. White (2001) commented that random cracking does not occur in soils and argued that cracking geometries can be deduced from soil structure characteristics. Chertkov (2001) responded that random cracking has been observed in intact clay and mine tailings and that, from the viewpoint of an observer, the intersection of cracks with an arbitrary line is random.

Causes of crack initiation

There is evidence that the unexpectedly rapid and extensive desiccation of clay layers in barrier-type cover systems for landfills is caused by vertical water vapor transport. An upward hydraulic gradient was measured in unsaturated soil of a cap at a site in Georgia (Khire et al. 1997). Choo and Yanful (2000) noted that vertical water vapor transport controlled total head profiles in laboratory columns simulating a cover system after only 3 days of testing. However, Döll (1997) simulated both water vapor and heat transport and was not able to fully capture nonisothermal water vapor flux in unsaturated soils.

In unsaturated soils, water evaporates from film water and the capillary fringe. The water above the capillary fringe is held by surface adsorption and surface tension (matric potential). Although barometric pressure changes affect the water held by matric suction and could act like a pump, simulation of the influence of barometric pressures changes on the water content of soils is not generally viewed as necessary. Heat flow in soils has been widely studied (Lettau 1954, 1971; de Vries and Afgan 1975; Kimball et al. 1976; Sepaskhah and Boersma 1979; Hillel 1982; Horton et al. 1983). Similarly, evaporation from soil has been widely studied (Philip and de Vries 1957; de Vries 1958; Richie 1972; Milly 1984; Nobre and Thomson 1993; Schelde et al. 1998; Bachmann et al. 2001), but theoretical questions regarding model parameter estimation for evaporation from the soil surface have not been completely resolved (Qui et al. 1999). Where coupled water vapor transport and heat transport are simulated, Fick's law for water vapor and Fourier's law for heat (and modifications thereof) are used to simulate water vapor transport and heat transport, respectively.

Models such as HELP and UNSAT_H have been developed to capture the moisture behavior at the clay-barrier interface.

Climatic changes

The models HELP and UNSAT_H use daily average climatic data and are not sufficiently refined to capture diurnal drying effects in the soil profile. Under actual field conditions, a cover is very dynamic. Episodes involving precipitation, runoff, and infiltration of different magnitude and duration preclude steady state. The need for transient modeling of these phenomena is well known. However, diurnal variations in air and soil temperatures and water vapor pressures are not usually simulated, and variations in these quantities are equally pronounced in the soil profile on diurnal, seasonal, and annual time scales. Thibodeaux (1996) gives examples of how the use of average daily temperatures underestimates both evaporation of water and volatilization of chemicals from soil surfaces. The overall effect is that use of average daily climatic data underpredicts evaporation and the potential for desiccation of clay barriers in caps. For a simulation of 200+ years, significant computational power is required to simulate diurnal effects on water balance.

Water vapor transport

Water vapor transport in the soil gas must be included to simulate the desiccation effects that have been observed, and HELP and UNSAT-H simply were not formulated or intended to simulate the complex physics of water vapor transport in soils.

Philip and de Vries (1957) and de Vries (1958) generalized Richard's equation to account for storage and diffusion of water vapor in the soil gas under nonisothermal conditions. Milly (1984) introduced an alternative mathematical expression based on matric head and temperature derivatives. Bulk flow of soil gas is not simulated. The model includes terms for matric pressure dependent vapor diffusion and thermally induced vapor diffusion. An enhancement factor is included in the definition of the thermally induced vapor diffusion coefficient. The enhancement factor is a function of porosity and water content. The thermally induced vapor diffusion coefficient was defined as a function of the enhancement factor, molecular diffusion coefficient for water vapor in air, temperature, the ratio of the average temperature gradient in the soil gas to the overall average temperature gradient of the soil, and the partial derivative of

absolute humidity with respect to temperature. This definition of a thermally induced vapor diffusion coefficient, shown in Equation 2a (Milly 1984), has no adjustable parameters.

$$D_{Tv} = \rho_l^{-1} \, D_a \, f \, \zeta \left. \frac{\partial \rho_v}{\partial T} \right|_{\psi} \qquad (2a)$$

where:

D_{Tv} = thermally induced diffusion coefficient
D_a = molecular diffusivity of water vapor in air (temperature dependent)
ρ_v = absolute humidity of the soil gas
T = temperature
ψ = matric potential.

The parameter f is the enhancement factor defined as follows:

$$f = n \qquad \text{for} \quad \theta \le \theta_k \qquad (2b)$$

$$f = \theta_a + \frac{\theta_a}{n - \theta_k} \theta \qquad \text{for} \quad \theta_k < \theta \qquad (2c)$$

where:

n = porosity
θ = volumetric water content of soil
θ_a = volumetric air content of soil
θ_k = volumetric water content at which liquid flow is negligible (i.e., the matric pressure dependent vapor diffusion coefficient is an order of magnitude greater than the unsaturated hydraulic conductivity).

It follows from the definition of the f parameter that this enhancement factor is a tortuosity type correction factor. The parameter ζ is the thermal gradient ratio,

$$\zeta = \frac{(\nabla T)_a}{\nabla T} \qquad (2d)$$

In Equation 2d, the numerator is the overall average temperature gradient in the soil gas, and the denominator is the overall average temperature gradient in the soil (i.e., macroscopic).

Bachmann et al. (2001) applied the Philip and de Vries (1957) and Milly (1984) theory to laboratory soil columns under nonisothermal conditions to investigate the effect of water repellency on evaporation. Water repellency refers to soil hydrophobicity, i.e., dislike for water. Water repellency is associated with organic coatings (fungal hyphae, humic acids, or partly decomposed plant material) on soil particles. Soils may display some degree of water repellency after drying below some critical water content. To obtain good agreement between predicted and observed evaporation fluxes and soil water content, Bachmann et al. (2001) found it necessary to multiply D_{Tv} by a factor of 3.5.

Döll (1997) applied the Philip and de Vries (1957) and Milly (1984) approach to three nonisothermal laboratory experiments and one non-isothermal field experiment. Multipliers of 3.3 to 4.5 for the thermally induced vapor diffusion coefficient were needed to simulate the laboratory experiments, and a multiplier of 13 was needed to simulate the field experiment. Multipliers of 3 to 5 imply vapor diffusion that is approximately as large as vapor diffusion in free air without soil (Döll 1997). Uncertainties in the field data cloud the significance of the multiplier required for the field data.

Schelde et al. (1998) modeled diurnal variations in heat and water flux in a 25-m² bare soil plot. Their model formulation for water vapor flux is not as complicated as that of Philip and de Vries (1957) and Milly (1984), as they do not conduct separate calculation of matric pressure dependent vapor diffusion and thermally induced vapor diffusion. The treatment is Fickian with correction for tortuosity and volumetric air content of the soil. Schelde et al. (1998) found that a multiplier of two provided the best fit, especially during drying. Modeled water vapor flow was significant compared with liquid flow and improved the agreement between observed and measured diurnal water tension. Model predictions were sensitive to the soil surface energy balance, gradients in water tension near the surface, and enhancement of water vapor flow. Schelde et al. (1998) noted a trend for overestimation of soil water content in the first 5 cm of soil toward the end of the experiment (10 days). The discrepancy could not be explained,

but the preclusion of hysteresis from the modeling was suggested as a possible explanation.

Modification of diffusion coefficients

Application of Fick's law to water vapor transport is overly simplistic except under strictly isothermal and isobarometric conditions requiring an adjustment of the diffusion coefficients in heat and water vapor transport models (Bachmann et al. 2001; Döll 1997; Schelde et al. 1998).

During the heat of the day, thermal gradients in the soil induce small eddies at the soil water-soil gas interface. This phenomenon has been studied in other environmental media (Thibodeaux 1996) and is modeled as eddy diffusion. At the microscopic scale, eddies form as evaporation transfers heat from liquid water to the soil gas. As the soil gas is heated, it expands, and the expansion is propagated away from the interface by eddy diffusion. Eddies impart turbulence to the soil gas, causing water-laden soil gas to mix with soil gas at lower water vapor pressure. This mixing effect enhances vapor flux more than is predicted by diffusive transport models.

Analysis of heat conduction in limnological and oceanographic studies has led to the application of an eddy conductivity or turbulent coefficient of thermal conductivity. Modification of Fourier's law of heat conduction yields (Thibodeaux 1996)

$$q = -\left(k^l + k^t\right)\frac{dT}{dy} \tag{3}$$

where:

q = heat flux
k^l = thermal conductivity
k^t = turbulent coefficient of thermal conductivity or eddy conductivity
y = distance.

Thermal conductivity, k^l, represents molecular movements, and eddy conductivity, k^t, represents random bulk movements. Figure 3 is a definition sketch for application of Equation 3 in the context of water vapor transport in the unsaturated soils above a clay barrier in a landfill cap.
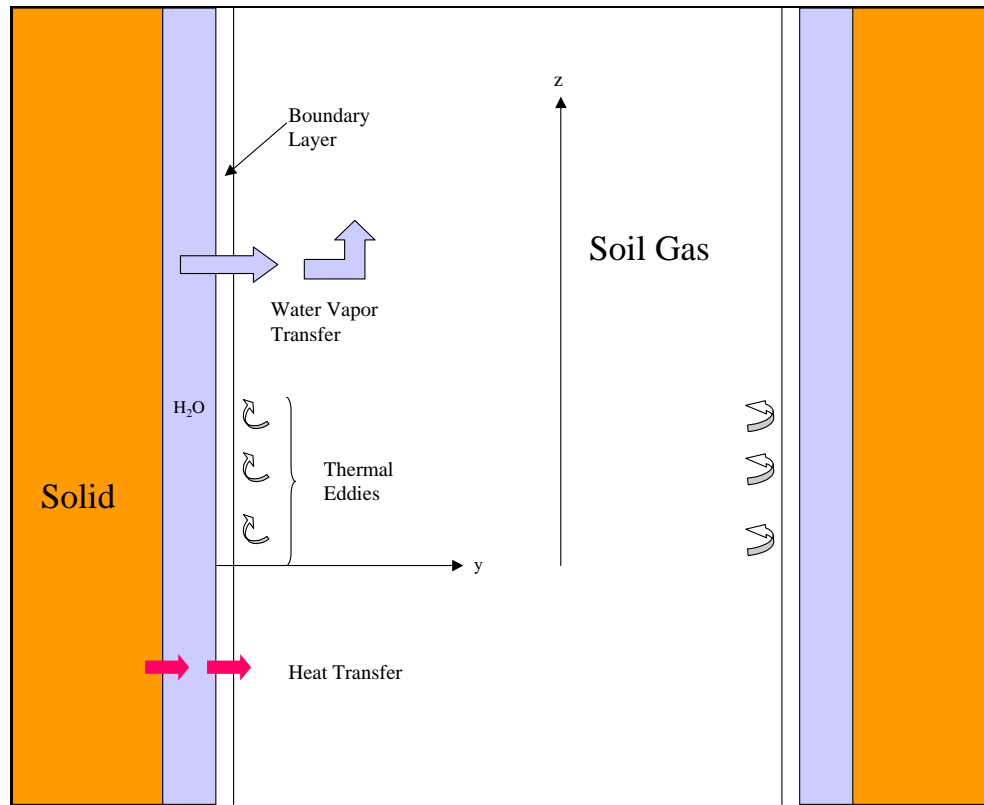
Figure 3. Heat and mass transfer in a soil tube.

Eddy conductivity is not applicable for the soil solids (motionless) and the water film (stagnant). Change in soil moisture during desiccation is assumed to be due to evaporation (shrinkage of the water film). Thus, the water film is treated as stagnant. The bulk of heat transfer during the day is downward and takes place in the soil solids and water films. Heat transfer in the soil solids-water continuum is modeled using Fourier's law, using a thermal conductivity coefficient that represents the combined media. Soil temperatures can be successfully modeled in this fashion. Few if any models simulate heat transfer in the soil gas because it can be neglected when simulating soil temperature profiles (Schelde et al. 1998).

An eddy thermal diffusivity can be defined as

$$D^t = \frac{k^t}{\rho \hat{C}}$$

(4)

where:

D^t = eddy thermal diffusivity
ρ = density of the fluid
$\hat{C}$ = heat capacity of the fluid.

Koh and Fan (1970) reviewed the magnitude of the eddy thermal diffusivity in water and found maximum values at the surface of lakes (~10 cm²/sec) and minimum values in the thermocline of lakes (~0.1 cm²/sec). Turbulence on a lake surface is primarily wind induced; however, turbulence in the thermocline is partially and sometimes primarily induced by the thermal gradient across the thermocline. Since analysis of heat conduction in lakes indicates thermally driven turbulence in the thermocline and air is less viscous than water, it is reasonable to hypothesize eddy diffusion at the soil gas-water interface in unsaturated soils.

By analogy to Equation 3, application of Fick's law to water vapor transport in unsaturated soils can be modified as shown in Equation 5.

$$J = -\left(D^l + D^t\right)\frac{dC}{dz} \tag{5}$$

where:

J = mass flux of water vapor
D^l = molecular mass diffusion coefficient
D^t = turbulent mass diffusion coefficient
C = water vapor concentration
z = distance, vertical direction.

The turbulent mass diffusion coefficient in Equation 5 represents bulk movement of soil gas by thermally induced eddies. For $D^t > 0$, mass transfer is enhanced over that predicted by molecular diffusion. Equation 5 and the above discussion provide a physical basis for the discrepancy between predicted and observed water vapor transport reported by Bachmann et al. (2001); Döll (1997); and Schelde et al. (1998).

Turbulent mass diffusion coefficients and eddy thermal diffusivities are not fluid properties alone, but depend on position and direction as well as

soil gas pressure and temperature gradients. They are highly variable near interfaces where they are most important, and thermal gradients in this region are usually unknown. For these reasons, Newton's law of cooling, which is basically a definition of a heat transfer coefficient, is often used to model heat and mass transfer across interfaces (Thibodeaux 1996). Heat and mass transfer coefficients are semi-empirical parameters that lump all the unknowns of a complicated process(es) into a single adjustable parameter that has physical meaning. Newton's law of cooling for heat transfer is stated below.

$$q_o = h\left(T_o - T_b\right) \tag{6}$$

where:

q_o = heat transfer across the soil gas-water interface
h = the local heat transfer coefficient
T_o = temperature at the soil gas-water interface
T_b = temperature in the mixed region away from the boundary layer.

An equivalent expression could be written for mass transfer of water, but such treatment would amount to one empirical coefficient for another. A model equation for water vapor transport in the z-direction (vertical) that accounts for thermally induced eddy effects on the soil gas transport properties and that is not strictly empirical remains to be developed.

Centrifuge analysis

Abu-Hejleh and Znidarčić (1995) recommended centrifuge modeling as a technique for verifying their desiccation cracking theory, especially in terms of verifying the crack-formation mechanism. Abu-Hejleh and Znidarčić (1995) further state "Short of an actual well-controlled field case, it is probably the only technique available to study crack development, since the field stress conditions that control crack propagation are properly simulated in centrifuge models." Abu-Hejleh and Znidarčić (1995) developed their theory for hydraulically placed fine grain deposits, such as mine tailings and dredged material, and the cracking associated with dewatering such materials. Implementation of Abu-Hejleh and Znidarčić (1995) recommendation in the context of clay barriers in landfill caps is not as straightforward as it might be for hydraulically placed deposits

since the clay barriers do not desiccate by drainage and evaporation, but primarily by evaporation. Cracking in both instances, however, is initiated in response to water loss, be it by drainage or by evaporation.

In the short time frames of the studies on desiccation cracking of clay barriers in landfill caps, movement of overlaying soil into cracks in clay barriers has not been reported (Benson and Khire 1995; Khire et al. 1997; Albrecht and Benson 2002). Paruvakat (2002), in commenting on the Albrecht and Benson (2001) paper, reasoned that cover soil could fill desiccation cracks. Centrifuge modeling could extend the time frame of analysis for crack fill-in to hundreds of years. Such modeling would be important because, if cover soil eventually migrates into cracks in the clay barrier, this material may hold the cracks open and prevent eventual self-healing in years of higher than normal precipitation. The potential for crack fill-in is therefore important for long-term performance assessment.

On the surface, the centrifuge would seem an ideal testing mechanism to capture the long-term effects of clay cracking, because of its ability to accelerate time. However, centrifuge modeling of water vapor diffusion is not possible according to the Philip and de Vries (1957) and Milly (1984) theory of heat and water vapor transport in unsaturated soils, since there is no gravitational term in Fickian models. Therefore, the centrifuge lacks the critical element necessary to incite further cracking due to drying effects of the soil. As will be shown in Chapter 4, the overburden stresses play an insignificant role in the prevention of crack behavior. As a result, the centrifuge does not offer much in the way of advancing the state of knowledge of cracking mechanisms. Therefore, it is recommended that a more comprehensive, static test be conducted to allow time for clay evaporation to study the phenomenon of crack propagation.

Summary

Laboratory and field studies have shown the following key phenomena in compacted clay liner systems:

- Cracking of clay liners occurs quickly, typically penetrating the entire layer thickness less than 10 years after construction.
- The cracks do not self-heal either by intrusion of overburden or by rewetting during cyclic seasonal changes.
- Geomembranes and GCLs are inadequate long-term barriers to protect against clay cracking.

- Diffusion (water vapor transport) explains the moisture loss at the clay surface but not the crack propagation phenomenon.
- Studied diffusion models do not predict the secondary porosity and, therefore, the high water intrusion detected in cracked clay liners.
- Centrifuge testing does not enable scaling of diffusion characteristics, but can provide both the influence of overburden and scaling of permeability.

The most direct way to assess the mechanisms of crack propagation is through a static test conducted over an extended time period to allow for diffusion. The resulting behavior could then provide the validation criteria for a numerical model capable of simulating the secondary porosity resulting from development of a cracking network within the clay mass.

3   Experimental Program

Introduction

The literature review describes the inevitably of crack generation in a clay liner when the clay surface is subjected to changing humidity conditions. A series of suggestions were proposed to better define the water vapor pressure and resultant humidity condition near the clay surface, which can then be translated into a moisture condition within the clay soil. A model is required that can predict the crack generation occurring from the clay surface downward as a function of the tensile stresses in the clay mass. The tensile stresses in the clay are a function of the moisture content, and this constitutive interaction will be addressed in the numerical modeling chapter. An experimental program was developed to address the behavior of the clay liner once the tensile stresses are sufficient to induce crack formation. From these experiments, a proper numerical model can be developed to determine the degradation of clay liner systems after crack initiation.

To understand the nature of cracking in a clay soil, a series of three experiments was conducted to determine the processes of horizontal and vertical cracking in a highly plastic soil. These experiments were designed sequentially, each having a unique purpose, and each experiment was built upon the lessons learned from the previous experiment.

- Experiment 1: The initial experiment was designed to test concepts for concentrating (or training) clay to form a crack in a predetermined location and to determine the effectiveness of measuring a lateral soil pressure sensor during cracking.
- Experiment 2: A simple experiment was performed to test the effectiveness of using time-lapse photography to observe and measure the cracking phenomenon. This test was undertaken using a highly plastic soil, which was compacted and allowed to dry in a cylindrical container without side restraints.
- Experiment 3: This experiment incorporates the best techniques learned for crack training, instrumentation of pressure sensors, and use of time-lapse photography into a single, larger scale test bed to observe the long-term crack generation of compacted clay during drying. Results obtained from Experiment 3 will be used to validate the

behavior of the numerical cracking model described in the following chapter.

Experiment 1

This first experiment was designed to test concepts for constructing a test bed of sufficient size for monitoring crack behavior, for concentrating (or training) clay to form a crack in a predetermined location, and for determining the effectiveness of a lateral soil pressure sensor during cracking.

Experimental setup

To best represent the cracking response of a soil in a predetermined area, in this case the middle of a square box, the surface area of a test bed must be large enough such that the sidewall influence does not inhibit crack development in the center of the soil bed. To achieve this, the chosen experimental setup consists of a reinforced, Plexiglas box that is 18 in. (45.7 cm) on a side and 4.5 in. (11.4 cm) in depth (Figure 4)—determined from experimentation with subsequently smaller boxes to encompass the desired cracking effects. To encourage the soil to crack in a preferential direction, a series of plastic soil bolts were fabricated and screwed into two opposing sides of the soil container at random positions. This technique was developed to prevent the soil from separating from the container walls, with bolted sides to encourage a primary crack to form in the middle of the soil box, parallel to the bolted sides. The other two sides of the box do not have soil bolts to enhance the potential for generating a long crack. The supposition is that, during drying, the soil will slide along the sides of the box without bolts, generating a single primary crack along which sensors can be placed to capture lateral stress effects.

To further encourage preferential drying and formation of a defined primary crack, a drying apparatus was designed that would allow air to move across the clay surface concentrating drying in narrow band of soil, expediting crack formation. Figures 5 through 7 show the conceptual design and operation of the airflow device and its proximity to the proposed primary crack. The drying box was designed and constructed (Figure 8) having a length that equals the length of the soil container (45.7 cm) and a width of 10 cm. An air hose connecter is located on top of the box, and numerous drilled holes are on both sides of the box. Air can be pushed into the drying box either through the connector or by applying a vacuum.

Soil bolts were fabricated into two opposite sides of the soil container box as shown in Figure 9.
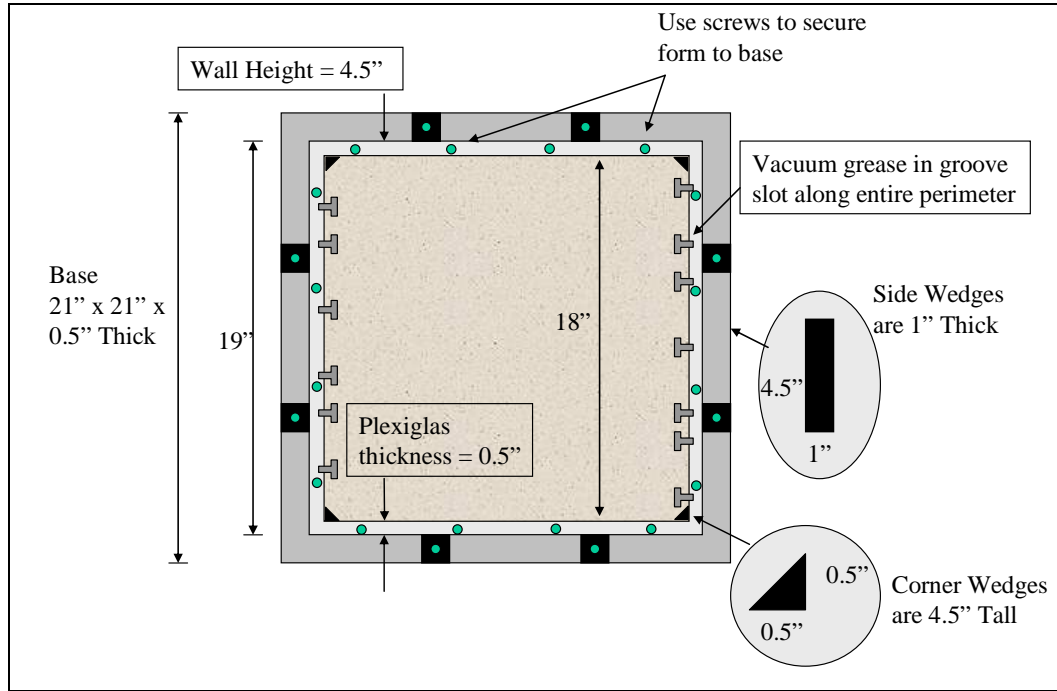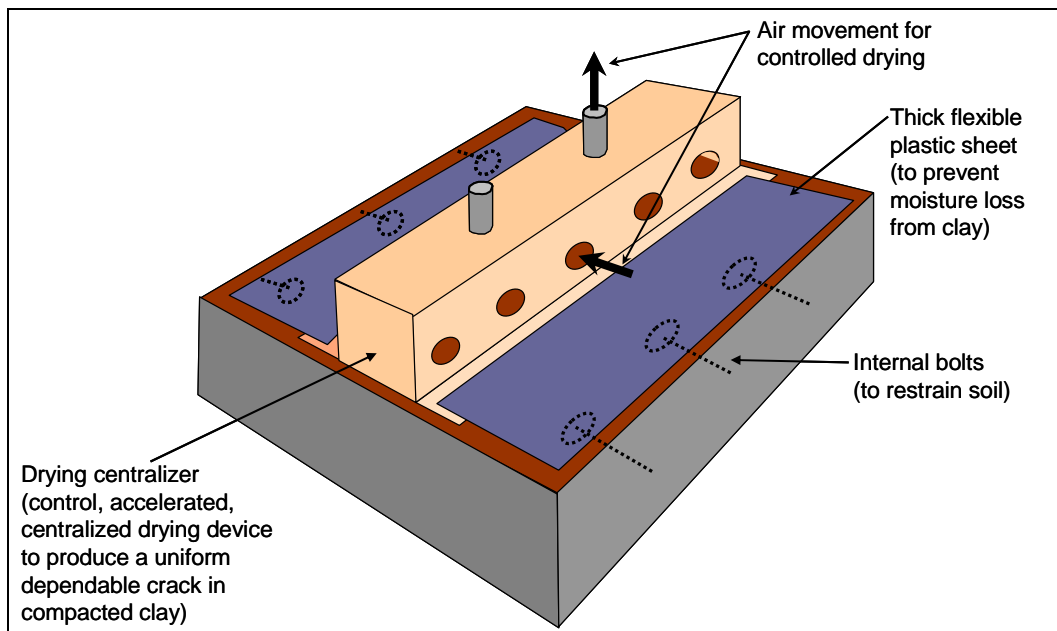

Figure 4. Soil test bed dimensions.

Figure 5. Conceptual view of drying apparatus for developing a primary crack.
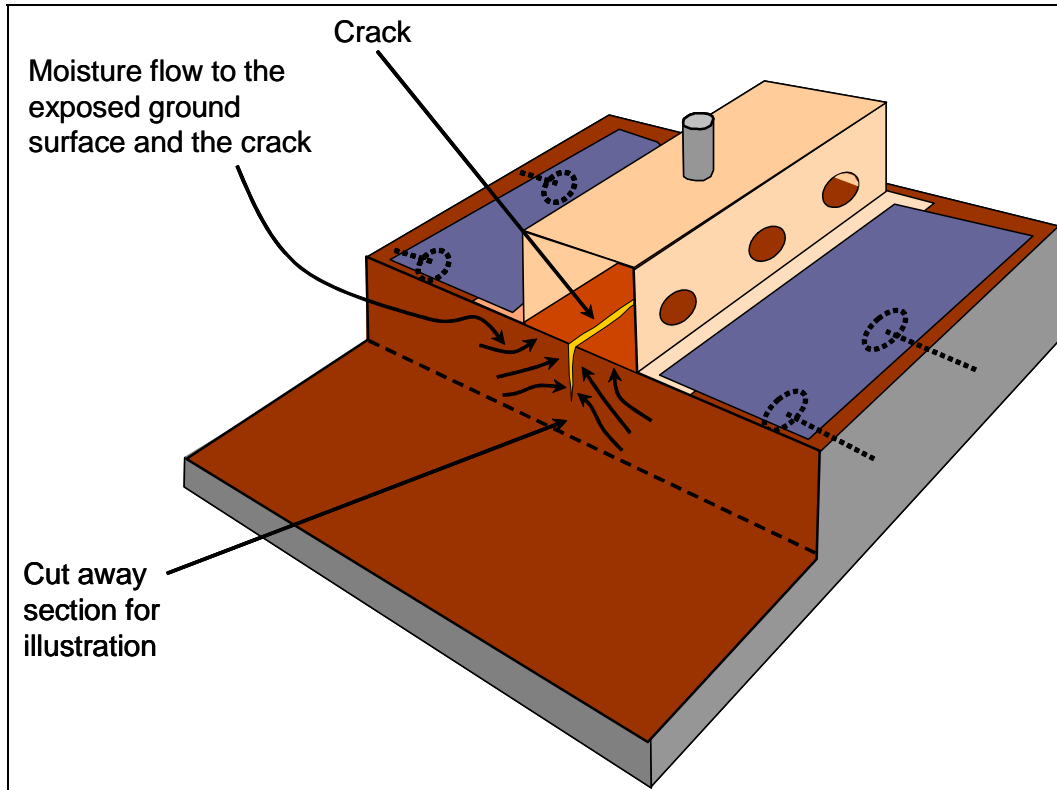
Figure 6. Intent of drying action on the soil surface.
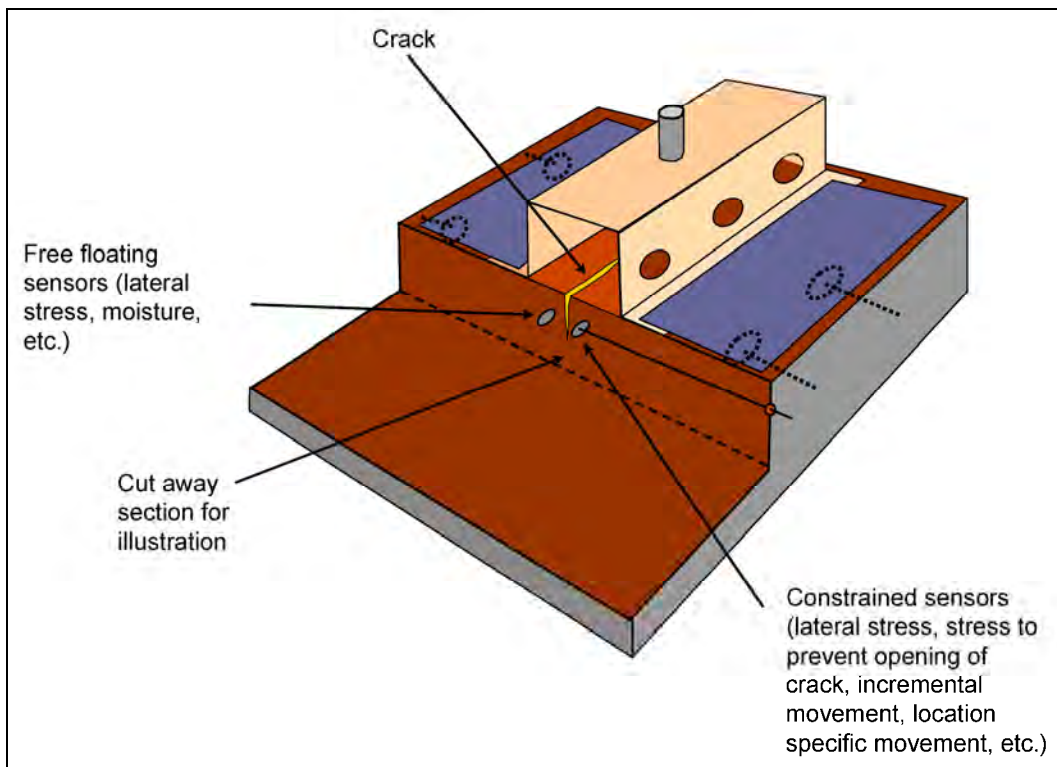

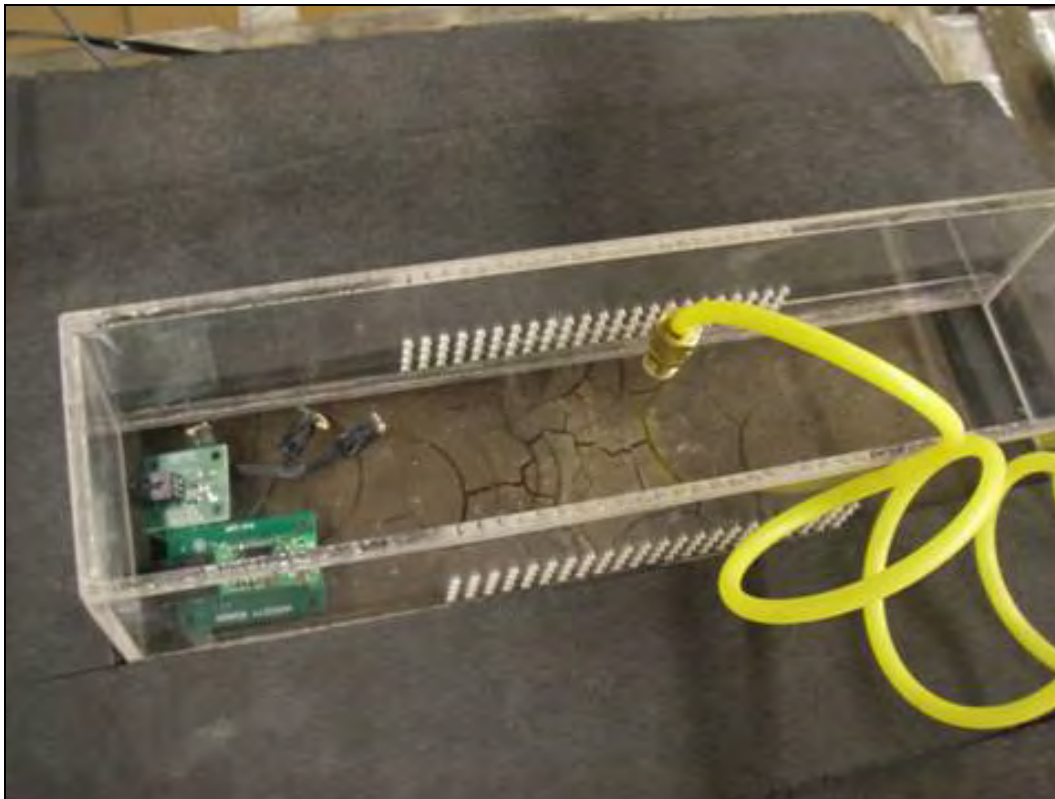Figure 7. Instrumentation concept around potential primary crack.

Figure 8. Drying box.

Figure 9. Soil box with soil bolts.

Soil tested

A high plasticity (CH) soil was used in the study and was obtained from a borrow pit located in Yazoo City, MS. The soil characterization data are presented in Table 1. The mineralogy of the CH is predominantly illite. This material is typical of low-permeability soils used in the design and construction of waste containment liners (Mitchell et al. 1965).

Table 1. Material properties for illitic, highly plastic clay.

Soil Property	Value
Particle size analysis	
% Sand	4.6
% Silt (<0.075 mm)	50.0
% Clay (<2 μm)	45.4
Specific gravity, G_s	2.74
Unified Soil Classification	CH
Atterberg limits	
Liquid limit, LL	76
Plastic limit, PL	24
Plasticity index, PI	52
Activity, A	1.15
Compaction (Standard Proctor)	
Optimum water content (%)	32.2
Maximum dry unit weight (kg/m^3)	13.2
Compression indices	
Coefficient of compressibility, C_c	0.317
Coefficient of recompression, C_r	0.011
Permeability, K (cm/sec) (Lambe and Whitman 1969)	$<1 \times 10^{-8}$

The CH soil used in this experiment was wetted to approximately the optimum water content given in Table 1 ± 2%. The soil was wetted and mixed using a hand-held mixer, shown in Figure 10, and then sealed in containers for 7 days of hydration to promote water absorption. Prior to soil compaction, the soil was remixed and soil moisture samples were taken to ensure uniform moisture distribution. During remixing, the large soil clods were broken down into smaller clods (maximum equivalent diameter <0.76 cm). The loose soil was then placed in the Plexiglas mold and compacted in four equal lifts, each approximately 3 cm thick. The lifts were compacted using a standard proctor hammer (ASTM D698), which was dropped a sufficient number of times to achieve the desired dry density

Figure 10. CH soil wetting and mixing.

in Table 1. Figure 11 shows a close-up of a single compacted soil layer after about half the compaction blows have been delivered. The final compacted depth of soil in the box was approximately 11.2 cm. Figure 12 shows the test box filled with the four compacted clay layers and the operation of the compaction hammer. The compaction effort smoothed out the chunky nature of the loosely placed soil into a smooth tight surface.

A thin sheet of plastic wrap was used to cover the entire soil specimen after compaction to protect it from drying until the experiment was conducted. The areas outside of the drying box were further overlain by a heavier, 1-cm-thick piece of rubber to insulate the clay surface from the surrounding dry air. Figure 13 shows the contrast at the end of the experiment between the light-colored, cracked clay located under the drying box and the smooth, darker surface that was protected from exposure to the air.

Figure 11. Surface of compacted soil layer after half the required hammer blows.

Figure 12. Soil box filled with compacted clay and compaction rammer.

Figure 13. Contrast between dried clay under drying box and protected clay under plastic sheet at end of experiment

Instrumentation

To measure lateral stresses occurring in the soil during crack propagation, an array of micro-electrical-mechanical systems (MEMS) pressure sensors were obtained and placed in the soil parallel to the constrained sides of the box (Figure 7). The lateral pressure measurements were performed with a new type of MEMS pressure sensor (shown in Figure 14) obtained from Phidget™ Inc. Several sensor sizes were available from the manufacturer, and the two smallest sensors were used—with diameters of 5 and 14 mm. These sensors use a universal serial bus (USB) based data acquisition circuit board (Figures 15 and 16) that is controlled by Visual Basic software. These sensors change the circuitry resistance with increased load. Consequently, a voltage splitter is required to convert resistance change to voltage. Calibration of the voltage output to a known pressure was conducted at the end of Experiment 3. The Phidget™ sensors experience a pressure saturation limit on the order of 150 psi (1 MPa), a value well in excess of any pressures anticipated during experimentation.

Different diameter pressure sensors were placed at varying distances from the center of the soil specimen and at two shallow depths below the ground surface. Figure 17 shows the general arrangement of the pressure

Figure 14. Phidget™ pressure sensor (5-mm diam).

Figure 15. Acquisition board for Phidget™ sensors.
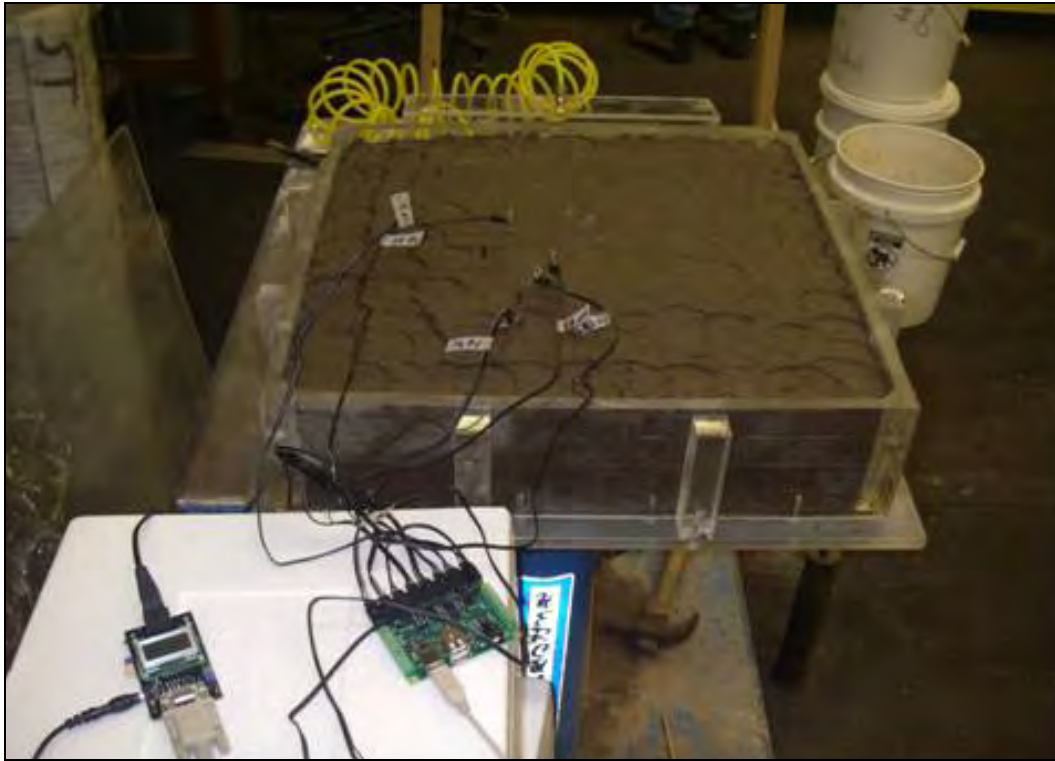
Figure 16. Acquisition board size relative to model.
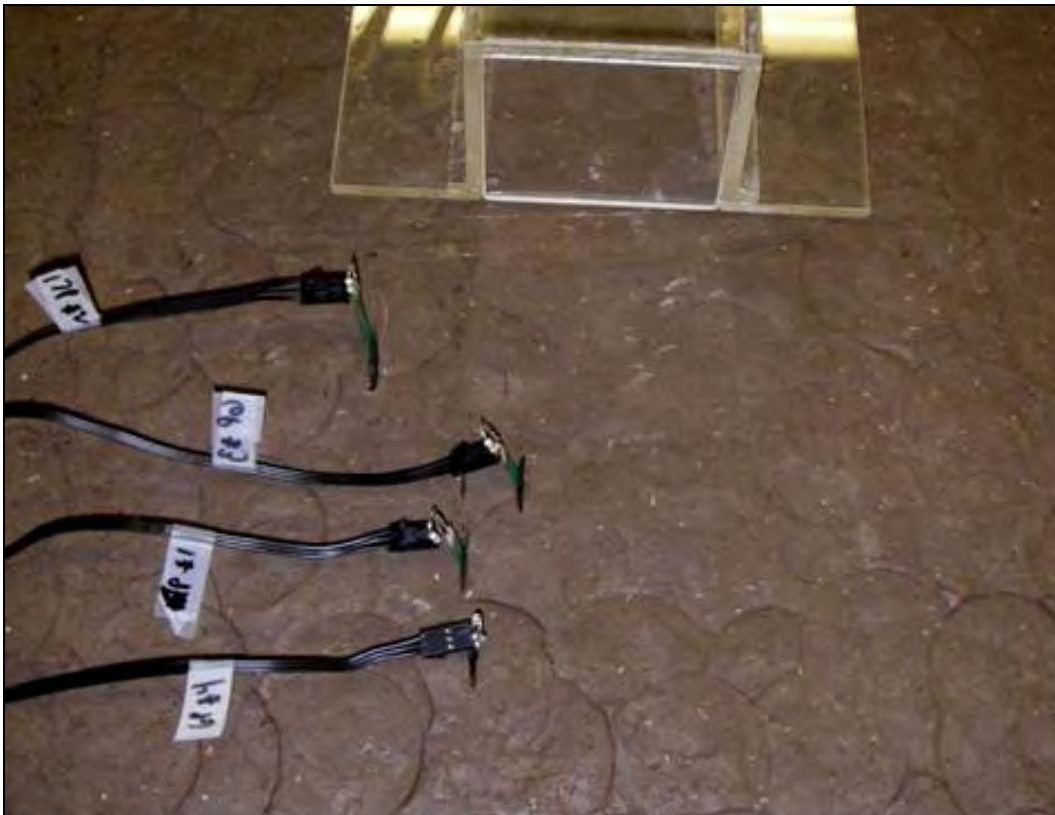
Figure 17. Positions of pressure sensors.

sensors before the drying box (shown in the background) is placed over the sensors. Figure 18 shows a MEMS humidity sensor from Sensirion™ Inc. inserted into a piece of polyvinyl chloride (PVC) pipe and buried near the surface of the final compaction lift to measure the change in relative humidity of the clay mass during the drying period. Note that the dark lines in Figures 16 and 17 are not cracks; they are depressions left from the last series of hammer blows on the soil surface.

Figure 18. Sensirion™ relative humidity sensor placement.

Results

Sensor data

The outputted voltage results from the pressure sensor measurements are shown in Figure 19. The pressure levels on the vertical axis are in terms of data acquisition bit levels because the calibration discussed in the section on instrumentation had not yet occurred. However, the trend in response was found to be the most revealing aspect of the experiment. The general trend observed in all cases is an initial compressive stress generated upon insertion of the sensors and subsequent compaction of clay around each sensor. As the soil surface begins to dry and tensile cracks open up, the lateral stress decreases to a point of zero compression (soil is in tension).
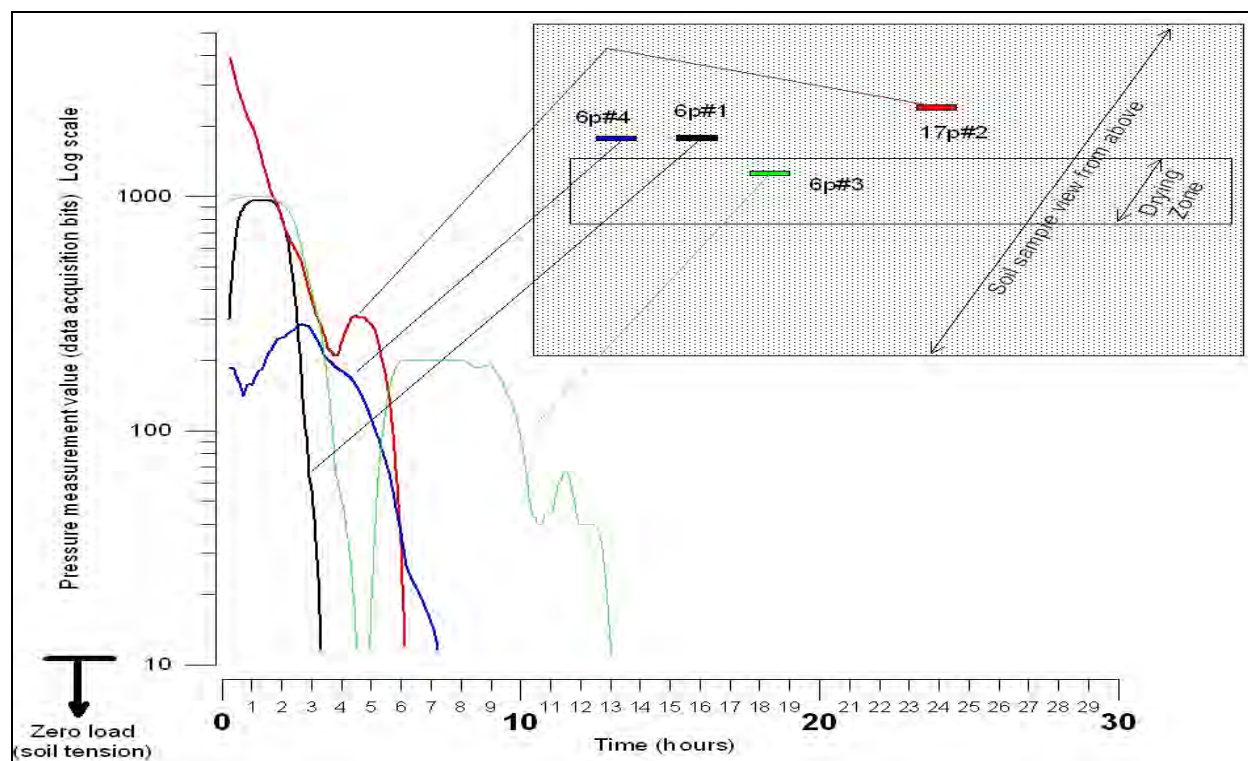
Figure 19. Voltage output from lateral pressure sensors.

All the pressure sensor measurements drop to zero within 7 hr of test initiation. This behavior is noted for both exposed and covered clay, with the difference being the time at which the soil enters into a fully tensile condition. Even though the area outside of the drying box is not exposed to drying air, it is still affected by soil moisture migration toward soil directly beneath the soil-drying box. For the single pressure sensor within the soil-drying box area, the pressure measurement dropped to zero at 4.5 hr, rebounded to a compressive state, and then dropped again to zero at 13 hr after start of the experiment. This phenomenon will be investigated in Experiment 3.

The relative humidity sensor was inserted immediately prior to the drying of the clay soil and was found to be ineffective over the 13-hr duration of the experiment. For this application, the sensor required greater than 13 hr to achieve an equilibrium state with the relative humidity within the clay soil, thereby missing the window of opportunity to provide information on changing conditions within the clay soil.

Digital imaging

A small digital camera was placed on top of the soil-drying box to take photos at different times during the latter half of the experiment. This effort was initiated because it might prove to be a means of visualizing the behavior of crack generation. Figure 20 shows one of the captured images that were later combined with other snapshots to create a time-lapse PowerPoint presentation. The generated cracks and resulting isolated "desiccated clay islands" appear to float and move by mechanisms that are not yet understood. It was noticed that microcracking occurred initially during the drying process, followed by generation of more severe, primary cracks. Once the soil began to constrict in these clay islands, the interior microcracks began to dissipate. This was the logical explanation of the rebounding of compressive stresses noted in the pressure sensor placed under the drying box.

Figure 20. Image of cracks using digital camera.

Crack propagation behavior

In the end, the soil-drying box did not produce a primary crack running down the middle of the soil specimen and was subsequently abandoned as a crack-training device in Experiment 3. However, there was a single crack

under the drying box, which was neither uniform nor symmetric. The vertical projection of the downward crack was observed to only occur to the depth of a compacted layer, approximately 1 in., even though a bonding scarification was performed between lifts. Horizontal cracking, or peeling of clay layers, was observed along the horizontal interfaces between compaction lifts. Consequently, the crack progression would initially cut a given compaction lift vertically, then crack horizontally between lifts, and then resume vertically cracking into the next lower compaction lift in a stair-step fashion, as shown in Figure 21. Tracking how a crack propagated downward through the compacted layers is not easy or obvious as shown in Figure 22. Figure 23 shows a deep-seated crack from the bottom to the top of the photo. The drying box was positioned at the same relative location (Figure 24) as during the experiment to show that the observed deep-seated crack occurs in the vicinity the drying box. In general, crack generation follows a path of minimum resistance as it moves both vertically and horizontally through the clay mass, creating a preferential flow path for moisture. This conclusion follows closely with observations made in excavated field liners noted extensively in the literature review.

Figure 21. Downward propagation of cracks.

Figure 22. Cracks in and through layers.
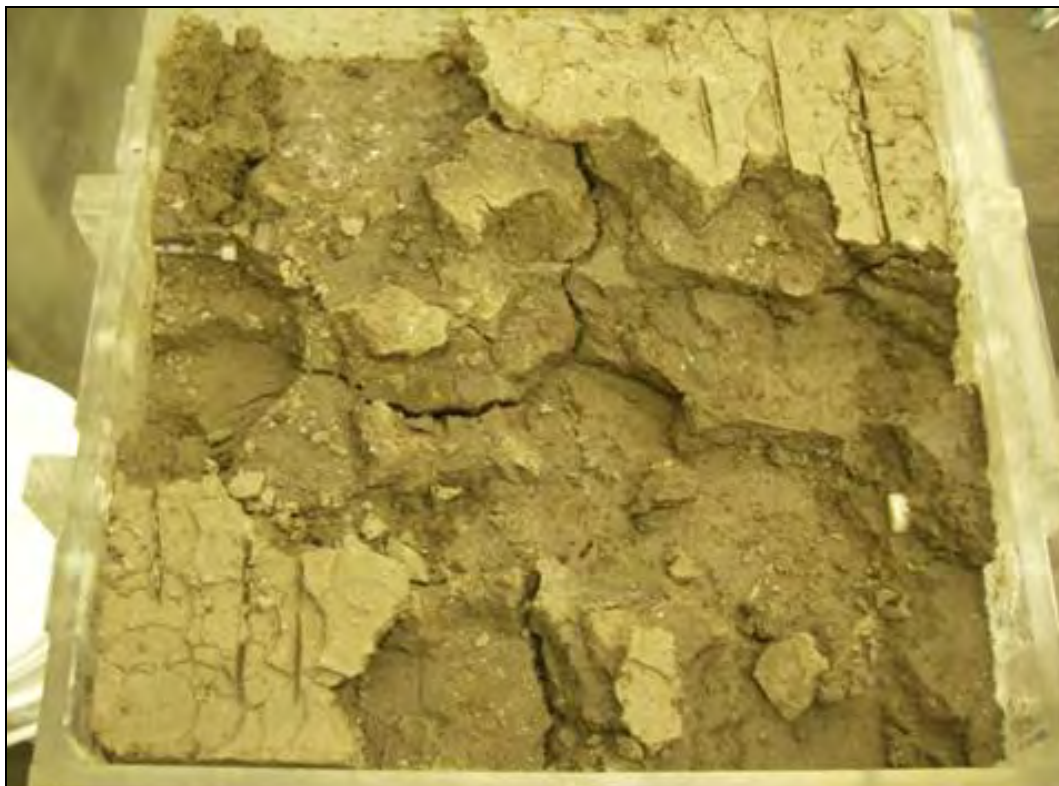
Figure 23. Deep-seated cracks in lower layers.
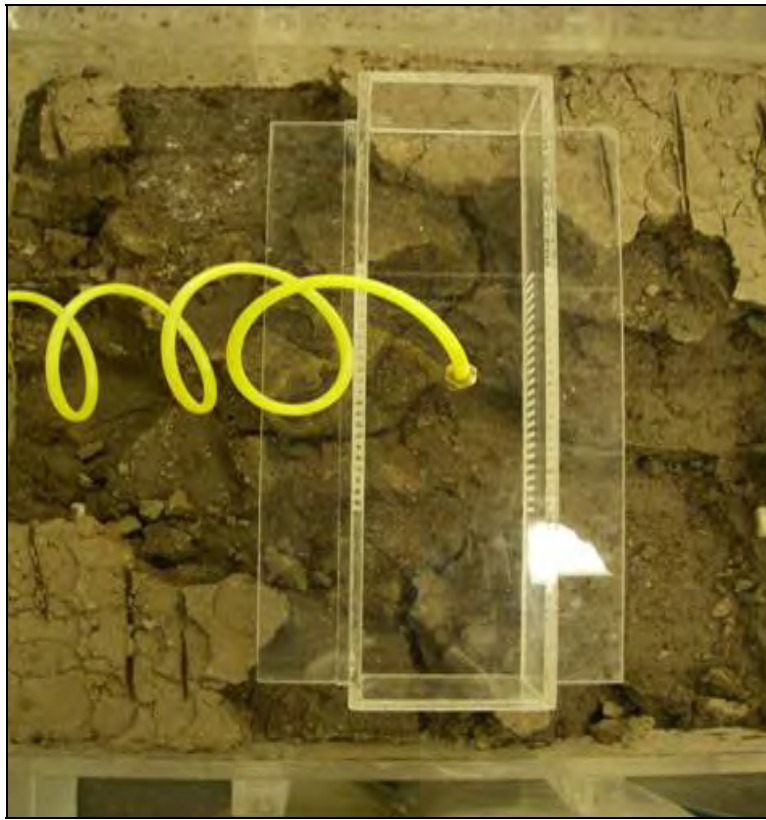
Figure 24. Orientation of drying box to deep-seated cracks.

Experiment 2

This experiment was designed to test the concept of using a time-lapse video camera and computer-controlled digital camera to capture the physical motion of cracking response on the soil surface. This study was also used to observe the drying response of the highly plastic clay without side restraints.

Experimental setup

This experiment used a compacted CH soil sample placed in a small 8-cm-diam metal container as shown in Figure 25. Unlike the larger scale sample box, this small container does not have side bolts to prevent the clay sample from pulling away from the container wall. The soil sample was compacted using a standard proctor hammer to an equivalent dry density as was found in Experiment 1.

Figure 25. Sample container for small scale drying test.

A video camcorder and digital camera were set up directly over the compacted clay specimen. This experiment was performed in an office rather than a humidity-controlled room and, as such, daily sunlight variations affected the video images. This experiment was performed over an interval of approximately 1 month. The computer-controlled digital camera was set to generate images at 2-hr intervals while the digital camcorder generated 0.5-sec images every 90 min.

Results

After approximately 1 month of observation, it was found that too many images were generated from the digital camcorder for the purpose of making a fast-acting animated digital movie. Therefore, only selected images were extracted from the video catalogue at various time stamps and assembled in a PowerPoint presentation that allows the user to cycle through the selected images to observe the crack propagation and healing. A time-lapse video was made of the digital camera images, which presents a smooth-flowing view of the cracking response over the month-long experiment.

Even though this experiment was designed to solely test digital imaging methods, the resulting time-lapse videos revealed the effect of microcrack generation (Figure 26), primary crack generation (Figure 27), and apparent crack closing (Figure 28) that would be difficult to discern otherwise. It was observed that the clay cracking began rather quickly, within a few hours, and crack size increased until the clay sample separated from the container walls (Figure 27). As the sample separated from the container wall, the thickness of the interior cracks began to diminish until only a fine outline of the original crack system remained (Figure 28). This process took approximately 13 hr from the initiation of the test, which is, interestingly, very similar to the time frame of the pressure response observed in Experiment 1. At the end of 1 month, these initial microcracks were either completely closed or showed only a slight indication of a past crack (Figure 28). This was the researchers' first observation of the cracking process from microcracking to primary cracking to apparent closing of microcracks, to be better defined in Experiment 3.

Figure 26. Microcrack generation.

Figure 27. Soil separation from container walls.

Figure 28. Closing of cracks after 1 month.

Experiment 3

This experiment was designed to measure the lateral pressure response of the clay during the three noted cracking phases—micro, primary, and healing—and tie in the physical measurements to a visual behavior of the soil to validate the measured response using the best techniques learned from the previous two experiments. The duration of the experiment was also extended to 6 weeks to ensure that a complete crack network was developed in the clay mass.

Experimental setup

The highly plastic CH soil was compacted in the wide area rectangular box to the same specifications used in Experiment 1 and subjected to a continuous drying cycle over a period of 6 weeks. The final moisture content and dry unit weight of the soil was determined to be 31.1% and 12.9 kg/m³, respectively, values that are reasonably close to the target moisture and density. This experiment was performed in a humidity-controlled room with a constant relative humidity of 23% and a temperature of 21.7 ºC. These environmental conditions were chosen to foster expedient crack generation to expedite the experiment. Figure 29 shows the cross section of the conceptual layout of the experiment. Changes in tensile stress were measured using a series of five 5-mm-diam Phidget™ lateral pressure sensors.
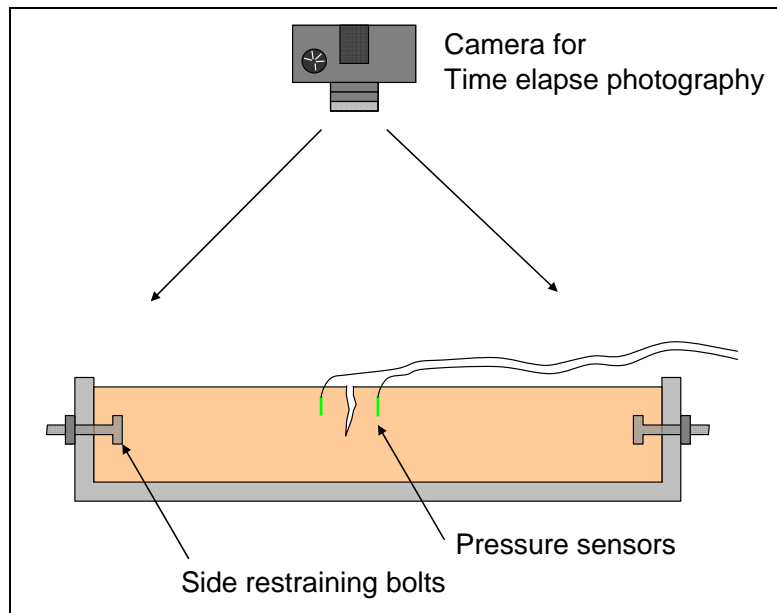
Figure 29. Conceptual view of soil box, instrumentation, and camera setup.

The techniques used to encourage a primary crack to form across the test box running north to south on the page and parallel to the sensor array involved using soil bolts (similar to Experiment 1) and scoring of the soil surface. Based on the success of controlling the direction of clay cracking with the soil bolts in the first experiment, the idea was used again with no modification. The soil-drying box from Experiment 1 was replaced with scoring the soil to train a soil crack, much like the methods used for the finishing of concrete floors. A 5-mm-deep line was scored along the middle of the sample and parallel to the soil bolted sides (Figures 30 through 33).

Image processing to monitor the surficial characteristics of crack development for this experiment was achieved through two approaches (see camera setup in Figures 34 and 35). The most successful approach used a standard high-resolution digital camera connected to a personal computer set up over the top of the test bed. The other approach used a standard High8 digital video camcorder in a similar mounting arrangement. After the experiment, the camcorder movie was downloaded to a computer and compressed to a shorter total movie length. However, more flexibility was found in using computer-controlled digital camera images to generate movies compared to using digital camcorders. The processed camcorder movies can generate excellent time-lapse movies, but only if the time-lapse interval is constant. In the case of clay drying and crack generation, this time-lapse interval is not constant but similar to an inverse log relationship. A majority of the action occurs within the first several hours of crack development, at which point any physical change of the surface begins to rapidly slow down.

The digital camera approach uses an Olympus camera, model D-595, controlled by Cam2Cam software via a USB cable. The Cam2Cam software allows the time interval and camera exposure to be remotely controlled. Each image from the camera is downloaded to a computer after each photo is taken. One camera image is taken every 10 min. At the end of the experiment, the selected images were combined into a movie file using Ulead Photo Explorer software. However, the final movie file did not include all the 10-min interval images from the experiment. Such a movie would show lots of action at the start and then be increasingly slow as the movie progressed. The key was to adjust the sequence of images to produce a movie that shows movement through all time periods. For example, the equivalent real-time interval at the beginning of this movie was 20 min per movie second and 1 month per movie second at the end of the movie.

Figure 30. Insertion of lateral pressure sensors.

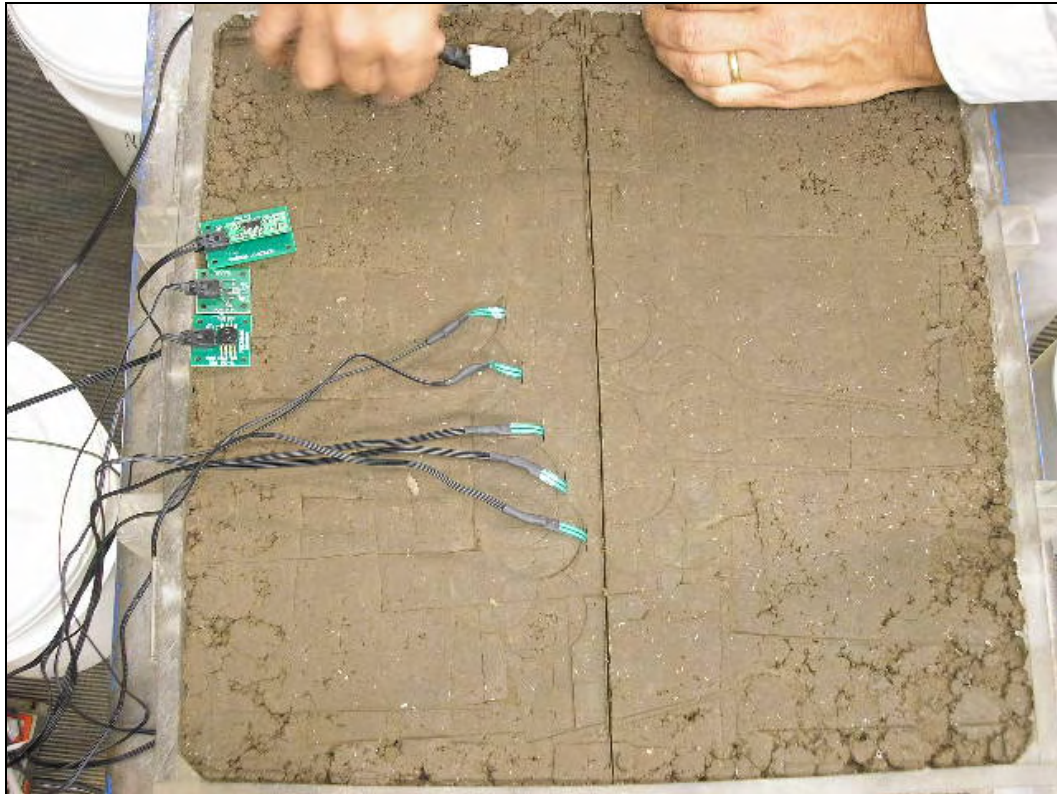Figure 31. Piston used for compaction around sensor holes.

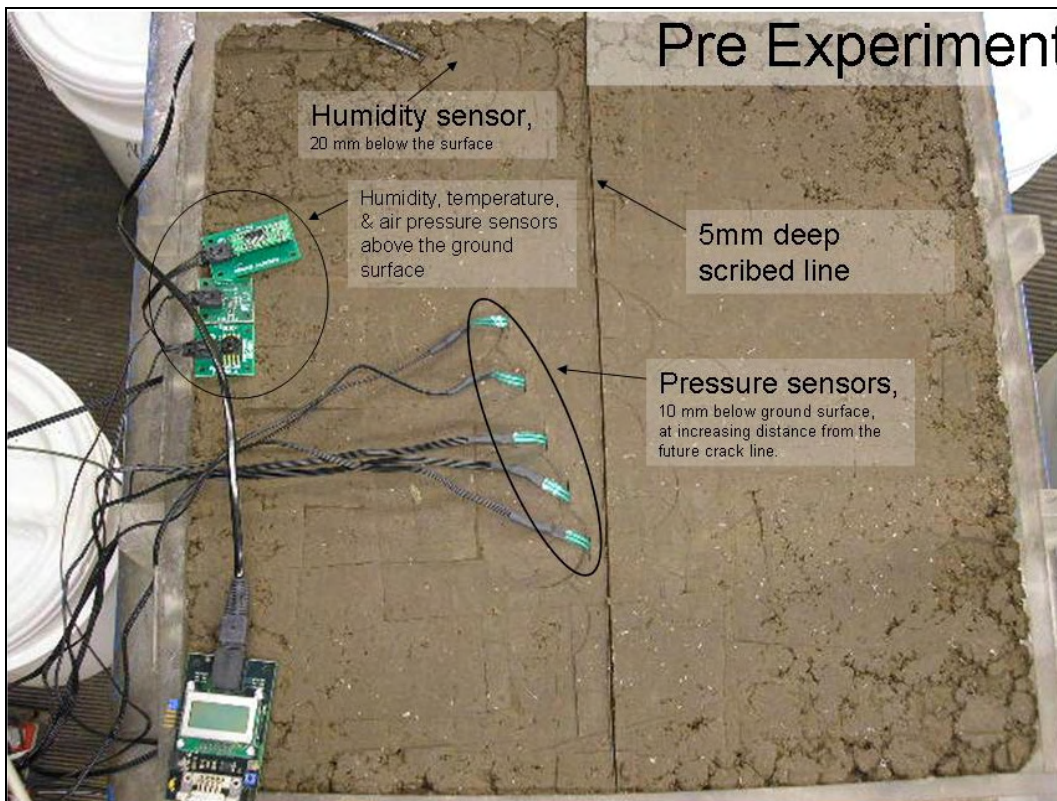Figure 32. Insertion of Sensirion™ relative humidity sensor.

Figure 33. Locations of all sensor instrumentation prior to drying.
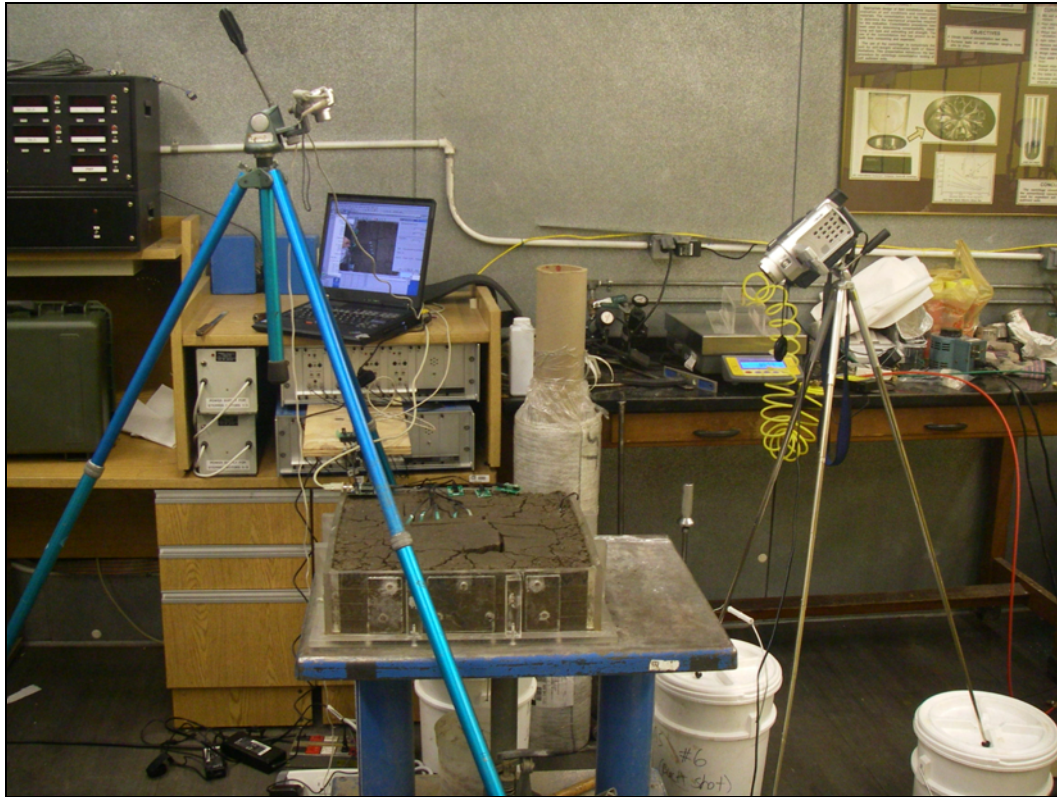
Figure 34. High-resolution camera digital camera setup.

Figure 35. Digital video camcorder setup.

Picking the best equal interval camera images to use in a movie will ensure continuous motion from the start of the experiment to the end of the experiment. The resulting cracking videos provide a means for the observer to see the effects of action and reaction during the experiment. At present, it takes considerable post-processing time to generate a representative movie. It is suggested, for future laboratory experiments, that custom software be used to automatically select the best equal interval photo files in order to generate the inverse time log based movies.

Instrumentation

The lateral Phidget™ pressure sensors were placed into the soil parallel to and at various distances from the scored line. Unlike Experiment 1, all pressure sensors were the same size, specifically the 5-mm-diam sensors, and all sensors were at the same depth below the ground surface (7 mm from the surface to the middle of the pressure sensor). The pressure sensors were placed into cut slice holes produced using a very thin knife (Figure 30). After all the slice holes were cut and sensors placed, the surrounding soil was lightly compacted using the weighted, 1.5-in.-diam compactor piston (Figure 31) to seal the holes and provide an initial compressive stress similar to the surrounding compacted soil. A relative humidity MEMS sensor was placed within a small piece of PVC pipe to protect it from compaction (as shown in Figure 32), but at a greater depth than in Experiment 1. All sensor locations are shown in Figure 33.

In order for the results of the pressure sensors to be applicable to the validation of a numerical model, the voltage output must be calibrated to a known physical pressure. To accomplish this task, a Tekscan™ pressure calibration machine (Figure 36) was obtained and modified with a digital pressure recorder. This device allowed all the sensors to be inserted at the same time, such that they were all exposed to the same pressure level. Pressure was gradually increased, noting the voltage output of each sensor, and was recorded using ERDC-designed Visual Basic software as shown in Figure 37. A summary plot of the pressure versus voltage output is shown as Figure 38. (Note that there existed a high degree of repeatability within replicate sensor calibrations.) Third-order polynomial fits were determined to represent each calibration curve, which in turn was used to back-calculate the observed pressure in the soil from Experiment 3.
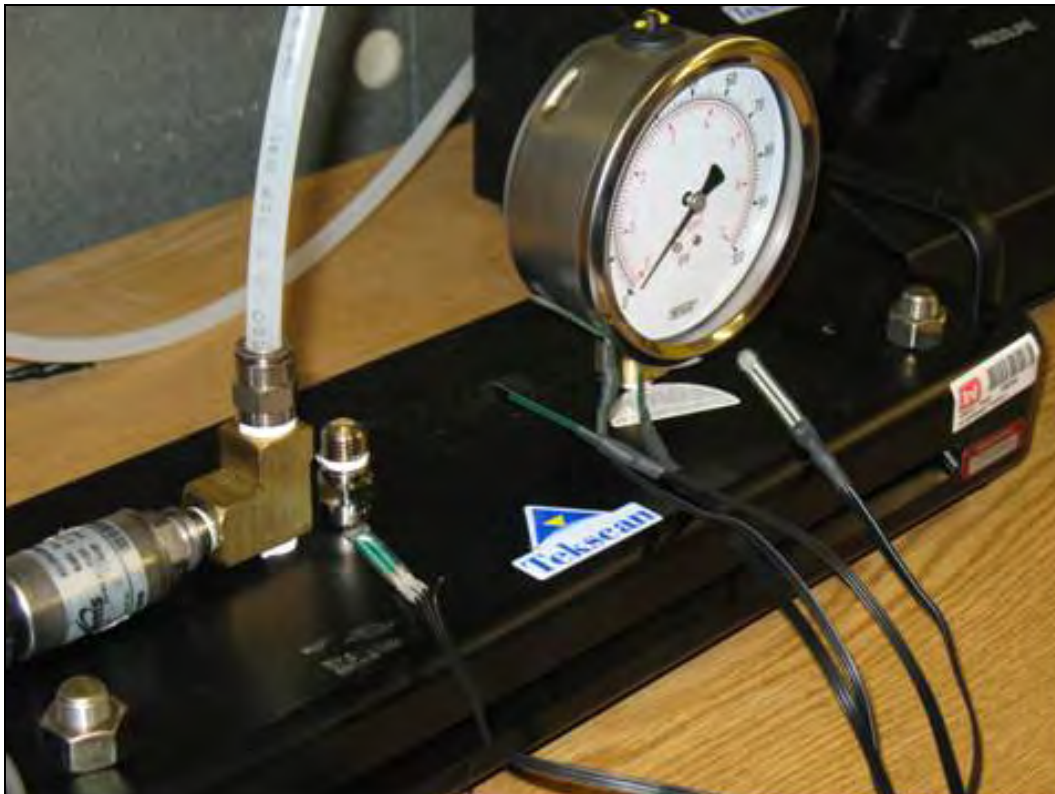
Figure 36. Tekscan™ pressure calibration unit and accompanying
Phidget™ pressure sensors.
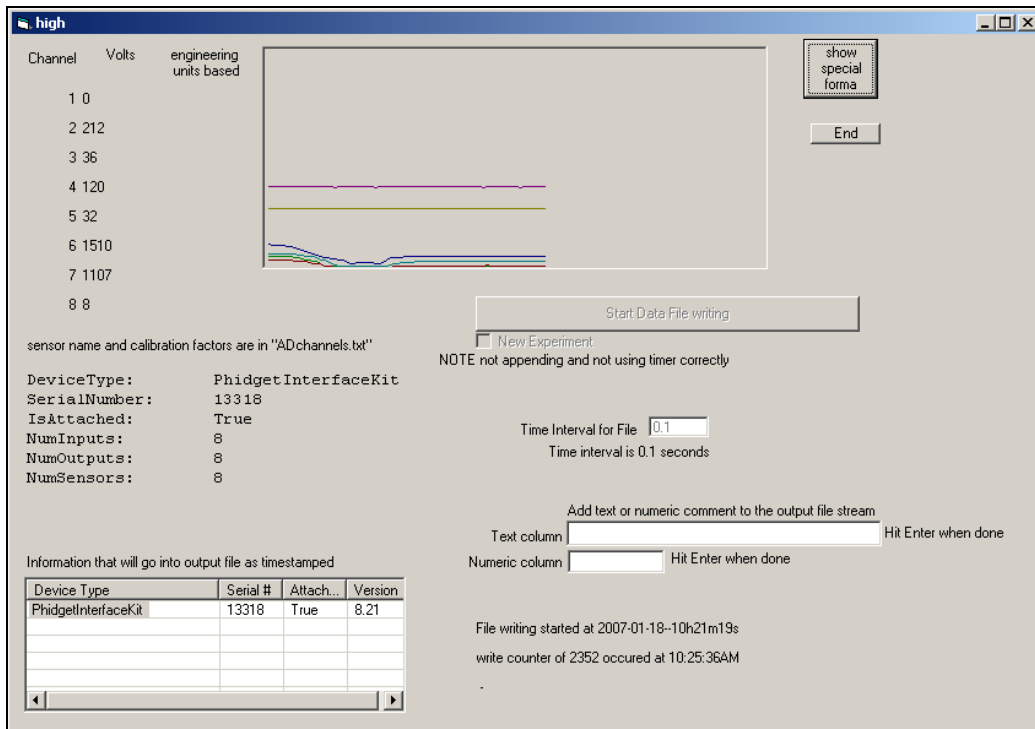
Figure 37. ERDC designed visual basic software designed for recording
Phidget™ sensor calibration data.
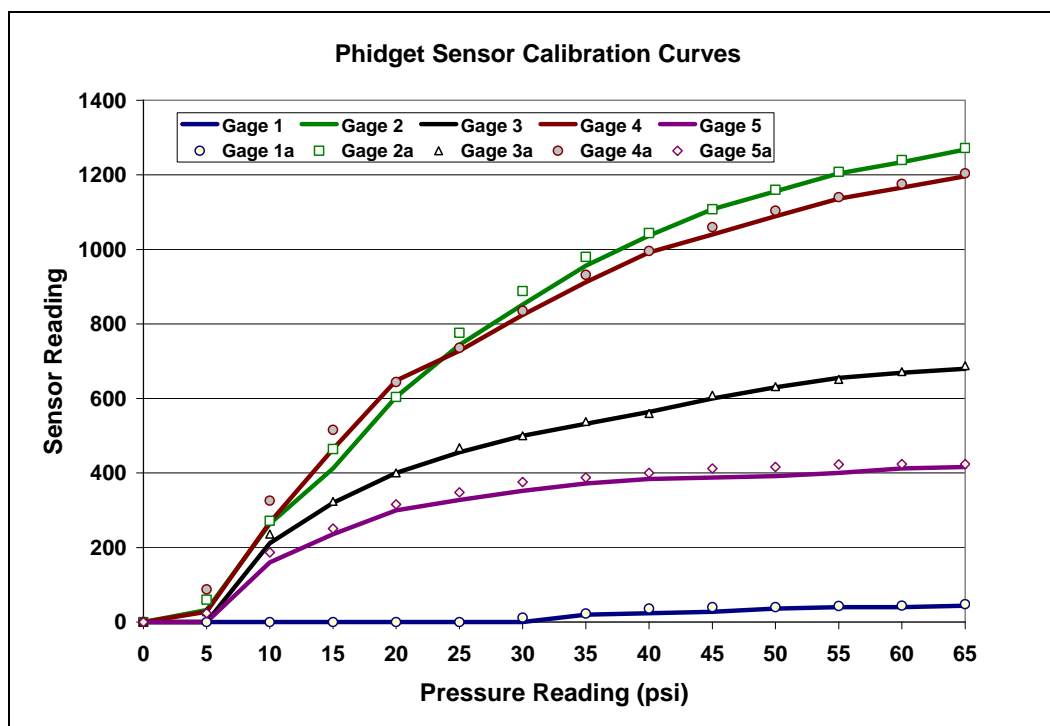
Figure 38. Calibration curves for Phidget™ sensors used in Experiment 3.

Results

Once the sensors were installed and the data acquisition units engaged, the time clock on the experiment began, as the dry ambient conditions would begin to cause cracking of the clay surface in only a few hours. The cameras were all turned on, and recording of the time-lapse pictures began. The test bed was left untouched for a period of approximately 6 weeks, at which point forensic studies were performed. The sample was carefully taken apart layer by layer to examine the nature of the cracking below the observable surface. Data were then post-processed to determine the magnitude of stresses, and the videos of the clay cracking were created.

Sensor data

The resulting calibrated stress levels [pounds (force) per square inch (psi) and pounds (force) per square foot (psf)] from the pressure sensor measurements are shown in Figure 39. The high initial stress levels represent the residual lateral stress in the soil from the piston compaction, presumably close to the passive resistance level for this clay. The zero measure on the x-axis represents a condition when the soil has undergone the transition from a compacted stress condition into pure tension as a result of crack formation.
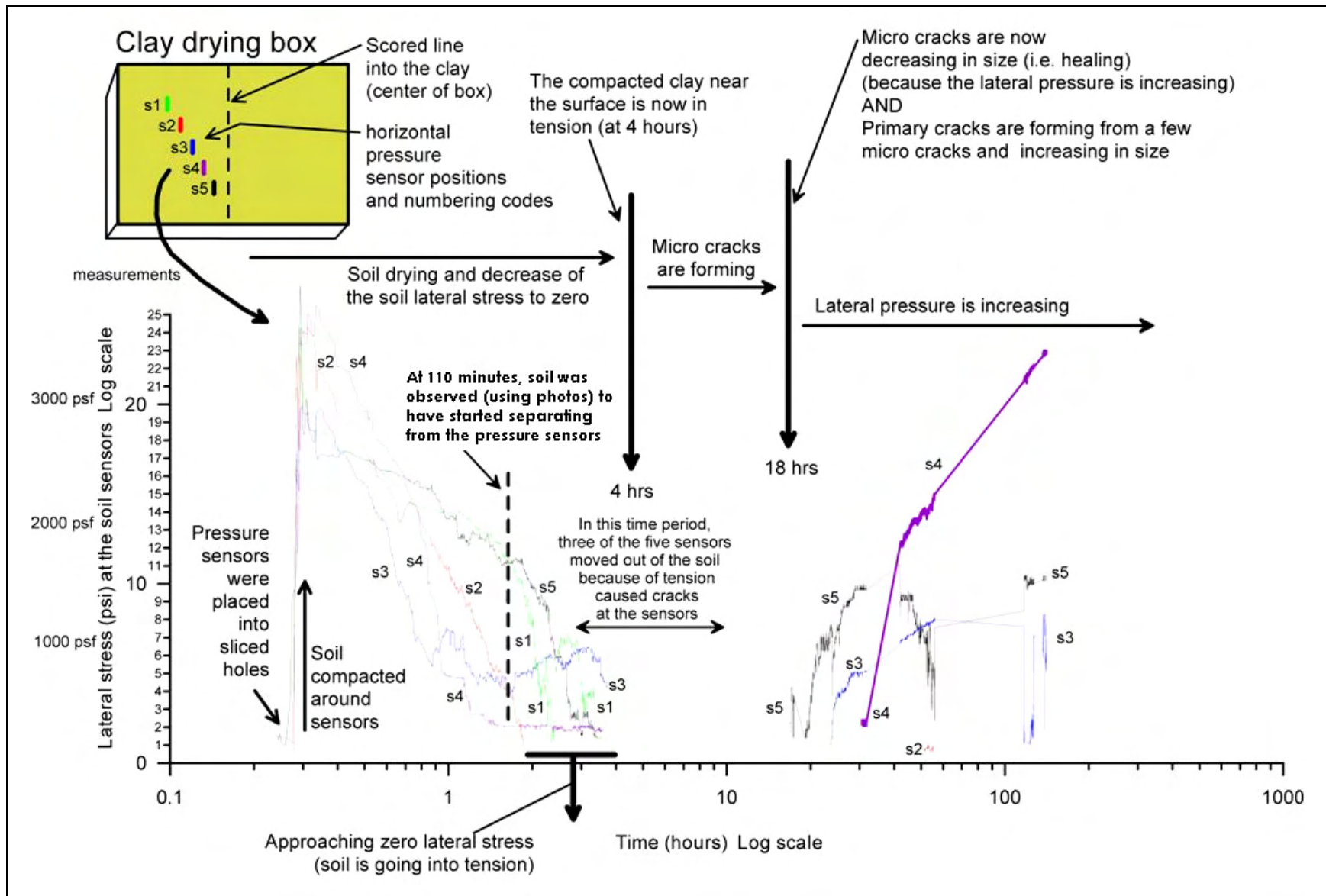
Figure 39. Resultant lateral pressure sensor measurements.

The key observation from pressure sensors results is that in all cases, the pressure decreased from an initial compacted lateral stress to a state of zero stress (tension) within about 4.5 hr after exposure to the air (Figure 40), specifically within a time period of 1.5 to 4.5 hr. From photo record examination, no microcracks were observed until after the lateral stress levels had dropped to zero. Figure 41 shows a few microcracks starting to form at about 6 to 8 hr from test initiation. The presence of microcracks occurring only after the lateral stress reaches zero indicates that when tensile stresses within the clay exceed the strength of the clay, lateral strains (or cracks) are induced. Consequently, once the soil has gone into tension, the formation of a primary crack network is the next step.

Between 18 and 30 hr (Figure 42), a few of the microcracks have expanded into large primary cracks while other microcracks have begun to decrease in size and will appear to heal. The pressure sensors at this time period (20 hr) are starting to show positive lateral compression stresses. Therefore, when microcracks decrease in size, it is an indicator that portions of the total soil specimen are returning to a compressive state. Microcracks decreasing in size infer the opening of primary cracks, causing tensile
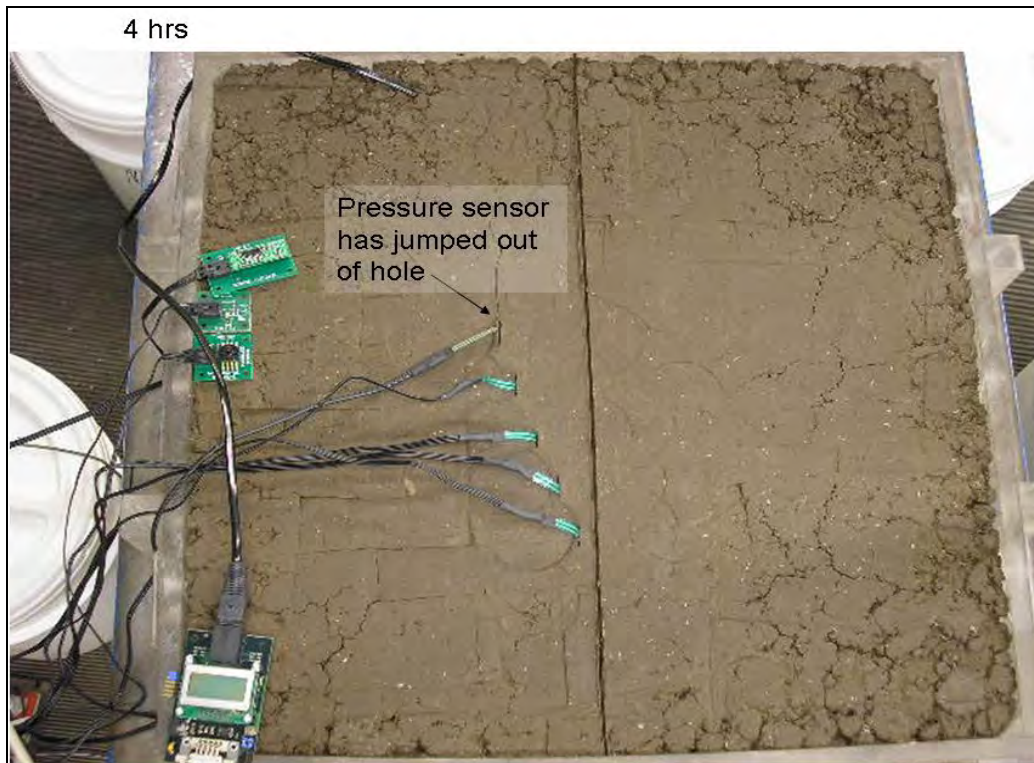
Figure 40. Clay mass when lateral stress level decreases to zero.
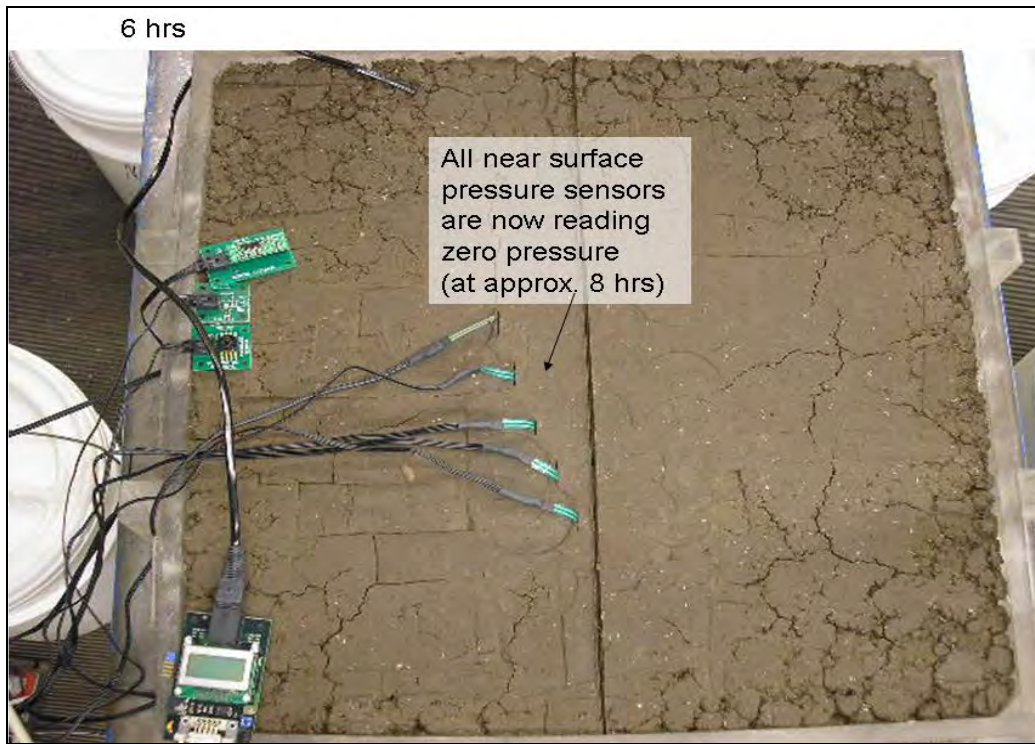
Figure 41. Microcrack formation at 6 to 8 hr from test initiation.
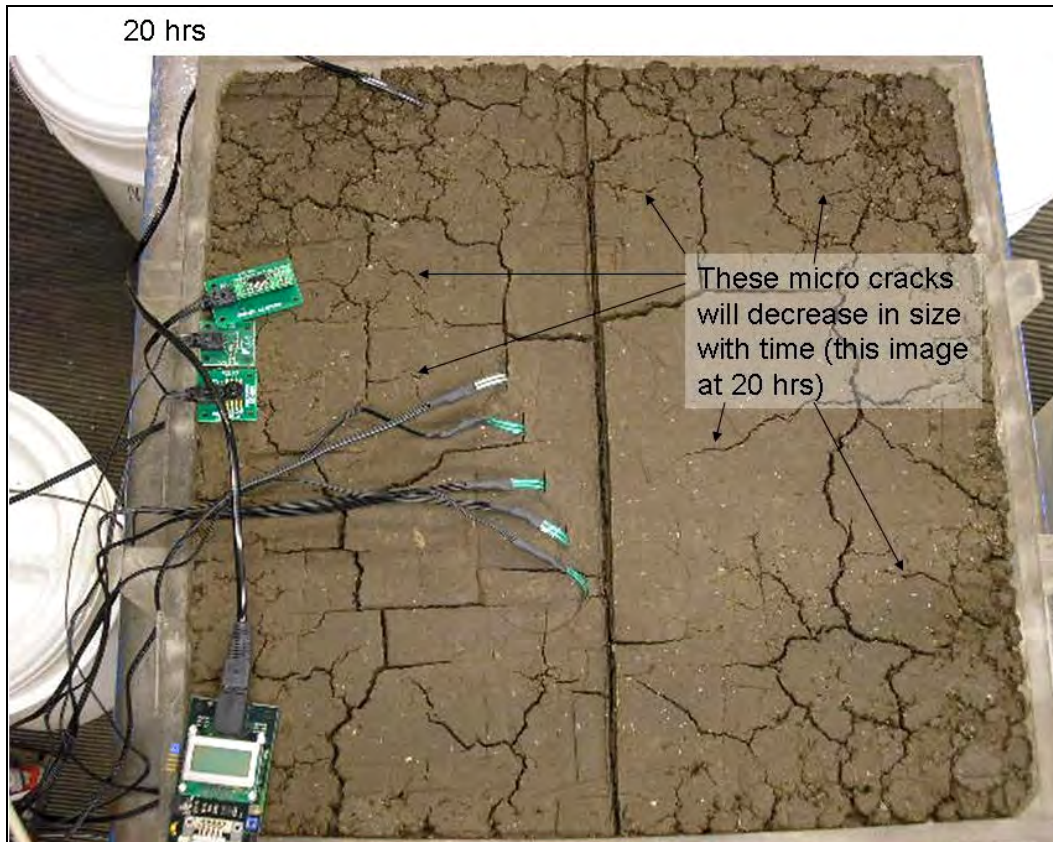
Figure 42. Onset of primary crack formation at 20 hr.

stress relief throughout the total specimen. As was observed in Experiment 2, the initial cracking can be defined as a web of thin microcracks. As time evolves, a few of these microcracks become primary cracks while several of the other microcracks slowly decrease in size and almost appear to close.

The other important observation is that most of the pressure sensors eventually returned to a positive compression stress level and, in one case, to a compressive state near the initial stress. This is observed in the formation of "clay islands," a block of soil bounded on all sides by a primary crack with healed microcracks within its interior. These clay islands begin to move and shift along the surface, suggesting a detachment between the underlying soil layer (Figure 43). The sliding is a result of the lateral restraints imposed by the soil bolts forcing one-dimensional movement. Figure 44 represents the conditions after 1 month.
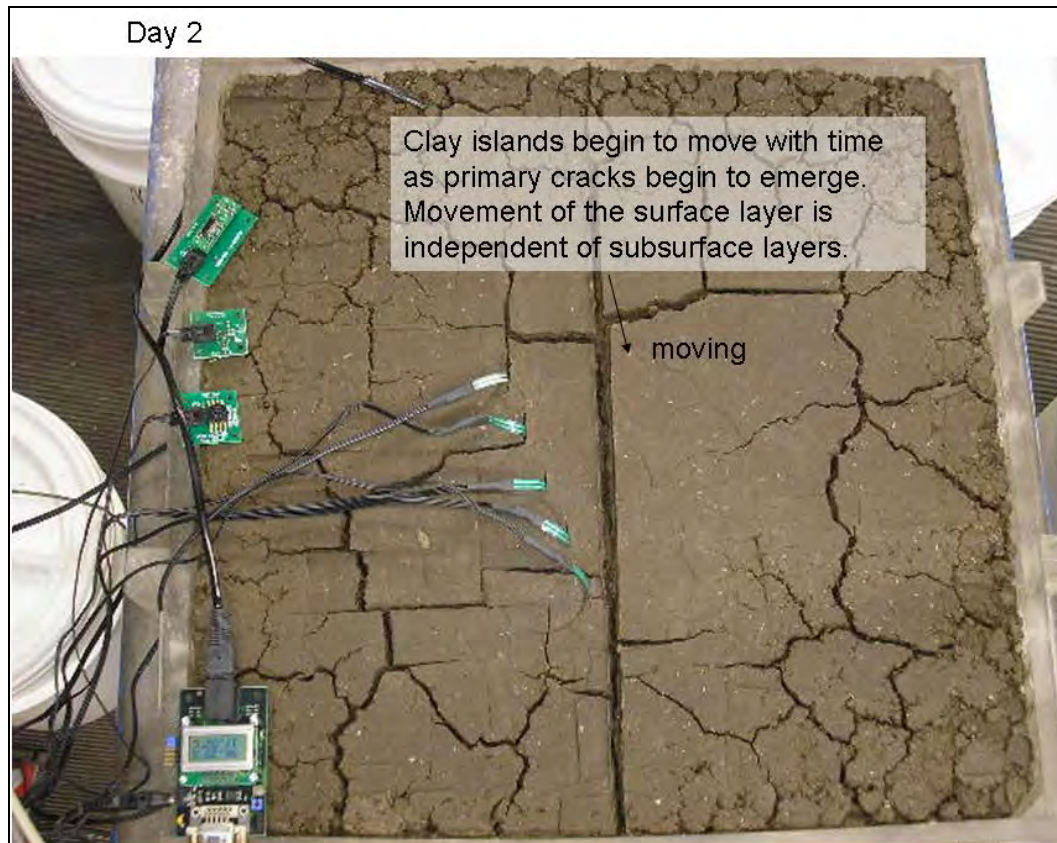
Figure 43. Primary crack size widening coupled with movement of clay islands.

Figure 44. Major crack faulting after 1 month.

Qualitatively, the following cracking processes were observed to occur:

- Microcrack generation
- Primary crack generation
- "Clay island" formation followed by block movement due to desiccation
- Microcrack closing
- Directional cracking with depth
- Curling of desiccated clay islands
- Relaxation of clay curling with time

Although every attempt was made to use the MEMS humidity sensor in this experiment, in this instance the soil cracked very near the sensor, rapidly exposing it to the outside environment and rendering its data output invalid for measuring changes in internal relative humidity in the clay during desiccation. Changes in the implementation of this device will be made upon use in any future experiments.

Volumetric effects

Surface curling is defined as the upward movement of primary cracks due to drying (and tension) on the top side of individual floating soil plates (illustrated in Figure 45). Figure 46 shows an example of surface curling of the soil after only 2 days. The curling is due to the unbalanced stress loads from the top to bottom of an individual compacted lift as the top shrinks faster than the bottom. Once this curling has occurred, soil begins to break away from the main soil mass to form individual floating plates (Kodikara et al. 2004). Once sufficient time has been given for drying to occur throughout the depth of a soil layer, curling dissipates as equalization of stress occurs from top to bottom. In this experiment, this was found to occur after about 7 days of drying.
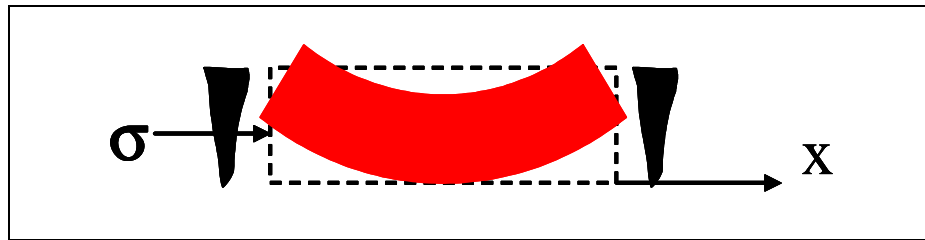
Figure 45. Curling response of soil undergoing changes in lateral tension.

Figure 46. Surface curling in clay mass after 2 days.

Scoring and instrumentation effects

Deep scoring of the compacted soil's surface along the center of the specimen caused a majority of the specimen to crack along that line, but only for the uppermost compacted layer (Figure 47). The surface score forced a crack along only 70% of its length in the uppermost layer and did not influence any underlying crack generation. A close-up of the cut score is shown in Figure 48 (taken near the top of the specimen shown in Figure 47). Note how the upper segment length of the surface crack in Figure 47 does not follow the entire scored line. After removal of several of the near-surface individual soil panels (compaction lifts) (Figure 49), the location of the primary crack shifted in subsequent compacted layers. The underlying observed crack in Figure 50 did not follow any portion of the surface cut score line in the middle of the specimen.

More soil removal (shown in Figure 50) reveals numerous smaller score marks (one score mark is illustrated with a pointer stick in the photo). These score marks were inserted during the soil compaction process at the completion of a compacted lift and prior to beginning the next lift. Providing a disturbance to the soil surface produces a better bond between each compaction layer. Several of these shallow score marks were observed in Figure 51; however, the deepest mark, in the bottom of the test bed,

Figure 47. Primary crack formation along score at end of test.

Figure 48. Close up of cut score at end of test.

Figure 49. Offset of primary crack formation in subsurface layers.

Figure 50. Crack influence due to score mark between compacted lifts.

Figure 51. Effect of cracking along scoring lines between compacted lifts.

appears to be where a primary crack occurred. Consequently, a single imperfection (i.e., a deep score mark) in the compacted soil layer just below the surface layer determined the location of a deep crack. This suggests that imperfections below the observable compacted surface can dictate crack initiation just as well as surface imperfections.

The pressure sensors for this experiment were offset from a single line to prevent formation of a single long crack that went through all the sensors. However, the pressure sensors do appear to be influencing the density of primary cracks. Figure 52 illustrates a higher crack density in the area of the pressure sensors compared to an area opposite from the sensors. The cracking did not appear to adversely affect any pressure data collected, in that a consistency between sensor responses is evident. It is recommended that future research consider using a wider spacing of pressure sensors, and likely on both sides of the scored line to minimize the impact in any one area of the compacted sample.
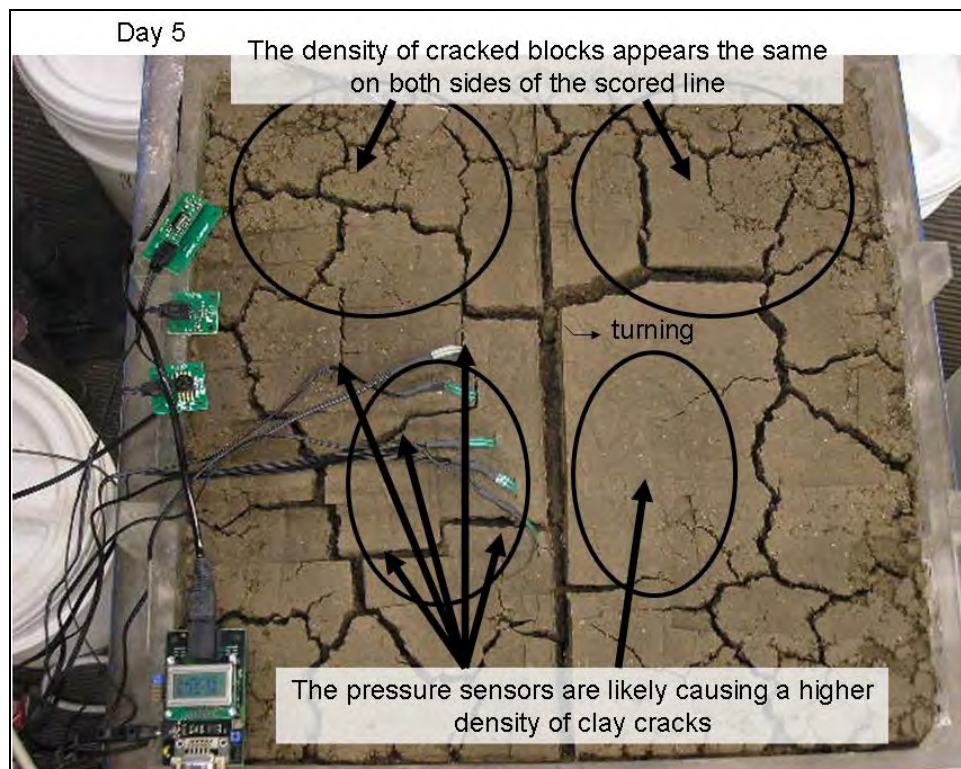

Figure 52. Localized cracking effects near placement of sensors.

Summary

From Experiments 1 through 3, the following qualitative and quantitative observations were made:

- Crack formations are very diverse along the surface layer and as they migrate downward. Shapes of cracks are neither uniform nor symmetric—evolving from thin webs of microcracks to a select number of wide primary cracks that, in turn, can seal off existing microcracks.
- Pressure sensors readings confirm this transition from microcracking to primary cracks to healing—an initial large lateral stress reducing to a zero lateral stress under tension, followed by a rebound in compressive stress when cracks begin to heal as a result of shifting soil layers.
- Cracks choose the path of least resistance, as evidenced by the changing location of the primary crack with layer depth. Drying action occurs along a primary crack followed by drying between compacted layers as curling occurs and, then, formation of primary cracks at deeper levels within the soil mass.
- Unbalanced stress loads from top to bottom of a given compaction lift induce a curling effect on the clay surface. As the soil continues to dry with depth and the boundary moisture conditions come into equilibrium, an uncurling effect is noted.
- Imperfections in compaction, such as the scoring between compacted lifts, causes formation of deep cracks.
- A high density of cracks around the sensors suggests preferential paths caused by incisions made from the installation of the sensors.
- The test box with the soil nails provided an effective means of directing the widening of the primary crack perpendicular to the direction of the intruding soil nails. This in turn directed the lateral pressure readings during movement of the surrounding "clay islands" perpendicular into the pressure sensors, providing a good measured response of the clay mass behavior.

The results of Experiment 3 can be used to validate a numerical model designed to predict the cracking network of a soil with similar material properties. The imaging provides a detailed network of crack response that can be used as a baseline to ensure that crack propagation is maintained in the model. Stress magnitudes measured with the accompanying pressure sensors will enable validation of the numerical constitutive laws to ensure that proper tensile stress development is occurring based on the calibrated model parameters.

4   Numerical Modeling Effort

Introduction

This chapter describes the development of a numerical model that simulates the progressive cracking in clay barriers. The numerical model seeks to address the following questions: first, how can drying penetrate a significant distance beneath the surface in the face of low-permeability clay and, second, to what extent is the permeability of the mass increased? To address these questions, and to provide a means to evaluate field sites, an investigation of the cracking process was initiated in three steps. The first step was to perform experiments on the cracking process to gain understanding of the mechanics of the cracking process (Chapter 3). The second step was to obtain numerical parameters for shrink-swell models necessary for a quantitative model of cracking. Finally, a numerical model was to be developed that could simulate the cracking process.

Research on soil desiccation and cracking

Research on crack development in soil is motivated by observation that secondary porosity created by macroscale features such as cracks contribute to most of the moisture movement in clayey soils. Intact clay has permeability values ranging from 10^{-5} cm/sec to less than 10^{-7} cm/sec. Water flow under purely gravity potential is effectively inhibited within the lower portion of this permeability range, making these soils attractive as water barriers for various types of waste disposal and retention sites. Unfortunately, clay is prone to shrinkage upon drying, which causes cracking that virtually destroys its capacity to act as a barrier to water. As a result, composite designs are now common in which a geomembrane is combined with a soil layer. For example, Albright et al. (2004) measured the percolation rates through clay barriers throughout the United States and found that composite barriers were generally effective while conventional barriers with soil-only barriers generally were not effective because of preferential flow through cracks and other defects. It is worth noting that only one of these soil-only sites evaluated was in an arid climatic condition. Thus, improvements of soil-based barriers must involve controlling soil desiccation and its attendant cracking. More recently, Benson et al. (2007) investigated a Wisconsin site where they identified a combination of cation exchange and dehydration as the cause of inordinately

high percolation rates in geosynthetic clay liners. The geosynthetic clay liners employ thin layers of bentonite encased between geotextile sheets. It was noted that, throughout most of the year, downward hydraulic gradients exist for only short time periods while upward gradients predominate, owing to the response to evapotranspirative demand. Whereas the tendency for long periods of upward gradients predominates in both arid and temperate climates, a strong potential for desiccating clay liners will always exist, regardless of geographic location.

Suction shrinkage relationships

A common feature of the desiccation models for soft soils is the observation that shrinkage occurs in the saturated state; desaturation occurs at the shrinkage limit, beyond which no further deformation occurs. The stress state during shrinkage can be described by the traditional Terzaghi effective stress principle in which the total stress (σ_{ij}) is decomposed into the effective stress (σ'_{ij}) and the pore pressure ($-p\delta_{ij}$). Tensile stress is taken to be positive. Pressure is likewise positive. Pressure acting on a boundary is equilibrated by a compressive (negative) stress. Therefore, in the case of saturated media, suction is a negative pore pressure that increases the mean compressive effective stress, σ_m, and causes a reduction in volume. The effective stress required for a given change in volume increases exponentially, as is evident from the traditional e-log σ_m plot. The shrinkage limit is the point at which the effective stress required to reduce the volume cannot be sustained by a continuous pore water phase, and the soil desaturates. The shrinkage can therefore be modeled using the principles of traditional mechanics of saturated soil.

Compacted soils are neither saturated nor are they at the shrinkage limit. Thus, for a compacted soil, a model based on partially saturated soil is required. In the case of a partially saturated state, the Terzaghi effective stress principle must be expanded to include both pore water pressure and pore air pressure. The soil mechanics literature contains numerous attempts to modify the effective stress principle that will not be reviewed here, although they are discussed in Berney (2004). The present work is based on a thermodynamic approach developed by Berney et al. (2003) and described in detail by Berney (2004). In this theory, the total stress is not assumed to have a definite decomposition into identifiable components. Rather, the constitutive response of the changes in total stress and suction potential is assumed to be coupled to the changes in strain and volumetric water content. The model does recognize the distinction

between the total stress, from which the balance of momentum equations are written, and the inter-granular stress, which is that stress transferred through the solid grains.

The theory is built upon an analysis of the work performed on a soil element. It is concluded that the thermodynamic conjugates for the deformation process are (σ_{ij}, ε_{ij}) and (p, θ), whereby the virtual work performed on an element of soil is given by

$$dW = \sigma_{ij}\delta\varepsilon_{ij} + p\delta\theta \tag{7}$$

where it is assumed that the suction, p, can be treated as a scalar, although it can be argued from micro-mechanical principles that in fact the suction should be treated as a tensor because the suction stress in general is not hydrostatic. The assumption of hydrostatic suction stress is retained in the present work as a reasonable simplifying assumption.

It follows that incremental constitutive relationships, shown in Figure 53, can be written as

$$d\sigma_m = K_1 d\varepsilon_v + K_2 d\theta \tag{8}$$

and

$$dp = K_2 d\varepsilon_v + K_3 d\theta \tag{9}$$

Taking $d\theta$ as a free parameter that can be eliminated from the equations, a relationship can be obtained:

$$d\sigma_m = K_s \left(d\varepsilon_v + K_\theta dp\right) \tag{10}$$

where:

$$K_s = K_1 - \frac{K_2^2}{K_3} \tag{11}$$

and

$$K_\theta = \frac{K_2}{K_1 K_3 - K_2^2} \tag{12}$$

By defining $d\varepsilon_\theta = -K_\theta dp$, a relationship analogous to that for thermal expansion (Zienkiewicz 1977) can be obtained:

$$d\sigma_m = K_s \left(d\varepsilon_v - d\varepsilon_\theta \right) \tag{13}$$

The case where θ can be treated as a free parameter occurs when the equations of equilibrium are not coupled to the equations of flow. Specifically, the suction (either prescribed or measured) is known. Such an assumption is valid for the case of low permeability. In this case, the water content can change near a boundary that is exposed to a suction condition but where significant flow is not induced away from the boundary.

The cracking process

The model development is based on the hypothesis that cracking in clay barriers is progressive and can extend to considerable depths despite the low permeability of the clay. The process is illustrated in Figure 54. Regardless of the low permeability of the clay soil, the clay will dry out at the surface, causing the clay to shrink and cracks to form. However, cracking is not a local phenomenon. Once a crack is formed, increasing the width of the crack at the surface by additional shrinkage will also extend the depth of the crack below that surface. The cracking exposes new surfaces to air, which initiates drying, causing further cracking. The key point is that the cracks driven by shrinkage within the dried zone expose material to the atmosphere beyond the ostensible depth of drying. Thus, the exposure of surfaces creates an avenue for more drying and its attendant cracking. The cracking can continue, provided the suction potential within the cracks is greater than that of the soil and at least one principal stress is tensile. Capturing this process with traditional groundwater models is impossible for two reasons. First, the progression of drying and cracking occurs with virtually no moisture movement in the intact soil, beyond what occurs immediately beneath the exposed surfaces. Thus, because the porosity created by the cracking system is not considered, the depth to which drying can extend is limited. Second, even with models that consider multiple continuum phases, the geometric distribution of the phases is specified a priori and does not capture the evolution of the cracking systems.

$$d\sigma^s = K_1 d\varepsilon_v + K_2 d\theta$$

$$dp = K_2 d\varepsilon_v + K_3 d\theta$$

$\sigma^s =$ Total stress

$\varepsilon_v =$ Volumetric strain

$p =$ Suction potential

$\theta =$ Water content

Compression

$d\varepsilon_v$

$p = 0$

$d\sigma^s$

Free Swell

$d\varepsilon_v$

$d\sigma^s = 0$

$d\theta$

Swell Pressure

$d\sigma^s$ $d\varepsilon_v = 0$

$d\theta$

Suction

dp $\sigma^s = 0$

$d\theta$
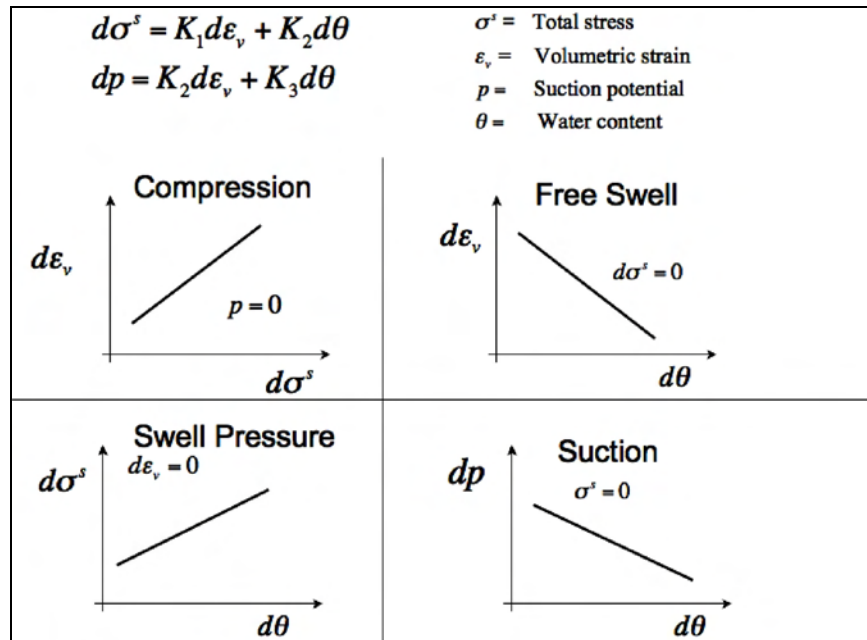
Figure 53. Incremental constitutive equations.

(The mechanical and moisture effects are coupled through a set of non-linear relationships shown here in their incremental linear form. The constants for the model can be determined from conventional soil tests.)

saturation line

a. Initial crack at surface

b. Crack driven below saturation line

c. Cracks allow access of atmospheric suction creating more cracks

Figure 54. Cracking processes.

(The crack is driven mechanically by the shrinking soil as it dries, creating surfaces at depth from which more drying can occur.)

Conditions are expected to be less conducive to cracking as depth increases. Water is transported through the crack system via the vapor phase, which necessitates a gradient in suction potential. Thus, the suction at crack surfaces should diminish with depth. Similarly, the stress state will be compressive below a depth where the compressive stress caused by the weight of the overburden is greater than the tensile stress induced by soil drying. Understanding these limiting factors of crack formation is one objective of developing the cracking model.
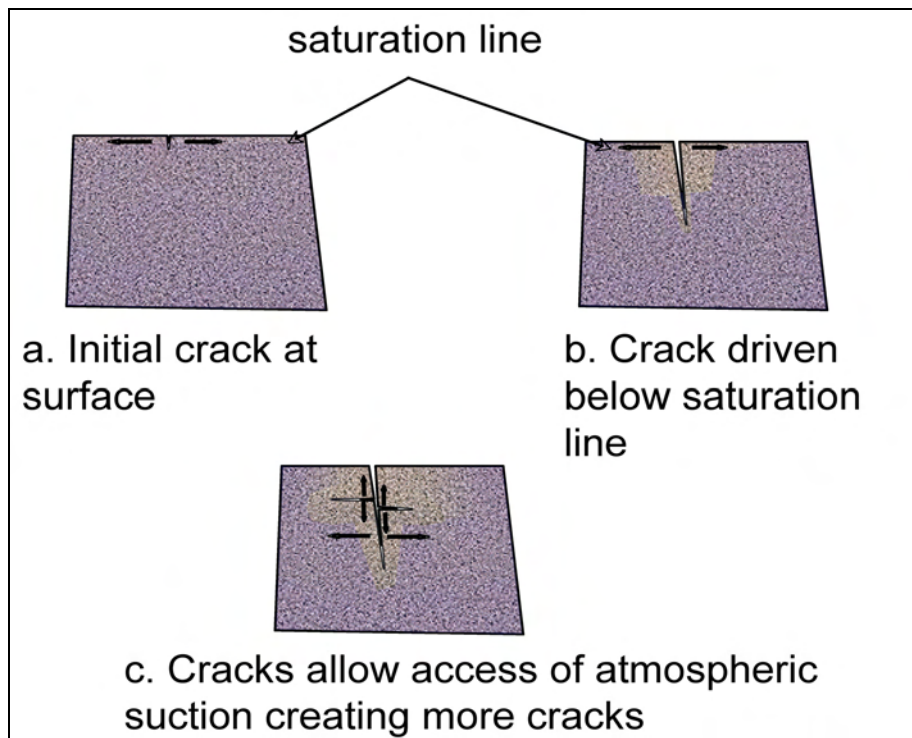
Model description

The cracking model consists of a finite element model of the soil shrinkage process that includes crack formation. Stresses within the intact material are caused by self weight (gravity stresses) and changes in water content (shrinkage). It is assumed that the water content within an element is in equilibrium with the suction potential. The suction potential within an element is approximated as the average value applied to the element boundaries (e.g., the average of the values applied to the nodes). As discussed previously, by specifying the suction potential, the water content becomes a free parameter that can be removed from the constitutive relationships. By this simplifying assumption, the water flow equations do not have to be explicitly included in the model.

The cracks are assumed to form at element boundaries. This assumption forces the crack system to conform to the geometry of the finite element system and, accordingly, might not produce cracks at their critical orientations. However, for the simple geometric configurations considered, this is believed to be a permissible approximation to the actual cracking process.

Finite element model

The finite element model is based on a three-dimensional regular grid as shown in Figure 55. Developed in-house by ERDC researchers, the model has several features conducive to efficient operation. The elements are identical; thus, element stiffness matrices are identical and do not have to be recomputed for each element. Further, the connectivity can be computed from the element number, which in turn is based on the logical (i, j, k) system that identifies the element with respect to the rows and columns in which it occurs. Thus, limited memory is required to describe model geometry; memory resources can be dedicated to the nodal degrees
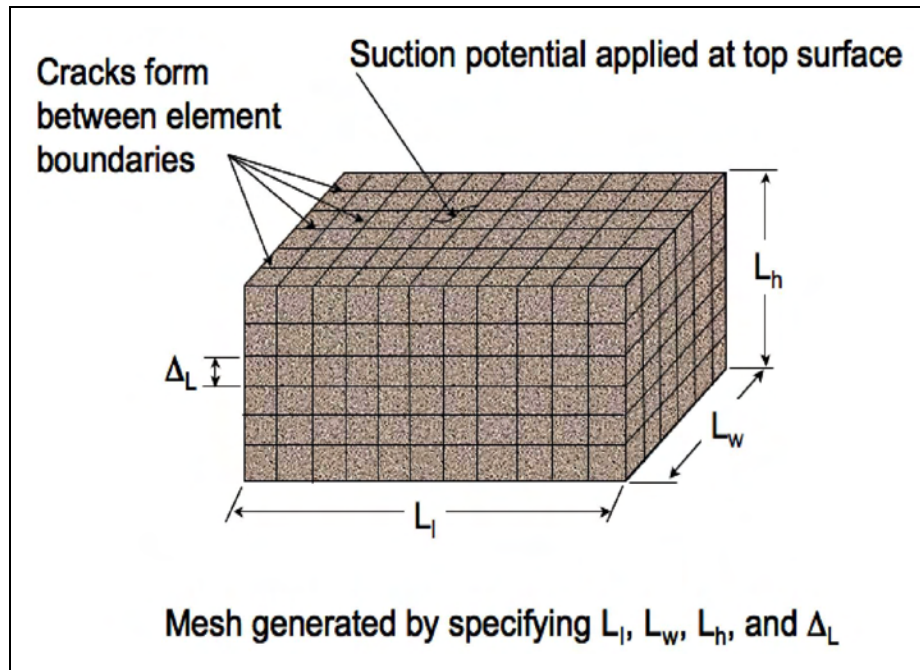
Figure 55. The rectangular finite element domain.

(The mesh details are generated within the program; the user only specifies the limits of the domain and the element size. The suction potential is applied at the top as a function of time. As cracks form at the top, the suction boundary condition is applied to newly formed crack surfaces.)

of freedom and state data. The element is defined by eight nodes and is an extension of a simple two-dimensional hybrid assumed-stress formulation described by Peters and Heymsfield (2004). The advantage of the element formulation is the need for an hourglass stabilization, which is obviated by the choice of stress assumption.

The stress response of the elements is assumed to be linear. The only non-linear aspect of the model is the crack formation that depends on the node-based state data. The state data are treated as an update in boundary condition. Therefore, the finite element computation is a sequence of linear stress computations, each of which is followed by an update of boundary geometry.

Stress computation

The stress computation is performed using explicit time integration of the dynamic equations of motion via a Verlet velocity scheme as it is described by Rieth (2003). A small damping is applied to the system such that, after several time steps, a static equilibrium condition is obtained. Therefore, there are two tiers of time stepping in the analysis. The main time

stepping, which denotes changes in the static equilibrium condition where the cracking condition is checked, and the internal stepping, which marches over the dynamic conditions, with fixed boundary conditions, until the static condition is obtained. Unless otherwise specified, all reference to time step implies the main time step. The internal stepping is merely a device to step from one static condition to another. The duration of the main time step is irrelevant and is only an indicator of the sequence of cracking events. Thus, the model does not provide information of the time involved in the cracking process, only its relative inevitability.

Cracking process

The cracking process is controlled by the normal stress acting on a potential crack plane. Cracks form between element boundaries by splitting the nodes into fragments, as illustrated in Figure 56. For the specific model considered here, cracks form in the coordinate directions (x, y, z) of the logical (i, j, k) coordinate system. Accordingly, each node consists potentially of eight fragments. When the stress across a pair of fragments exceeds the tensile strength, each fragment is assigned an independent degree of freedom which, from a connectivity standpoint, creates a crack. This process is illustrated in Figure 57 for a sequence consisting of forming a vertical crack followed by forming a horizontal crack.

The cracking process depends on stress values at the nodes. As for displacement-based finite element models in general, the stresses are computed within the element, not at the nodes. The stress values at the nodes are obtained from the consistent forces (f_i^e) computed from the
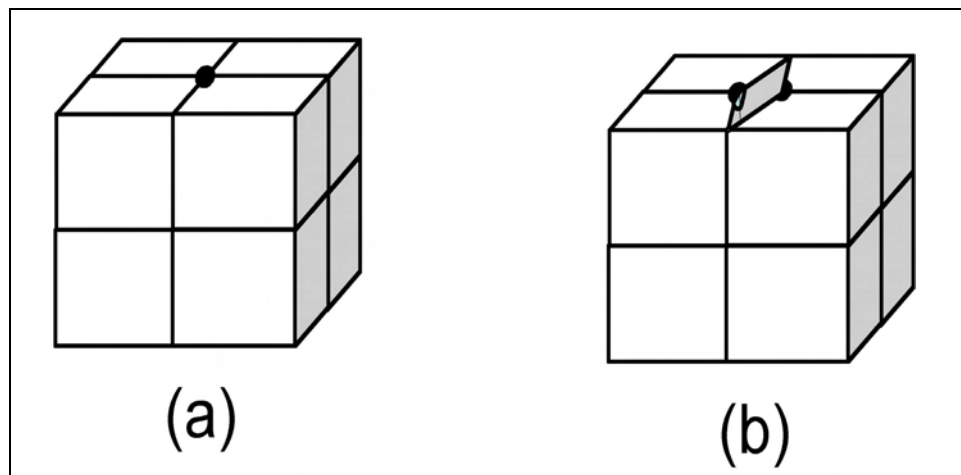

Figure 56. Crack formed in element group by splitting one node.
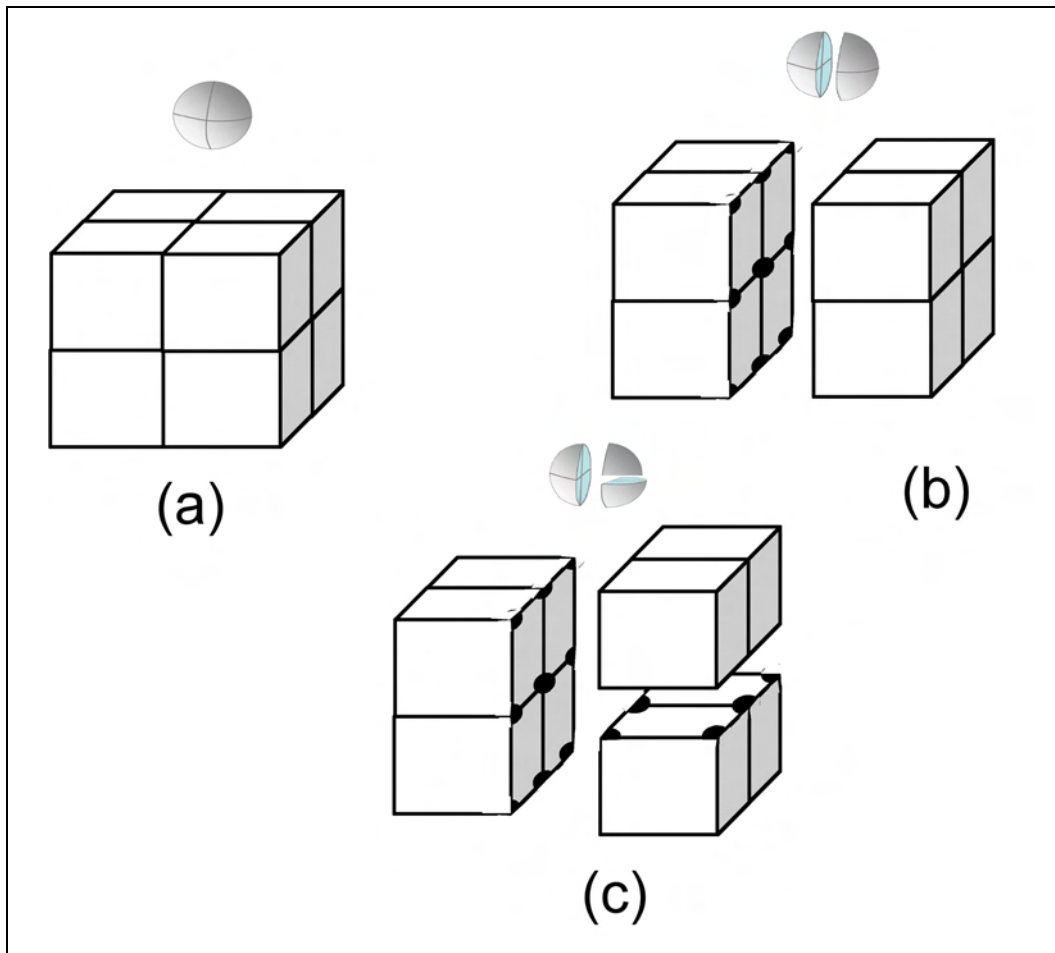
Figure 57. Process of subdividing nodes to create cracks along element boundaries.

For the eight elements shown (a), the vertical fracture is created by subdividing the nodes as shown in (b). Additional subdivision creates horizontal crack in right-hand element group, as shown in (c). The nodal subdivisions shown correspond to the central node.)

internal stress state. The three potential crack planes at the nodes correspond to three normal directions n_i^c. The cracking force is the projection of the nodal force projected on the potential crack direction,

$$f^c = f_i^e n_i^c \tag{14}$$

where repeated indices imply summation over the three coordinate directions. The crack stress, σ^c, is simply the cracking force divided by the area of the potential crack, $\sigma^c = f^c/A^c$. The area, A^c, of a node, depends on the cracking state of the neighboring nodes within the plane defined by n_i^c. As shown in Figure 58, the A^c is equal to

$$A^c = \frac{A^f}{2^{4-n^b}} \tag{15}$$

where:

$A^f = \Delta_f^2 =$ area of an element face

$n^b =$ number of neighboring nodes that are not cracked.

Note that one immediate effect of cracking a node is to reduce the contributing area available to adjacent nodes, thereby increasing their nodal stress.
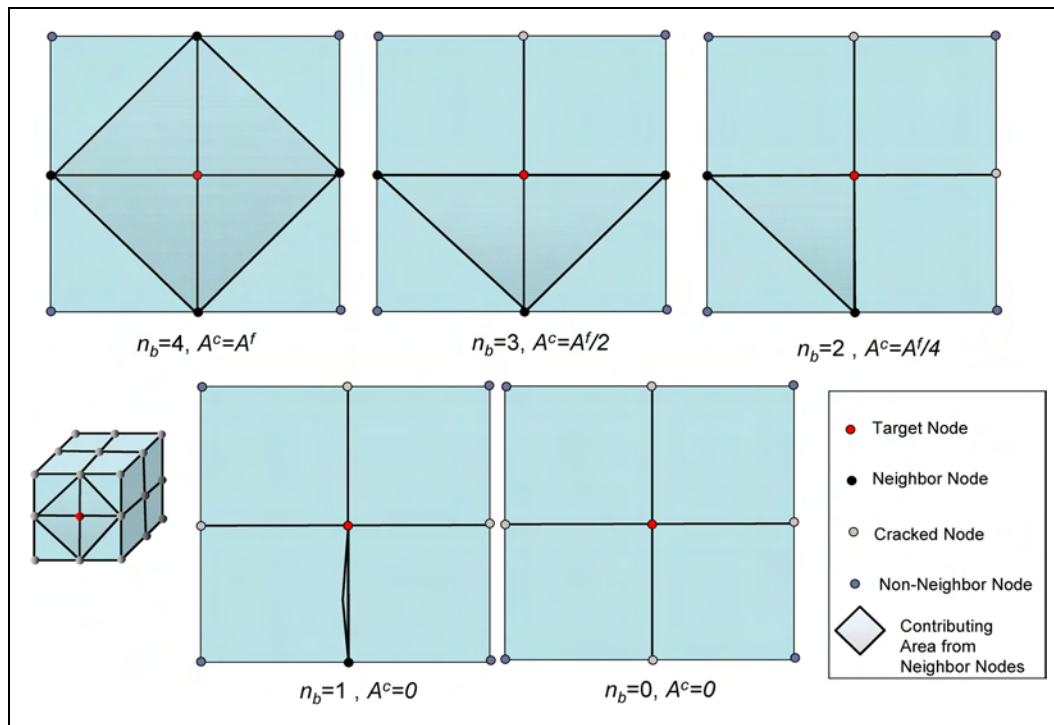
Figure 58. Assignment of area, A^c, to the central node (target node) based on the status of cracking on the neighboring nodes.

Crack model

Crack formation is controlled by a simple cohesive crack model. When the normal stress component across a crack boundary exceeds the crack resistance, a crack is formed (Figure 59). The cracking condition is checked at each node. The formation of the crack consists of creating new degrees of freedom at the node using the node fragmentation procedure described
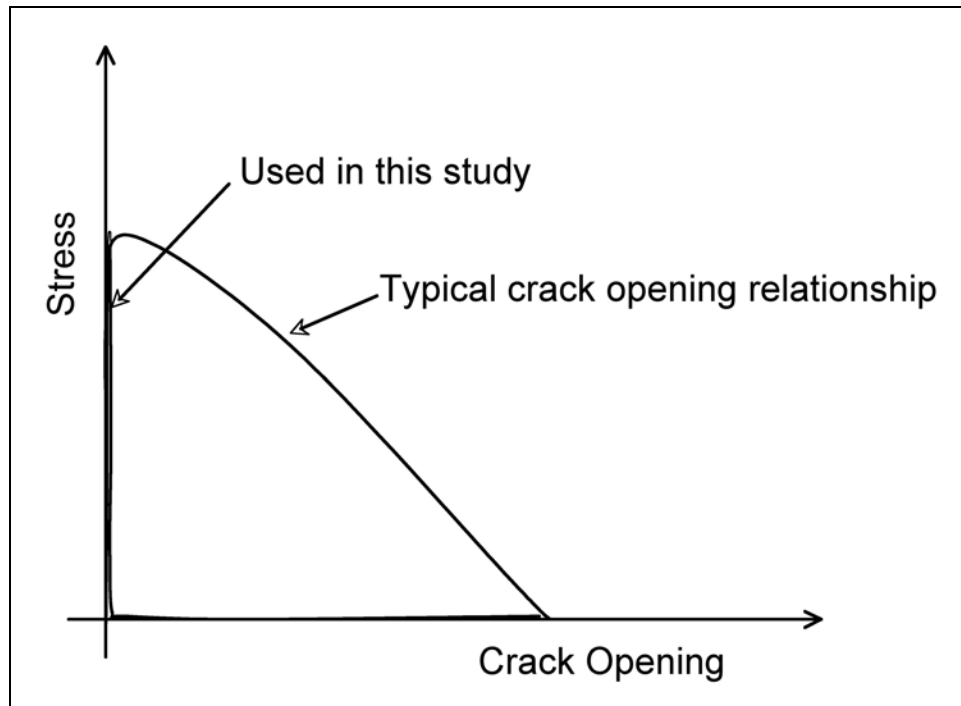
Figure 59. Relationship between crack opening and stress across crack interface.

*(This study employed a law in which the interface stress
dropped to zero upon reaching the fracture stress.)*

previously. The analysis proceeds in time, whereby the cracking condition
is checked at each time step. After a crack is formed, the domain is
changed in two ways. First, the crack plane becomes stress free, which
causes the stresses to redistribute around the cracked node. Second, the
suction condition is applied to the newly formed surface, which changes
the stress system. The changes combine to spread the cracking to adjacent
nodes or to induce cracking along other planes.

Parameter determination

The model relates the stress and suction changes to volumetric strain
through a coupled relationship that predicts shrink/swell behavior in an
unconfined condition and swells pressures in a confined condition. The
behavior is assumed to be reversible to simplify the analysis. Although
hysteresis is observed in actual experiments, cracking experiments
described in Chapter 3 showed that the shrink-swell process is nearly
reversible once cracks formed. The cracking itself is irreversible in that
cracks can close but do not heal.

The elastic parameters for the soil can be determined from standard soil experiments. The parameter, K_θ, can be determined from either swell tests or swell pressure tests. In the case of swell pressure, $d\varepsilon_v = 0$ and $d\sigma_m = K_s K_\theta dp$, where $d\sigma$ and dp are measured quantities, and K_s is determined from the elastic parameters. Presumably, the cracking stress, σ_c, can be measured from tensile tests on the soil. Unfortunately, tensile tests are difficult to perform. Alternatively, the approximation of $\sigma_c = FS_u$ was employed by Abu-Hejleh and Znidarčić (1995). A more direct approach is to perform a controlled drying experiment in which the increase in suction required to induce cracking is measured and the tensile stress computed for that suction.

Performing an analysis

The domain of the analysis is a rectangular region defined by the coordinates of its six faces (Figure 55). A grid of equal-size finite elements is automatically created to fill its volume. Therefore, the analysis requires no mesh generation. The geostatic stresses are computed from self weight such that the soil is in equilibrium. Suction potential is then applied at the surface based on the user-specified value. The analysis is then stepped through time as the soil responds to the shrinking/swelling driven by changes in suction at the evolving crack surfaces. If stress at element boundaries reaches a critical value, a crack is formed, creating a new boundary surface on which the surface suction is applied.

The applied suction potential can be specified as a function of time, providing a means to model both shrinking and swelling. The shrink/swell analysis is primarily intended for model validation. The present version of the model does not include transport of moisture within the cracks, and therefore represents a severe condition in which the suction potential at the surface is felt throughout the crack complex. A task for model improvement will be to implement a moisture-flow model for the vapor phase within the crack system to account for suction gradations.

Simulation of experimental test bed

Two analyses were conducted for the experimental setups described in Chapter 3. The first model domain corresponds to the drying box used in Experiment 1. As in the experiment, compacted clay having the dimensions of the drying box was allowed to dry from the surface. It was assumed that the soil was attached to the sides of the box and no moisture

flow occurred around the box boundaries. The second model domain cor-
responds to the drying box used in Experiment 3 with a pre-crack scored
down the center of the specimen. The soil consisted of a plastic (CH) clay,
which has a relatively large potential for cracking. The parameters used for
the model are given in Table 2.

Table 2. Model parameters for example problem.

Parameter	Symbol	Dimension	Value
Bulk modulus	K	psi	10,000.0
Shear modulus	G	psi	5,000.0
Cracking stress	σ_c	psi	0.4
Shrinkage index	K_θ	psi^{-1}	0.6×10^{-4}
Width	W	inches	18.0
Length	L	inches	18.0
Depth	D	inches	4.5
Element size	Δ_x	inches	1.0
	Δ_y	inches	1.0
	Δ_z	inches	0.25
Suction potential	P_s	psi	1.0

Figure 60 shows an example mesh for the analysis. Displacements were
fixed as zero on all boundaries except the top surface. The suction, P_s, was
applied to the entire top surface and to all crack surfaces as the cracks
formed. The model was cycled through five iterations to capture the pro-
gressive nature of the crack formation. The resulting crack formation for
Experiment 1 is shown in Figure 61. The curling on the top surface is
apparent, as is the dominance of cracks in the horizontal plane. In fact,
cracking occurred in all planes. Cracking in the vertical planes tended to
involve smaller displacement across the crack and is therefore more
difficult to distinguish in the image.

Remarks on cracking pattern

The cracking pattern obtained in the first example simulation agrees well
with observations from the experiments described in Chapter 3. One of the
explanations of the dominance of the horizontal cracks was the tendency
of the cracks to follow the path of least resistance, which is presumed to
be the horizontal compaction lift boundaries. However, the simulation
did not account for any anisotropy in the cracking or elastic properties.
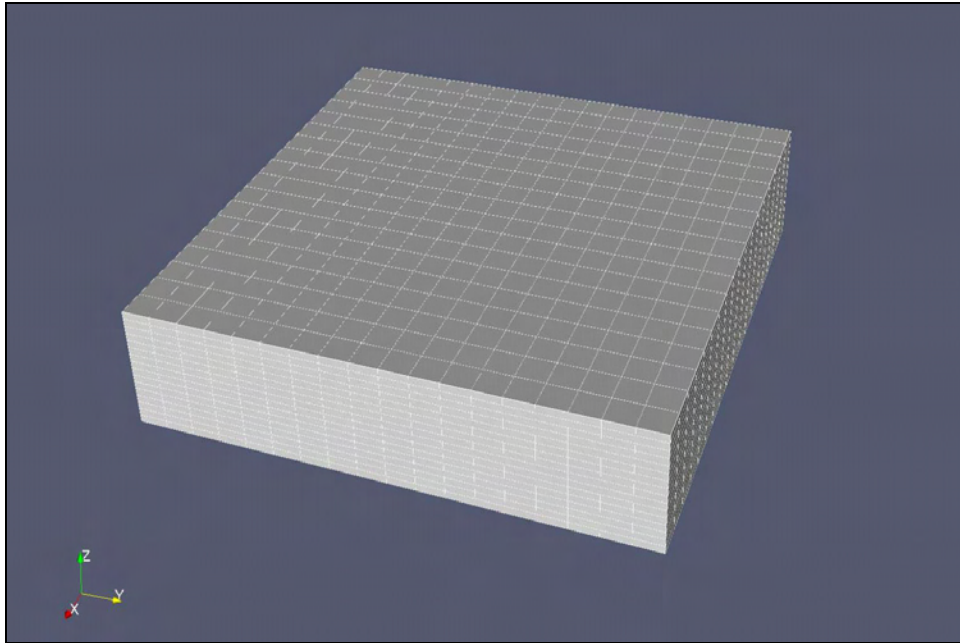
Figure 60. Finite element model for example problem.

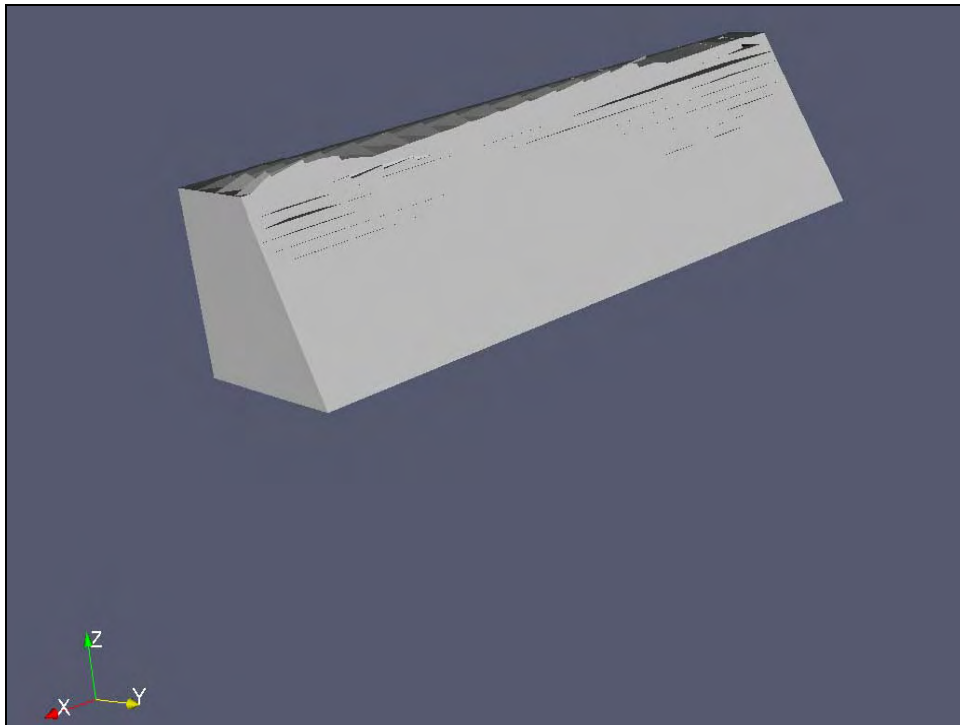**Figure 61. Cut-away view of end state of cracking.**

(Displacements have been exaggerated to make cracking apparent. The effects of curling in blocks created by surface cracks are clearly visible. Visible cracking is dominated by horizontal cracking. Vertical cracking also occurred throughout the thickness of the block, but with crack openings too small to be discernible in the image.)

Thus, the tendency to form horizontal cracks in the simulation is not a result of compaction lifts. It is more likely that the horizontal cracks are wider because the soil is confined in the horizontal direction, which favors vertical shrinkage strains resulting in horizontal cracks. Also, the sizes of the horizontal crack openings are enhanced by the curling tendency that results from the variation in shrinkage strain across the layers. The fact that the essential features of the cracking process can be captured without appealing to arguments based on unmeasurable lift properties simplifies interpretation of the cracking experiments.

The second analyses using the scored line produced the cracking behavior shown in Figure 62. In this experiment, a pre-crack is introduced along the middle of the specimen parallel to the constrained sides. The results, however, show little change in overall crack response from the first analyses. Surface curling was again evident as was horizontal cracking and therefore vertical cracking at depth. Figure 63 shows the cracking pattern with the soil mass removed. From this exaggerated view of the cracking pattern, vertical cracks are evident at each element seam but with irregularly sized horizontal cracking with depth. This is similar to the behavior observed in Experiment 3 as the primary crack locations varied with depth of the compacted layer. Therefore, the numerical model is able to capture the irregular cracking pattern indicative of typical field response versus a symmetric, uniform crack distribution.

Cracking reduction due to overburden stresses

It is possible for overburden stresses to restrain the cracking behavior of the soil, essentially by producing enough compressive stresses within the clay that the tensile strength of the clay mass is never exceeded. The magnitude of overburden required to achieve this is quite considerable owing to the high tensile stresses that are possible in a typical highly plastic clay that is subjected to long-term drying effects. The suction present in a clay mass can be determined based on the relative humidity present at the interface between the clay and its immediate surface. Equation 16 shows the conversion from relative humidity (*RH*) and temperature (*T*) to suction (Ψ).

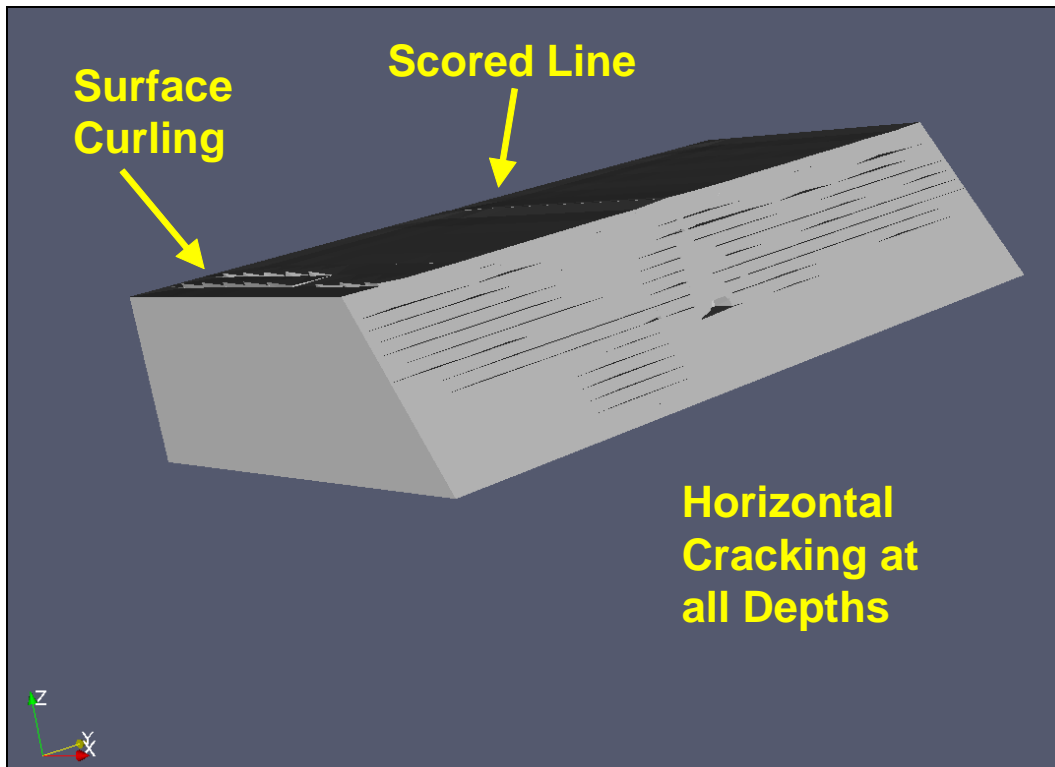$$\Psi = \frac{RT}{v_{wo}\omega_v}\ln(RH) \tag{16}$$

Figure 62. Model simulation of the end state of cracking within the clay mass with a scored line down center.

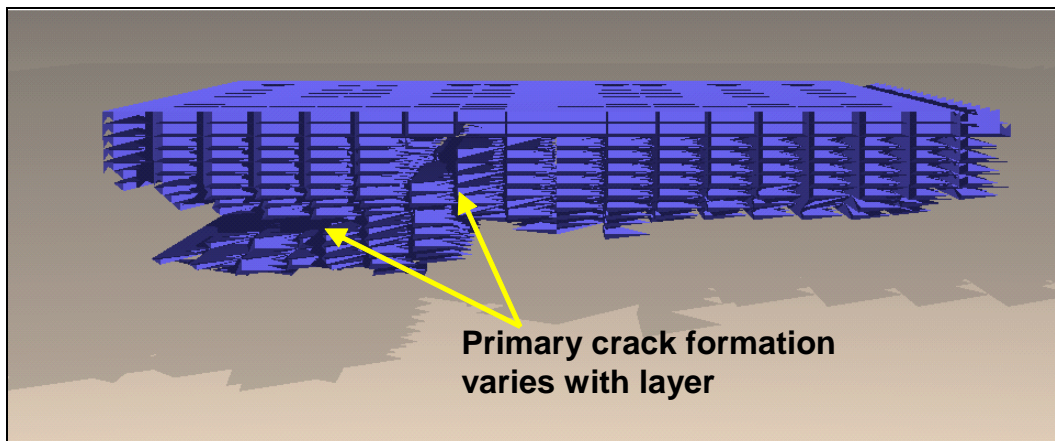*(Displacements have been exaggerated to make cracking apparent.)*

Figure 63. Image of crack surfaces within the clay mass with solids removed.

where:

Ψ = suction (kPa)
R = universal gas constant = 8.31432 J/(mol * °K)
T = temperature in Kelvin = (273.16 + °C)
v_{wo} = specific volume of water = 1/1000 m³/kg
ω_v = mass of water vapor = 18.016 kg/kmol
RH = relative humidity in decimal
Joule = kg/(m²*s²)
kPa = 1000 J/m³.

The result is the following general expression:

$$\Psi\ (kPa)\ =\ -460.573\ *\ (273.16\ +\ °C)\ *\ \ln\ (RH) \qquad (17)$$

A simple calculation of the required overburden thickness is conducted based on the model constraints. Consider the plastic clay at a nominal relative humidity of 99.5%, which is a reasonable estimate of relative humidity found within a few particle depths beneath the clay surface when in contact with a porous, unsaturated overburden layer. Assuming a subsurface temperature of 10 °C, one obtains a suction of 650 kPa within the clay mass. Assuming that if the tensile strength of the soil is not exceeded then no strains exist in the soil, a condition $d\varepsilon_v = 0$, then one can rewrite Equation 13 as

$$d\sigma_m = K_s (K_\theta dp) \qquad (18)$$

Using the model parameters from Table 2, the change in tensile stress associated with that magnitude of suction would be 0.6 * 650 kPa = 390 kPa. To prevent a tensile crack from forming, a horizontal compressive stress of 390 kPa would be required, and twice that much in the vertical direction, assuming 50% of the vertical load is transferred horizontally. Considering an effective unit weight of soil of 20.4 kg/m³, one obtains an overburden thickness of 780 kPa/20.4 kg/m³ = 38 m. This is an enormous volume of soil to place over the clay, suggesting that, as long as changes in moisture conditions are allowed to occur over the surface of the clay barrier, tensile cracking will occur.

Summary

The model is based on the following assumptions:

- Moisture movement through the primary porosity requires very long time periods and can therefore be ignored.
- Moisture can be removed from the immediate surface of the soil by evaporation, causing the soil to shrink.
- Secondary porosity is created by cracks that extend from the surface as a result of shrinkage.
- Mechanically induced stresses can drive cracks below the saturation front, thereby exposing the soil to drying well below the depth computed from moisture movement through the primary porosity.

The basis of the model is that the cracking is a mechanical process that involves moisture movement only at the immediate surface of the soil and is propagated in time by the creation of new surfaces. From this view, standard groundwater models are not applicable to understanding the cracking process. However, the model ignores the movement of moisture through the secondary porosity and therefore presents a severe condition for crack growth. In fact, it is expected that, as the crack system develops, a suction gradient would be required to move moisture from deeper portions of the crack to the surface.

Another issue implicit in the model is the scale of the cracking. The crack spacing is limited by the element size, Δ_f. Also, if suction is applied to the surface of the element, the entire element feels the effects. Thus, the depth to which the effects of suction extends is equal to Δ_f. Features of secondary porosity smaller than Δ_f cannot be captured by the model. The extent to which a crack system can be simulated depends on the computer resources.

5 Conclusion and Recommendations

Conclusions

This report investigated the nature of cracking behavior in compacted clay liners. A thorough literature review on the current state of practice for construction of compacted clay liners revealed that significant infiltration of water into clay barriers occurs despite predictions of hydrologic models that such infiltration should be minimized by the low permeability of the clay. Numerous field studies revealed that the cause of the high water intrusion is a direct result of cracks occurring as a result of vertical water vapor transport at the surface of the clay layer. These cracks will form quickly in compacted clay liners, independently of current techniques to mitigate cracking. Even composite caps that include clay liners overlain with geomembranes fail to provide effective resistance to water vapor transport because of defects that occur during the construction process. The studied hydrologic models do not account for the crack formation caused by drying which induces a secondary porosity that greatly increases the bulk permeability of the clay mass.

Results of the experimental program provided several important observations about crack propagation, which supported observed field behaviors and directed the design of an appropriate numerical model.

- Crack formations are very diverse along the surface layer and as they migrate downward. Shapes of cracks are not uniform or symmetric—evolving from thin webs of microcracks to a select number of wide primary cracks that, in turn, can seal off existing microcracks.
- The crack behavior was validated by pressure sensor readings exhibiting initially high compressive lateral stress that decreased to zero after 4 hr during microcrack formation (full tension). This was followed by a rebound to a compressive stress state after 20 hr, when the formation of large primary cracks began to cause closure o f the existing microcracks.
- Unbalanced stress loads from top to bottom of a horizontal crack induce a curling effect on the clay surface. As the soil continues to dry with depth and the boundary moisture conditions on the surfaces of the horizontal crack become balanced, an uncurling effect is noted.
- Time-lapse photography showed that the coupling of soil curling with primary crack formation leads to formation of "clay islands," which are free to

> shift and move along interfaces between compacted lifts. The exposed soil also allows drying to continue to deeper levels within the clay mass.

- Any imperfections in compaction, including scoring between compacted lifts, causes propagation of deep cracks, suggesting field defects can expedite cracking.

Once the mechanics of the cracking process were better defined, numerical parameters for shrink-swell models necessary for a quantitative model of cracking were obtained. The developed numerical model was based on the hypothesis that cracking in clay barriers is progressive and can extend to considerable depths despite the low permeability of the clay mass. Once an initial crack is formed at the surface, increasing the width of the crack by additional shrinkage will drive the crack deeper into the soil mass, exposing new surfaces to air. These fresh surfaces enable further drying and cracking, both horizontally and vertically within the soil mass. The cracking model consists of a finite element model of the soil shrinkage process that includes crack formation. Stresses within the intact material are caused by self weight (gravity stresses) and changes in water content, which induce shrinkage as a result of suction-induced tensile stresses. The cracks are assumed to occur at the element boundaries, forcing the crack system to conform to the geometry of the finite element system. This was assumed a satisfactory approximation to capture the simple geometry of the experimental program.

Results from the two numerical simulations on digital test beds representing Experiments 1 and 3 (continuous and pre-cracked) agreed well with the experimental observations. The model was dominated by horizontal cracking, not as a result of the influence of compaction lifts, but because the soil is confined in the horizontal direction, which favors vertical shrinkage strains resulting in horizontal cracks. Also, the size of the horizontal crack openings is enhanced by the curling tendency that results from the variation in shrinkage strain across the layers. In the second pre-crack simulation, little change was observed in the overall cracking response from the first analysis. From an exaggerated view of the cracking pattern, vertical cracks are evident at each element seam but with irregularly sized horizontal cracking with depth. This is a phenomenon very similar to the observed experimental behavior where primary crack locations varied with layer position. The fact that the essential features of the cracking process can be captured without appealing to arguments based on unmeasurable lift properties simplifies interpretation of the cracking

experiments. Therefore, the numerical model is able to capture the irregular cracking pattern indicative of typical field response versus a symmetric, uniform crack distribution.

Future research with the model will increase our understanding of how the physical soil parameters interact to complete the mechanistic model of the cracking process. Certainly, example simulations should be performed for geometries similar to barriers at actual waste sites. However, both field observations and the modeling effort point to the inevitability of cracking in clay soil that is exposed to drying. Therefore, better information on the mechanics of the cracking process does not necessarily lead to better barrier designs. The critical question to be answered beyond this project is how to protect the clay from drying.

The weight of the evidence from the published field studies, experiments, and numerical simulation clearly documents the inevitability of cracking in clay liners. The atmospheric suction potential, computed from relative humidity, is sufficient to cause cracking, even in temperate climates. The overburden stress is insufficient to offset the tensile stresses. It is concluded that clay liners are generally not adequate as a long-term moisture barrier.

At issue is that most liner designs strive to create an upward vertical gradient designed to keep water out of the overburden layers rather than infiltrating down into the waste material. This increases the instance of drying on the clay surface, which inevitably leads to cracking. This suggests that change to the current design criteria for engineered barriers is necessary to enable the clay surface environment to remain in a fixed, as-compacted state.

Recommendations for future research

The conclusions suggest the state of the practice for design of engineered barriers using a clay liner design cannot provide an intact layer sufficient to withstand moisture infiltration for 1000 years. The complex nature of crack propagation suggests that the best approach to achieving a successful design is to maintain the in situ characteristics of the compacted liner without change over the lifetime of the engineered barrier. This can be done in one of two ways: (1) developing improved characteristics of the clay liner such that it is much less susceptible to cracking or (2) developing multilayer soil systems that can maintain moist conditions at the surface

of the clay liner while still providing adequate evapotranspiration to prevent flooding of the liner system. To improve the characteristics of the clay barrier, several concepts are described that are in no way an exhaustive list of potential alternative cover designs.

Optimization of silt content

The silt content plays a critical role in the constitutive response of the fine-grained mass. Gap-graded materials such as clay-silt mixtures can exhibit radically different physical responses with small changes in size fractions (Figure 64), similar to those observed in more typical sand-clay mixtures (Berney and Peters 2004). An investigation into the development of optimum silt content to minimize clay cracking is proposed. This research effort would require a shrinkage analysis of silt-clay mixtures followed by prototyping the technology to adequately mix silt-clay fractions to achieve desirable shrink behavior. This prototyping could then be upsized to field-scale machinery for use in applications.
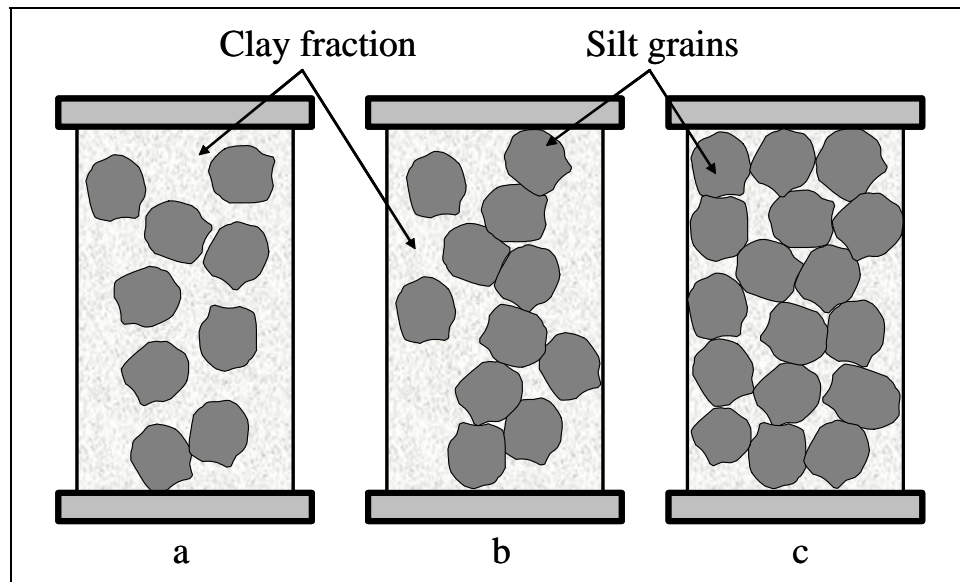

Figure 64.Illustration of clay-silt fractions.

*(Clay-dominated response (a) (high shrinkage), (b) transitional
point where silt-clay behavior is mixed (medium shrinkage),
(c) silt-dominated behavior (low shrinkage).)*

Stabilized overlying protective layer

The placement of geosynthetic liners poses a great risk in the effectiveness of an engineering barrier because any defect during placement can be a focal point for future leakage. It is proposed that application of a 5- to

15-cm layer of sand stabilized with virgin liquid asphalt, which does not degrade when in contact with water, be mixed and placed over the clay barrier (Figure 65). This could be laid down easily over the undulating surface of the compacted clay and would provide a flexible, impermeable and, more importantly, a vapor barrier preventing moisture from escaping the clay and keeping its compacted conditions constant. Other stabilizing additives such as surfactants or cement and applications such as foamed asphalt can be explored to satisfy current field construction techniques.
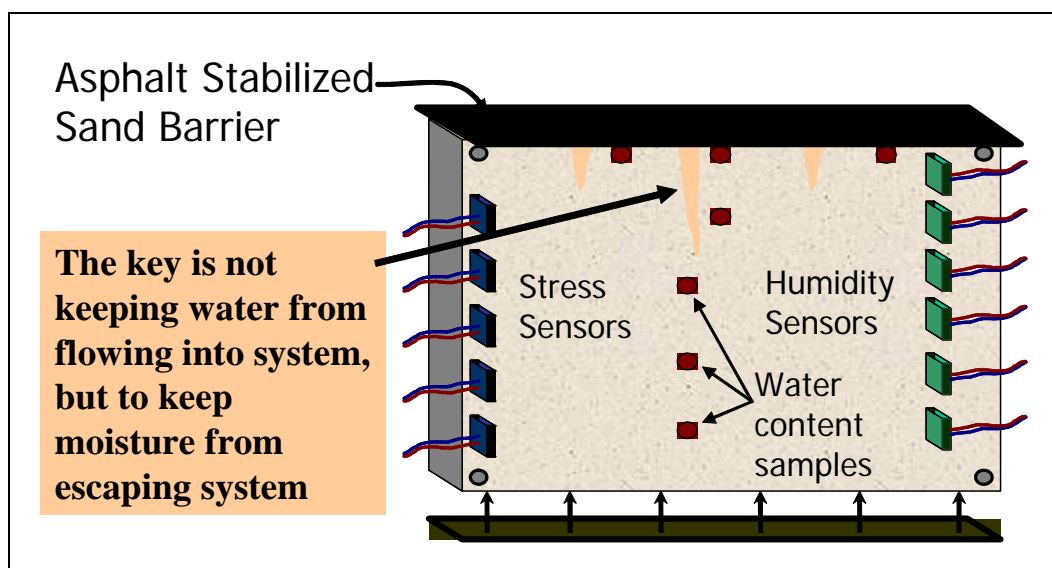

Figure 65. Laboratory investigation of stabilized surface layers overlying the compacted clay barrier.

Introduction of ultra-compact soils

There is the possibility that grain size distributions exist that can be classified as impermeable sand, a concept called ultra-compact soils. A proper gradation would be determined that would minimize clay content and cracking potential yet maximize impermeability in a strong flexible barrier that requires nothing more than proper compaction. Figure 66a shows a well-graded gradation currently thought of as best-practice guidance on building a strong soil. However, forces are carried through chains of larger particles in these types of gradations, leaving finer particles unstressed and therefore in an unstable state. Figure 66b shows an ultra-compact soil gradation (Vernet 2004) that suggests the usage of an even distribution of gap-graded particle sizes that, when compacted, provide a much tighter, interlocked system that is more resistant to failure and can provide impermeability without the risk of cracking.
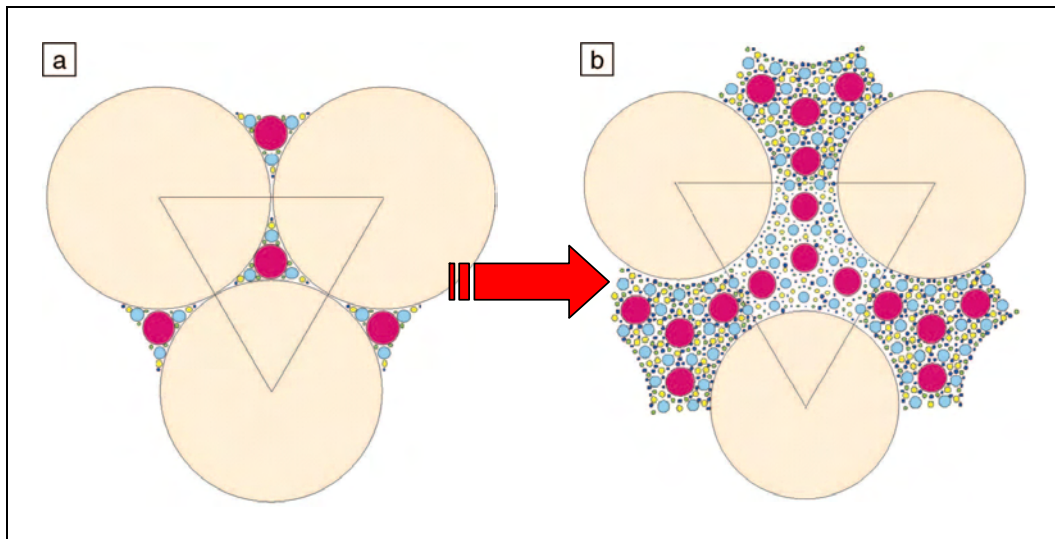
Figure 66. Idealization of (a) well-graded soil mixture versus (b) ultra-compact graded soil mixture (Vernet 2004).

Proper design of multilayer systems

The need exists to determine criteria for proper multilayer soil systems that may include sand filters and other material types that will perform a dual role: first, to allow moisture to the clay surface to prevent cracking and, second, to maintain sufficient evapotranspiration to prevent flooding of the liner system. A subsurface irrigation technique could also be employed to provide sufficient moisture to the clay surface while having little impact on moisture infiltration from rain events. The latter technique would require continual maintenance to monitor moisture migration and proper system operation.

6   References

40 Code of Federal Regulations (CFR). 2008. *Part 192—Health and environmental protection standards for uranium and thorium mill tailings.* Washington, DC: U.S. Environmental Protection Agency.

Abu-Hejleh, A. N., and D. Znidarčić, D. 1995. Desiccation theory for soft cohesive soils. *Journal of Geotechnical Engineering* 121(6):493–502.

Aitken, G.W., and R. L. Berg. 1968. *Digital solution of modified Berggren equation to calculate depths of freeze and thaw in multilayered systems.* Special Report No. 122. Hanover, NH: U.S. Army Cold Regions Research and Engineering Laboratory.

Albrecht, G. 1996. Effect of desiccation on compacted clay. MS thesis, Univ. of Wisconsin.

Albrecht, B. A., and C. H. Benson. 2001. Effect of desiccation on compacted natural clays. *Journal of Geotechnical and Geoenvironmental Engineering* 127(1):67–75.

_____. 2002. Closure to "Effect of desiccation on compacted natural clays." *Journal of Geotechnical and Geoenvironmental Engineering* 128(4):357–360.

Albright, W. H., C. H. Benson, G. W. Gee, A. C. Roesler, T. Abichou, P. Apiwantragoon, B. F. Lyles, and S. A. Rock. 2004. Field water balance of landfill covers. *Journal of Environmental Quality* 33:2317–2332.

Aldrich, H.P., and H. M. Paynter. 1953. *Analytical studies of freezing and thawing of soils, first interim report.* Technical Report No. 42. Concord, MA: U.S. Army Engineer Division, New England, Arctic Construction and Frost Effects Laboratory.

Aubertin, M., and B. Bussière. 2001. Discussion: Water flow through cover soils using modeling and experimental methods. *Journal of Geotechnical and Geoenvironmental Engineering* 127(9):810.

Bachmann, J., R. Horton, and R. R. van der Ploeg. 2001. Isothermal and nonisothermal evaporation from four sandy soils of different water repellency. *Soil Science Society of America Journal* 65:1599–1607.

Basnett, C., and R. Bruner. 1993. Clay desiccation of a single-composite liner system. *Geosynthetics '93 Conference, Vancouver, Canada.*

Benson, C. H. 1997. *A review of alternative landfill cover demonstrations.* Environmental Geotechnics Report 97-1. Madison, WI: University of Wisconsin.

_____. 2000. Liners and covers for waste containment. *Proceedings, Fourth Kansai International Geotechnical Forum, Creation of a New Geo-environmental, Japanese Geotechnical Society, 24–26 May 2000, Kyoto, Japan.*

_____. 2001. Waste containment: Strategies and performance. *Australian Geomechanics* 36(4):1–25.

Benson, C. H., and M. Khire. 1995. Earthen covers for semi-arid and arid climates. In *Landfill closures*. GSP No. 53, ed. J. Dunn and U. Singh, 201–217. Reston, VA: American Society of Civil Engineers.

Benson, C. H., and M. Othman. 1993. Hydraulic conductivity of compacted clay frozen and thawed in situ. *Journal of Geotechnical Engineering* 119(2):276–294.

Benson, C. H., T. H. Abichou, M. A. Olson, and P. J. Bosscher. 1995. Winter effects on hydraulic conductivity of compacted clay. *Journal of Geotechnical Engineering* 121(1):69–79.

Benson, C.H., D. E. Daniel, and G. P. Boutwell. 1999. Field performance of compacted clay liners. *Journal of Geotechnical and Geoenvironmental Engineering* 125(5):390–403.

Benson, C. H., P. A. Thorstad, H. Jo, and S. A. Rock. 2007. Hydraulic performance of geosynthetic clay liners in a landfill final cover. *Journal of Geotechnical and Geoenvironmental Engineering* 133(7):814–827.

Berney, E. S., IV. 2004. *A partially saturated constitutive theory for compacted fills*. ERDC/GSL TR-04-4. Vicksburg, MS: U.S. Army Engineer Research and Development Center.

Berney, E. S., IV, and J. F. Peters. 2004. Percolation threshold of sand-clay binary mixtures. *17th American Society of Civil Engineers Engineering Mechanics Conference*, Newark, DE.

Berney, E. S., IV., J. F. Peters, and D. M. Smith. 2003. The thermodynamics of three-phase partially saturated soil. In *Proceedings of the 16th Engineering Mechanics Conference*. Seattle, WA: Univ. of Washington.

Boardman, T., and D. E. Daniel. 1996. Hydraulic conductivity of desiccated geosynthetic clay liners. *Journal of Geotechnical Engineering* 122(3):204–208.

Chertkov, V. Y. 2000. Using surface crack spacing to predict crack network geometry in swelling soils. *Soil Science Society of America Journal* 64:1918–1921.

_____. 2001. Reply to comments on using surface crack spacing to predict crack network geometry in swelling soils. *Soil Science Society of America Journal* 65:1574.

_____. 2002. Characteristic crack dimension of saturated drying soils: Theory and applications. *Agricultural Engineering International: CIGR Journal of Scientific Research and Development*, Manuscript LW 02 00s, (IV, Dec).

Chertkov, V. Y., and I. Ravina. 1998. Modeling the crack network of swelling clay soils. *Soil Science Society of America Journal* 62:1162–1171.

_____. 1999. Tortuosity of crack networks in swelling clay soils. *Soil Science Society of America Journal* 63:1523–1530.

Choo, L., and E. K. Yanful. 2000. Water flow through cover soils using modeling and experimental methods. *Journal of Geotechnical and Geoenvironmental Engineering* 126(4):324–334.

Corser P., and M. Cranston. 1991. Observations on the performance of composite clay liners and covers. In *Proceedings, Geosynthetic Design and Performance.* Vancouver, BC, Canada: Vancouver Geotechnical Society.

Day, R. W. 1997. Discussion: Hydraulic conductivity of desiccated geosynthetic clay liners. *Journal of Geotechnical and Geoenvironmental Engineering* 123(5): 484–486.

de Vries, D. A. 1958. Simultaneous transfer of heat and moisture in porous media. American Geophysical Union. *Eos Transactions* 39(5):909–916.

de Vries, D. A., and N. H. Afgan. 1975. *Heat and mass transfer in the biosphere.* New York: John Wiley and Sons.

Department of Energy. 2002. *Alternative landfill cover: Innovative technology summary report.* EOE/EM-0558. Sandia, NM: Sandia National Laboratories.

Döll, P. 1996. Modeling of moisture movement under the influence of temperature gradients: desiccation of mineral liners below landfills. PhD thesis. Germany: Technical University of Berlin.

_____. 1997. Desiccation of mineral liners below landfills with heat generation. *Journal of Geotechnical and Geoenvironmental Engineering* 123(11):1001–1009.

Fayer, M., and Jones, T. 1990. *Unsaturated soil-water and heat flow model, version 2.0.* Richland, WA: Pacific Northwest Laboratory.

Gibson, R. E., G. L. England, and M. H. L. Hussey. 1967. The theory of one-dimensional consolidation of saturated clays, I. finite nonlinear consolidation of thin homogeneous layers. *Geotechnique* 17(3):261–273.

Giroud, J. P., and R. Bonaparte. 1989. Leakage through liners constructed with geomembranes, Part I: geomembrane liners. *Geotextiles and Geomembranes* 8(1):27–67.

Hauser, V. L., B. L. Weand, and M. D. Gill. 2001. Natural covers for landfills and buried waste. *Journal of Environmental Engineering* 127(9):768–775.

He, G., H. Solo-Gabriele, and K. V. Wong. 1998. Infiltration rates through landfill cover systems. *Journal of Solid Waste Technology and Management* 25(3–4):161–167.

Hewitt, P. J., and L. K. Philip. 1999. Problems of clay desiccation in composite lining systems. *Engineering Geology* 53:107–113.

Hillel, D. 1982. *Introduction to soil physics.* San Diego, CA: Academic Press.

Horton, R., P. J. Wierenga, and D. R. Nielsen. 1983. Evaluation of methods for determining the apparent thermal diffusivity of soil near surface. *Soil Science Society of America Journal* 47:25–32.

James, A. N., D. Fullerton, and R. Drake. 1997. Field performance of GCL under ion exchange conditions. *Journal of Geotechnical and Geoenvironmental Engineering* 123(10):897–901.

Khire, M. V., C. H. Benson, and P. J. Bosscher. 1997. Water balance modeling of earthen final covers. *Journal of Geotechnical and Geoenvironmental Engineering* 123(8):744–754.

Kim, W., and D. Daniel. 1992. Effects of freezing on hydraulic conductivity of compacted clay. *Journal of Geotechnical Engineering* 118(7):1083–1097.

Kimball, B. A., R. D. Jackson, R. J. Reginato, F. S. Nakazama, and S. B. Idso. 1976. Comparison of field-measured and calculated soil-heat fluxes. In *Proceedings Soil Science Society of America* 40:18–25.

Kodikara, J. H., H. Nahlawi, and A. Bouazza. 2004. Modeling of curling in desiccated clay. *Canadian Geotechnical Journal* 41(3):560–566.

Koerner, R. M., and D. W. Daniel. 1997. *Final covers for solid waste landfills and abandoned dumps*. New York: American Society of Civil Engineers.

Koh, R.C.Y., and L. N. Fan. 1970. *Mathematical models for the prediction of temperature distributions resulting from the discharge of heated water in large bodies of water*. 16130DW010/70. Washington, DC: US Environmental Protection Agency, Water Quality Office.

Kraus, J. F., C. H. Benson, A. E. Erickson, and E. J. Chamberlain. 1997. Freeze-thaw cycling and hydraulic conductivity of bentonitic barriers. *Journal of Geotechnical and Geoenvironmental Engineering* 123(3):229–238.

Lake, C. B., and R. K. Rowe. 2005. The 14-year performance of a compacted clay liner used as part of a composite liner system for a leachate lagoon. *Geotechnical and Geological Engineering* 23:657–678.

Lambe, W. T., and Whitman, R. V. 1969. *Soil mechanics*. New York: John Wiley and Sons.

Landreth, R. E., D. E. Daniel, R. M. Koerner, P. R. Schroeder, and G. N. Richardson. 1991. *Design and construction of RCRA/CERCLA final covers*. U.S. Environmental Protection Agency Seminar Publication, EPA/625/4-91/025. Washington, DC: Government Printing Office.

Lau, T. T. K. 1990. Desiccation cracking of soils. MSc thesis. Saskatoon, Saskatchewan, Canada: University of Saskatchewan.

Leavell, D. A., and J. F. Peters. 1988. *Uniaxial tensile test for soil*, Technical Report GL-87-10. Vicksburg, MS: U.S. Army Engineer Waterways Experiment Station.

Lettau, H. 1954. Improved models of thermal diffusion in the soil. *Transactions of the American Geophysical Union* 35:121–132.

Lettau, B. 1971. Determination of the thermal diffusivity in the upper layers of a natural ground cover. *Soil Science* 112: 172–177.

McBrayer, M.C., M. Mauldon, E. C. Drumm, and G. V. Wilson. 1997. Infiltration tests on fractured compacted clay. *Journal of Geotechnical and Geoenvironmental Engineering* 123(5):469–473.

Melchior, S. (1997). In situ studies on the performance of landfills caps. In *Proceedings International Containment Technology Conference*, 365–373. Germantown, MD: U.S. Department of Energy.

Miller, C. J., and M. Mishra. 1989. Modeling of leakage through cracked clay liners: II. A new perspective. *Water Resources Bulletin* 25:557–563.

Milly, P. C. D. 1984. A simulation analysis of thermal effects on evaporation from soil. *Water Resources Research* 20(8):1087–1098.

Mitchell, J. K., D. R. Hooper, and R. G. Campanella. 1965. Permeability of compacted clay. *Journal of the Soil Mechanics and Foundation Division* 91(SM4):41–65. American Society of Civil Engineers.

Montgomery, R., and Parsons, L. 1989. The Omega Hills final cover test plot study: Three year data summary. In *Proceedings 1989 Annual Meeting of the National Solid Waste Management Association, Washington, DC.*

Nobre, R. C. M., and N. R. Thomson. 1993. The effects of transient temperature gradients on soil moisture dynamics. *Journal of Hydrology* 157:57–101.

Office of Nuclear Regulatory Research. 2002. *Radionuclide transport in the environment: Research program plan*. Office of Nuclear Regulatory Research. Washington, DC: Nuclear Regulatory Commission.

Peters, J. F., and E. Heymsfield. 2004. FEM formulation of four and five noded elements using a linearly varying stress assumption. *International Journal of Solids and Structures* 41(7):1991–2009.

Peters, J. F., and D. A. Leavell. 1986. Uniaxial tensile test for soils. In *Advanced Triaxial Testing of Soil and Rock*, ASTM STP 977:169–188. Louisville, KY.

Philip, J. R., and D. A. de Vries. 1957. Moisture movement in porous material under temperature gradients. American Geophysical Union. *Eos Transactions* 38(2):222–232.

Piet, S. J., R. P. Breckenridge, D. E. Burns, and project team. 2003a. Testing, modeling, and monitoring to enable simpler, cheaper, longer-lived surface caps. In *Proceedings Waste Management '03 Conference, 23–27 February 2003, Tucson, AZ*. Tucson, AZ: WM Symposia, Inc.

Piet, S. J., J. J. Jacobson, P. Martian, R. Marineau, and R. Soto. 2003b. Modeling and simulation of long-term performance of near-surface barriers. *In Proceedings Waste Management '03 Conference, 23–27 February 2003, Tucson, AZ*. Tucson, AZ: WM Symposia, Inc.

Qui, G.Y., J. Ben-Asher, T. Yano, and K. Momii. 1999. Estimation of soil evaporation using the differential temperature method. *Soil Science Society of America Journal* 63:1608–1614.

Richie, J. T. 1972. Model for predicting evaporation from a row crop with incomplete cover. *Water Resources Research* 8:1204–1213.

Rieth, M. 2003. *Nano-Engineering in Science and Technology*. London: World Scientific Publishing Company.

Schelde, K., A. Thomsen, T. Heidmann, and Schjønning. 1998. Diurnal fluctuations of water and heat flows in a bare soil. *Water Resources Research* 34(11):2919-2929.

Schroeder, P.R., C. Lloyd, and P. Zappi. 1994. *The hydrologic evaluation of landfill performance (HELP) model, user's guide for version 3.0*. Cincinnati, OH: U.S. Environmental Protection Agency.

Sepaskhah, A. R., and L. Boersma. 1979. Thermal conductivity of soils as a function of temperature and water content. *Soil Science Society of America Journal* 43:439-444.

Smith, G. M., and Rager, R. E. 2002. Protective layer design in landfill covers based on frost penetration. *Journal of Geotechnical and Geoenvironmental Engineering* 128(9):794–799.

Suter, G. W., F. J. Luxmoore, and E. D. Smith 1993. Compacted soil barriers at abandoned landfill sites are likely to fail in the long term. *Journal of Environmental Quality* 22(2):217–226.

Tatterson, G. B. 1991. *Fluid mixing and gas dispersion in agitated tanks*. New York, McGraw-Hill, Inc.

Thibodeaux, L. J. 1996. *Environmental chemodynamics*, 2nd ed. New York: John Wiley and Sons.

Vernet, C. P. 2004. Ultra-durable concretes: Structure at the micro- and nanoscale. *Materials Research Society Bulletin* 29(5).

White, E. M. 2001. Comments on using surface crack spacing to predict crack network geometry in swelling soils. *Soil Science Society of America Journal* 65:1573–1574.

Wong, L., and M. Haug. 1991. Cyclical closed-system freeze-thaw permeability testing of soil liners and cover materials. *Canadian Geotechnical Journal* 28:784–793.

Ziehm, R. 2003. Engineered near surface disposal facility of the industrial complex for solid radwaste management at Chernobyl Nuclear Power Plant. In *Proceedings Waste Management '03 Conference, 23–27 February 2003, Tucson, AZ*. Tucson, AZ: WM Symposia, Inc.

Zienkienwicz, O. C. 1977. *The finite element method*, third edition. London: McGraw–Hill.

REPORT DOCUMENTATION PAGE

1. REPORT DATE *(DD-MM-YYYY)* June 2008	2. REPORT TYPE Final report	3. DATES COVERED *(From - To)*

4. TITLE AND SUBTITLE	5a. CONTRACT NUMBER
Assessment of the Effectiveness of Clay Soil Covers as Engineered Barriers in Waste Disposal Facilities with Emphasis on Modeling Cracking Behavior	5b. GRANT NUMBER
	5c. PROGRAM ELEMENT NUMBER

6. AUTHOR(S)	5d. PROJECT NUMBER
Ernest S. Berney IV, Wayne D. Hodo, John F. Peters, Tommy E. Myers, Richard S. Olsen, and Michael K. Sharp	5e. TASK NUMBER
	5f. WORK UNIT NUMBER

7. PERFORMING ORGANIZATION NAME(S) AND ADDRESS(ES)	8. PERFORMING ORGANIZATION REPORT NUMBER
U.S. Army Engineer Research and Development Center Geotechnical and Structures Laboratory Environmental Laboratory 3909 Halls Ferry Road Vicksburg, MS 39180-6199	ERDC TR-08-X

9. SPONSORING / MONITORING AGENCY NAME(S) AND ADDRESS(ES)	10. SPONSOR/MONITOR'S ACRONYM(S)
U.S. Nuclear Regulatory Commission Office of Nuclear Regulatory Research Washington, DC 20555	11. SPONSOR/MONITOR'S REPORT NUMBER(S)

12. DISTRIBUTION / AVAILABILITY STATEMENT
Approved for public release; distribution is unlimited.

13. SUPPLEMENTARY NOTES

14. ABSTRACT

This research investigated the nature of cracking behavior in compacted clay liners used for nuclear waste disposal facilities. A literature review found that, in all documented in-place clay liner studies, cracking occurred in the clay liner within 10 years, leading to failure of the liner system. Further, all moisture-flow models studied failed to capture clay cracking and the resultant high permeability associated with these failed liner systems. A laboratory investigation was undertaken to define the mechanics of the clay cracking process for a numerical model. Visual and numerical observations of cracking during drying of a highly expansive clay showed that crack formations are very diverse along the surface layer and as they migrate downward. Shapes of cracks are neither uniform nor symmetric, evolving from thin webs of microcracks to a select number of wide primary cracks that, in turn, can seal off existing microcracks. A finite element model of the soil shrinkage process was then developed, which included crack formation. Stresses within intact soil are caused by self weight (gravity stresses) and changes in water content, which induce shrinkage as a result of suction-induced tensile stresses. Two numerical simulations were run on a digital test bed similar to the laboratory study. The simulations agreed well with laboratory experimental observations, capturing all the relevant crack phenomena. The report concludes that a change in the current design criteria for clay liner systems is necessary to enable the clay to remain in a fixed, as-compacted state.

15. SUBJECT TERMS	Evapotranspiration	Nuclear waste	Soil suction
Clay cracking	Finite element numerical modeling	Percolation	Thermodynamics
Desiccation	Moisture barrier	Shrink swell	

16. SECURITY CLASSIFICATION OF:			17. LIMITATION OF ABSTRACT	18. NUMBER OF PAGES	19a. NAME OF RESPONSIBLE PERSON
a. REPORT UNCLASSIFIED	b. ABSTRACT UNCLASSIFIED	c. THIS PAGE UNCLASSIFIED		108	19b. TELEPHONE NUMBER *(include area code)*